

Lecture Notes in Civil Engineering

Satyajit Patel
C. H. Solanki
Krishna R. Reddy
Sanjay Kumar Shukla *Editors*

Indian Geotechnical Conference 2019

Geotechnics for Infrastructure
Development & Urbanisation
(GeoINDUS)

 Springer

Lecture Notes in Civil Engineering

Volume 140

Series Editors

Marco di Prisco, Politecnico di Milano, Milano, Italy

Sheng-Hong Chen, School of Water Resources and Hydropower Engineering,
Wuhan University, Wuhan, China

Ioannis Vayas, Institute of Steel Structures, National Technical University of
Athens, Athens, Greece

Sanjay Kumar Shukla, School of Engineering, Edith Cowan University, Joondalup,
WA, Australia

Anuj Sharma, Iowa State University, Ames, IA, USA

Nagesh Kumar, Department of Civil Engineering, Indian Institute of Science
Bangalore, Bengaluru, Karnataka, India

Chien Ming Wang, School of Civil Engineering, The University of Queensland,
Brisbane, QLD, Australia

Lecture Notes in Civil Engineering (LNCE) publishes the latest developments in Civil Engineering—quickly, informally and in top quality. Though original research reported in proceedings and post-proceedings represents the core of LNCE, edited volumes of exceptionally high quality and interest may also be considered for publication. Volumes published in LNCE embrace all aspects and subfields of, as well as new challenges in, Civil Engineering. Topics in the series include:

- Construction and Structural Mechanics
- Building Materials
- Concrete, Steel and Timber Structures
- Geotechnical Engineering
- Earthquake Engineering
- Coastal Engineering
- Ocean and Offshore Engineering; Ships and Floating Structures
- Hydraulics, Hydrology and Water Resources Engineering
- Environmental Engineering and Sustainability
- Structural Health and Monitoring
- Surveying and Geographical Information Systems
- Indoor Environments
- Transportation and Traffic
- Risk Analysis
- Safety and Security

To submit a proposal or request further information, please contact the appropriate Springer Editor:

- Pierpaolo Riva at pierpaolo.riva@springer.com (Europe and Americas);
- Swati Meherishi at swati.meherishi@springer.com (Asia—except China, and Australia, New Zealand);
- Wayne Hu at wayne.hu@springer.com (China).

All books in the series now indexed by Scopus and EI Compindex database!

More information about this series at <http://www.springer.com/series/15087>

Satyajit Patel · C. H. Solanki ·
Krishna R. Reddy · Sanjay Kumar Shukla
Editors

Indian Geotechnical Conference 2019

Geotechnics for INfrastructure Development
& UrbaniSation (GeoINDUS)

 Springer

Editors

Satyajit Patel
Department of Civil Engineering
Sardar Vallabhbhai National Institute of
Technology (SVNIT)
Surat, Gujarat, India

C. H. Solanki
Department of Applied Mechanics
Sardar Vallabhbhai National Institute of
Technology (SVNIT)
Surat, Gujarat, India

Krishna R. Reddy
Department of Civil and Materials
Engineering
University of Illinois at Chicago
Chicago, IL, USA

Sanjay Kumar Shukla
Department of Civil Engineering
Edith Cowan University
Joondalup, WA, Australia

ISSN 2366-2557

ISSN 2366-2565 (electronic)

Lecture Notes in Civil Engineering

ISBN 978-981-33-6589-6

ISBN 978-981-33-6590-2 (eBook)

<https://doi.org/10.1007/978-981-33-6590-2>

© The Editor(s) (if applicable) and The Author(s), under exclusive license to Springer Nature Singapore Pte Ltd. 2021

This work is subject to copyright. All rights are solely and exclusively licensed by the Publisher, whether the whole or part of the material is concerned, specifically the rights of translation, reprinting, reuse of illustrations, recitation, broadcasting, reproduction on microfilms or in any other physical way, and transmission or information storage and retrieval, electronic adaptation, computer software, or by similar or dissimilar methodology now known or hereafter developed.

The use of general descriptive names, registered names, trademarks, service marks, etc. in this publication does not imply, even in the absence of a specific statement, that such names are exempt from the relevant protective laws and regulations and therefore free for general use.

The publisher, the authors and the editors are safe to assume that the advice and information in this book are believed to be true and accurate at the date of publication. Neither the publisher nor the authors or the editors give a warranty, expressed or implied, with respect to the material contained herein or for any errors or omissions that may have been made. The publisher remains neutral with regard to jurisdictional claims in published maps and institutional affiliations.

This Springer imprint is published by the registered company Springer Nature Singapore Pte Ltd. The registered company address is: 152 Beach Road, #21-01/04 Gateway East, Singapore 189721, Singapore

Preface

The Indian Geotechnical Society, Surat Chapter, and Sardar Vallabhbhai National Institute of Technology (SVNIT), Surat, India, organized the Indian Geotechnical Conference (IGC) in Surat during 19–21 December 2019. The main theme of the conference was “GeoINDUS: Geotechnics for INfrastructure Development & UrbaniSation”. The subthemes of the conference included:

1. Characterization of Geomaterials and Physical Modelling,
2. Foundations and Deep Excavations,
3. Soil Stabilization and Ground Improvement,
4. Geoenvironmental Engineering and Waste Material Utilization,
5. Soil Dynamics and Earthquake Geotechnical Engineering,
6. Earth Retaining Structures, Dams and Embankments,
7. Slope Stability and Landslides,
8. Transportation Geotechnics,
9. Geosynthetics Applications,
10. Computational, Analytical and Numerical Modelling,
11. Rock Engineering, Tunnelling and Underground Constructions,
12. Forensic Geotechnical Engineering and Case Studies,
13. Other Topics: Behaviour of Unsaturated Soils, Offshore and Marine Geotechnics, Remote Sensing and GIS, Field Investigations, Instrumentation and Monitoring, Retrofitting of Geotechnical Structures, Reliability in Geotechnical Engineering, Geotechnical Education, Codes and Standards and other relevant topics.

The proceedings of this conference consist of selected papers presented at the conference. The proceedings are divided into six volumes, including a special volume with all keynote/invited presentations.

We sincerely thank all the authors who have contributed their papers to the conference proceedings. We also thank all the reviewers who have been instrumental in giving their valuable inputs for improving the quality of the final papers. We greatly appreciate and thank the student volunteers, especially Vemula Anand Reddy, Mohit Mistry, Rahul Pai, Manali Patel, Rohan Deshmukh, Hrishikesh

Shahane, Anand M. Hulagabali, Jiji Krishnan and Bhavita Dave, for their unwavering support that was instrumental in preparation of these proceedings. Finally, thanks to the Springer team for their support and full cooperation for publishing six volumes of these IGC-2019 proceedings.

Surat, India

Surat, India

Chicago, USA

Joondalup, Australia

Satyajit Patel

C. H. Solanki

Krishna R. Reddy

Sanjay Kumar Shukla

Contents

Recent Advancements in Predicting the Behaviour of Unsaturated and Expansive Soils	1
Aritra Banerjee, Anand J. Puppala, Surya S. C. Congress, Sayantan Chakraborty, and Aravind Pedarla	
Recent Advances on Dynamic Load Testing of Bored Piles and Other Cast-in-Situ Piles	23
E. Anna Sellountou and Brent Robinson	
Recent Advances in Geotechnical Infrastructure	31
Bindumadhava Aery	
Forensic Geotechnical Investigation of Settlement Failure of Pile Group Supporting Columns of Conveyor Belt	41
C. N. V. Satyanarayana Reddy and M. Nagalakshmi	
Field Application of High-Strength Deep Mixing Method for Waste Water Pipeline in Soft Ground	51
E. C. Shin, J. K. Kang, Y. K. Rim, and J. J. Park	
Sustainable Remediation of a Dumpsite	65
P. Sughosh, N. Anusree, B. Prathima, and G. L. Sivakumar Babu	
Micro-structural and Mineralogical Studies to Evaluate the Effectiveness of Industrial Solid Wastes for Stabilization of Expansive Soils	77
H. N. Ramesh, B. V. Manjunatha, and Madhavi Gopal Rao Kulkarni	
Geotechnical Engineering Accompanied by Risk	95
Ikuo Towhata	
Quantitative Assessment of Life Cycle Sustainability (QUALICS): Application to Engineering Projects	111
Krishna R. Reddy, Girish Kumar, and Jyoti K. Chetri	

**Geological and Geotechnical Investigations and Interpretations
Thereof for Statue of Unity Foundation 127**
Sandeep Ghan

Early Warning of Water-Triggered Landslides 139
Vikas Thakur, Katherine Robinson, Emir Oguz, Ivan Depina,
Ankush Pathania, Praveen Kumar, Prateek Chaturvedi, Kala Venkat Uday,
and Varun Dutt

Editors and Contributors

About the Editors



Dr. Satyajit Patel is Associate Professor at the Civil Engineering Department, Sardar Vallabhbhai National Institute of Technology, Surat, India. His research area includes utilization of industrial solid wastes in civil engineering constructions, geoenvironmental issues, soil stabilization, ground improvement, and geosynthetics for road pavements. He has published 13 journal papers and presented 7 research papers internationally. He has guided more than 29 M.Tech students and 9 students are currently pursuing their PhD under his guidance. He is a life member of Indian Geotechnical Society, Institution of Engineers (India), and Indian Road Congress (IRC). He has received a research grant from the Department of Science and Technology, Government of India.



Dr. C. H. Solanki is Professor (Geotechnical Engineering) at the Civil Engineering Department, Sardar Vallabhbhai National Institute of Technology, Surat, India. He has guided 50 postgraduate dissertations and 16 PhD thesis and he is currently supervising 11 PhD research scholars. He has published 165 research papers in the reputed national, international journals and conferences. Dr. Solanki received the “Shri. M.S. Jain Biannual Award” for the Best Paper in IGC 2013, Prof. Dinesh Mohan Award in IGC 2017 and “Distinguished Faculty Award” form The Venus International Faculty Awards-2016. He has organized

20 national level events including STTP, FDP, conferences and seminars and he was the chairman for the Indian Geotechnical Conference (IGC 2019) held at Surat, Gujarat. Dr. Solanki has been elected as a member of executive committee of IGS for the terms (2015–2022). His research interests include subsoil characteristics, predictions in geotechnical engineering, soil dynamics, ground improvement and geoenvironmental engineering. He has given 50 expert talks throughout India and abroad. He is a life member of Indian Geotechnical Society, Indian Society for Technical Education (ISTE), and Institution of Engineers (India).



Dr. Krishna R. Reddy is Professor of Civil and Environmental Engineering, Director of Sustainable Engineering Research Laboratory, and also Director of the Geotechnical and Geoenvironmental Engineering Laboratory at the University of Illinois at Chicago, USA. He received his Ph.D. in Civil Engineering from the Illinois Institute of Technology, Chicago, USA. Dr. Reddy has over 28 years of teaching, consulting, and research experience in the fields of civil engineering, geotechnical & geoenvironmental engineering, environmental engineering, and sustainable & resilient engineering. He is the author of 4 books, 246 journal papers, 21 edited books/conference proceedings, 22 book chapters, and 225 full conference papers. He has received several awards for excellence in research and teaching, including the ASCE Wesley W. Horner Award, ASTM Hogentogler Award, UIC Distinguished Researcher Award, the University of Illinois Scholar Award, and the University of Illinois Award for Excellence in Teaching.



Dr. Sanjay Kumar Shukla is the Founding Research Group Leader (Geotechnical and Geoenvironmental Engineering) at the Edith Cowan University, Perth, Australia. He is the Founding Editor-in-Chief of the International Journal of Geosynthetics and Ground Engineering. He holds the Distinguished Professorship in Civil Engineering at Delhi Technological University, Delhi, VIT University, Vellore, Amity University, Noida, Chitkara University, Himachal Pradesh and VR Siddhartha Engineering College, Vijayawada, India. He graduated in Civil Engineering from BIT Sindri, India, and earned his MTech in Civil (Engineering Geology) Engineering and PhD in Civil (Geotechnical) Engineering from the Indian Institute of Technology (IIT) Kanpur, India. His primary areas of research interest include geosynthetics and fibres for sustainable developments, ground improvement techniques, utilization of wastes in construction, earth pressure and slope stability, environmental, mining and pavement geotechnics, and soil–structure interaction. He is an author/editor of 15 books, including 7 textbooks, and more than 260 research papers, including 160 refereed journal papers. He has been honoured with several awards, including IGS Award 2018 by the International Geosynthetics Society, USA, in recognition of outstanding contribution to the development and use of geosynthetics. He is a fellow of Engineers Australia, Institution of Engineers (India), and Indian Geotechnical Society, and a member of American Society of Civil Engineers, International Geosynthetics Society, and several other professional bodies.

Contributors

Bindumadhava Aery Aurecon, Brisbane, QLD, Australia

E. Anna Sellountou Pile Dynamics, Inc., Cleveland, OH, USA

N. Anusree Indian Institute of Science, Bangalore, Karnataka, India

Aritra Banerjee Assistant Professor, Department of Civil and Environmental Engineering, University of Delaware, Newark, DE, USA

Sayantana Chakraborty Assistant Professor, Department of Civil Engineering, Birla Institute of Technology and Science, Pilani, Rajasthan, India

Prateek Chaturvedi Indian Institute of Technology, Mandi, Himachal Pradesh, India

Jyoti K. Chetri Department of Civil and Materials Engineering, University of Illinois, Chicago, IL, USA

Surya S. C. Congress Associate Research Scientist, Zachry Department of Civil and Environmental Engineering, Texas A&M University, College Station, TX, USA

Ivan Depina SINTEF, Trondheim, Norway

Varun Dutt Indian Institute of Technology, Mandi, Himachal Pradesh, India

Sandeep Ghan Chief Engineering Manager, Transportation Infrastructure IC, EDRC (RREC), L & T Construction, Mumbai, India

J. K. Kang Department of Civil and Environmental Engineering, Incheon National University, Incheon, South Korea

Madhavi Gopal Rao Kulkarni Bangalore University, Bengaluru, India; Presidency University, Bengaluru, India

Girish Kumar Department of Civil and Materials Engineering, University of Illinois, Chicago, IL, USA

Praveen Kumar Indian Institute of Technology, Mandi, Himachal Pradesh, India

B. V. Manjunatha Bangalore University, Bengaluru, India

M. Nagalakshmi College of Engineering, Andhra University, Visakhapatnam, India

Emir Oguz Norwegian University of Science and Technology, Trondheim, Norway

J. J. Park Department of Civil and Environmental Engineering, Incheon National University, Incheon, South Korea

Ankush Pathania Indian Institute of Technology, Mandi, Himachal Pradesh, India

Aravind Pedarla Geotechnical Engineer, CDM Smith, Dallas, TX, USA

B. Prathima Indian Institute of Science, Bangalore, Karnataka, India

Anand J. Puppala A.P. and Florence Wiley Chair Professor, Zachry Department of Civil and Environmental Engineering, Texas A&M University, College Station, TX, USA

H. N. Ramesh Department of Civil Engineering, Bangalore University, Bengaluru, India

Krishna R. Reddy Department of Civil and Materials Engineering, University of Illinois, Chicago, IL, USA

Y. K. Rim Department of Civil and Environmental Engineering, Incheon National University, Incheon, South Korea

Brent Robinson Pile Dynamics, Inc., Cleveland, OH, USA

Katherine Robinson Norwegian University of Science and Technology, Trondheim, Norway

C. N. V. Satyanarayana Reddy Department of Civil Engineering, College of Engineering, Andhra University, Visakhapatnam, India

E. C. Shin Department of Civil and Environmental Engineering, Incheon National University, Incheon, South Korea

G. L. Sivakumar Babu Indian Institute of Science, Bangalore, Karnataka, India

P. Sughosh Jawaharlal Nehru National College of Engineering, Shimoga, Karnataka, India

Vikas Thakur Norwegian University of Science and Technology, Trondheim, Norway

Ikuo Towhata Kanto Gakuin University, Yokohama, Japan

Kala Venkat Uday Indian Institute of Technology, Mandi, Himachal Pradesh, India

Recent Advancements in Predicting the Behaviour of Unsaturated and Expansive Soils



Aritra Banerjee , Anand J. Puppala , Surya S. C. Congress , Sayantan Chakraborty , and Aravind Pedarla

Abstract This study focuses on the advancements of characterization of unsaturated expansive soils which would allow better prediction of its swelling and mechanical behaviours. The paper has been divided into three parts. Firstly, a novel model is developed by considering two micro-soil parameters, soil-specific surface area and internal pore size distribution, to predict the natural swelling in expansive clayey soils. The model was validated by comparing the predictions with experimental results for eight soils. Secondly, the paper deals with the diffused-double-layer (DDL) theory-related electrostatic forces from individual clay minerals of expansive soils and their influence on soil swelling. A DDL-based model was also developed, which was validated for swell prediction for fourteen expansive soils. A good correlation was observed for both models when the results were compared with experimental results. Finally, the paper demonstrated the use of vapour pressure technique to control suction beyond 5 MPa for performing suction-controlled repeated load triaxial (RLT) test at high suction state. This novel

A. Banerjee

Assistant Professor, Department of Civil and Environmental Engineering,
University of Delaware, Newark 19716, DE, USA
e-mail: aritra@udel.edu

A. J. Puppala (✉)

A.P. and Florence Wiley Chair Professor, Zachry Department of Civil and Environmental
Engineering, Texas A&M University, College Station 77840, TX, USA
e-mail: anandp@tamu.edu

S. S. C. Congress

Associate Research Scientist, Zachry Department of Civil and Environmental Engineering,
Texas A&M University, College Station 77840, TX, USA
e-mail: congress@tamu.edu

S. Chakraborty

Assistant Professor, Department of Civil Engineering, Birla Institute of Technology
and Science, Pilani 333031, Rajasthan, India
e-mail: sayantan.chakraborty@pilani.bits-pilani.ac.in

A. Pedarla

Geotechnical Engineer, CDM Smith, Dallas 75251, TX, USA
e-mail: aravindcivil@gmail.com

technique mitigates the limitation of axis-translation technique for maintaining suction till the air-entry-value (AEV) of the ceramic disk. These new models and unsaturated laboratory testing techniques would aid in better characterization of expansive soils in their unsaturated state. This would also provide accurate prediction of swell and stiffness behaviours of soils, thereby reducing the uncertainties in the design of civil infrastructure built on expansive soils.

Keywords Unsaturated soils · Swelling · Expansive soils · Resilient modulus · High-suction state

1 Introduction

Expansive soils are known to be problematic for supporting civil infrastructure, such as low-height residential structures, pavements and others, due to the tendency of such soils to undergo significant volume changes with considerable moisture content fluctuations. These moisture fluctuations are commonly caused due to seasonal and daily variations in temperature and precipitation. However, due to the growth in population and associated urbanization, expansive soils are often used as foundation soils and construction still takes place on top of expansive soils [1]. Several cases of severe distress had been observed for such constructed structures and pavements due to the swell-and-shrink-related movements of these soils [2, 3]. These damages had been reported to be greater than those observed for the damages caused by floods, hurricanes, tornadoes and earthquakes [4, 5].

Many parts of the world lie within the arid and semi-arid regions, where precipitation is lower than the rate of evaporation. Hence, during most of the year the soil in such regions, especially at shallow depths are in unsaturated state, wherein theories of classical soil mechanics and geotechnical engineering of either dry or fully saturated soils doesn't apply. The study of unsaturated soil involves the principles of mechanics, hydraulics, thermodynamics and interfacial physics. Because of the complexity of the material properties and the requirement of sophisticated equipment to characterize the behaviour of unsaturated soils, limited research has been conducted, resulting in a lack of knowledge.

The negligence or oversimplification of the relations, required to accurately study the behaviour of unsaturated soils, has resulted in incorrect predictions of strength and volume changes of soil when it is subjected to various kinds of loads, such as structural and climatic loads [6]. This is especially true for expansive soils. Since the volume changes of expansive soils create severe distress to civil infrastructure, the study of the behaviour of expansive soils had motivated the unsaturated soil research [4, 7].

Additionally, the problems due to expansive soils might have risen due to the lack of consideration for soil mineralogy [8, 9]. Most of the previous correlations for predicting the behaviour of expansive soil adopted a PI-based methodology to propose simplistic relationships that were utilized to predict the swelling potential of

clayey soils, which may be an erroneous approach [8, 5]. In this study, an attempt was made to improve the understanding of the behaviour of expansive soil by identifying the parameters that affect the swelling characterization of clayey soils and also demonstrate the need for advanced setups to determine the resilient modulus–suction relationship in expansive soils. In the past, studies have been conducted to identify various micro-soil parameters such as clay mineralogy, surface area, matric suction and pore distribution, and their effect on behaviour of soils [2, 10–13].

The first part of research data presented in this study focuses on correlating two micro-soil parameters, soil-specific surface area and internal pore size distribution, with the swell behaviour of expansive clay. These two parameters account for the swell potential of clay minerals in soil and internal moisture distribution that provides moisture access to the clay minerals present in soils. The second part of this paper deals with the diffused-double-layer (DDL) theory-related electrostatic forces from individual clay minerals of an expansive soil and their influence on soil swelling, and a DDL-based model was developed and validated for swell prediction for expansive soils. Finally, the use of vapour pressure technique to control suction beyond 5 MPa was demonstrated for performing suction-controlled repeated load triaxial test at high suction state. This novel technique mitigates the limitation of axis-translation technique for maintaining suction till the air-entry-value (AEV) of the ceramic disk. This was performed to reduce the variation of resilient modulus for each loading sequence.

Some of the advancements presented in this study showcased improved characterization of expansive soils and mechanical characterization studies on unsaturated soils at field moisture conditions corresponding to high suctions. These studies, though requires additional studies and tests, will provide better and comprehensive characterization and assessments of soil behaviour that will lead to better infrastructure designs on these soils.

2 Swell Prediction Methods

The swelling potential of soils is mostly based on the clay mineralogy. Previous studies had demonstrated that by using parameters such as specific surface area, cation-exchange capacity and total potassium, the clay mineralogy of various clayey soils could be predicted [9]. Specific surface area (SSA) of the clay particles is the property of the material and is defined as the total surface area of the solid particles per unit of mass. This property represents the reactivity of clay minerals, which often translates to rate of moisture adsorption for clayey soils, which results in swelling [14]. There are a few methods to determine the value of SSA, among which the ethylene glycol monoethyl ether (EGME) method was used in this study. Previously, Carter et al. [15] and Cerato and Lutenegeger [16] had used this method and concluded that the test results were repeatable. Pedarla [17] had noted that SSA aids in indirectly quantifying the amount of expansive clay minerals, such as montmorillonite and illite, which are commonly found in soils.

Researchers had suggested that the moisture distribution and its access to clay minerals within soil could be estimated by determining the internal pore structure and pore distribution [18]. Mercury intrusion porosimetry (MIP) technique is used to evaluate the pore size distribution in a soil specimen. In MIP technique, a non-wetting liquid, i.e. mercury, is forced into the accessible pores within the soil specimen. From the MIP data, the average pore diameter and the pore void distribution of the soil were determined due to the ink bottle effect [17]. Researchers have attempted to study the effect of pore distribution and pore connectivity on the behaviour of expansive soil [19, 20]. These studies have concluded that the MIP technique is successful way to determine the pores and the structure of clayey soils. Pedarla [17] had selected different soils from various parts of the USA to study their swelling behaviour. A synopsis of these test results is shown in Table 1.

Two types of swell characterization studies were used by Pedarla [17]. One-dimensional swell tests were conducted on soil specimens of 2.54 cm height and 6.35 cm diameter. These tests were conducted in an oedometer in accordance to ASTM D4546 (2014). Additionally, three-dimensional swell strain tests were conducted on larger soil specimens with 10.16 cm height and 5.08 cm diameter. Figure 1 presents the schematic and illustrations of the 3D swell test setup used by Pedarla [17]. The details of the test setup and operating principles are discussed in Pedarla [17]. The volume change of soil specimen in the lateral direction was quantified from the changes in the water chamber volume readings. The soil specimen encased in the chamber was submerged in the water tub and then allowed to swell in all directions. Strains in both directions were measured and used to determine the volumetric strains of these soils at different moisture content levels.

Table 2 summarizes the volumetric swell strains for all eight soils when subjected to full saturation under different confining pressures. It was observed that Grayson soil swelled the most, while San Diego soil swelled the least. In general, soil specimens were observed to swell less with increasing confining pressures, which may be because the confining pressure resists the repulsive pressure induced due to hydration of diffused-double-layer systems of the clay particles.

As mentioned earlier, the surface area of clay minerals in soils plays a significant part in determining the amount of swelling in expansive soils. The minerals such as montmorillonite have a very high surface area when compared with minerals such as kaolinite and illite [21]. The soil specimens which have higher percentages of montmorillonite and illite minerals have a tendency to have more reactive surface area per unit of mass of soil, which results in higher affinity for moisture and such soils mostly experience larger amounts of swelling. Hence, specific surface area of clay minerals was attempted to be determined by Pedarla [17] to study the swelling behaviour of clayey soils.

The EGME method was used to determine the value of SSA, which has been used in agronomy circles [15], and was later validated for geotechnical applications by Cerato and Lutenegeger [16]. Cerato and Lutenegeger [16] had identified the potential of this method for a wide range of clay mineralogy in soils, where SSA ranges from 15 to 800 m²/g.

Table 1 Basic properties of the test soils

	Liquid limit (LL)	Plasticity index (PI)	USCS classification	Clay fraction (%)	MDUW (kN/m ³)	OMC (%)	SSA (m ² /g)
Grayson	75	49	CH	55	14.3	24	223.0
San Antonio	67	43	CH	52	15.8	22	192.4
Colorado	63	42	CH	46	16.2	19	185.0
Burleson	55	37	CH	52	16.0	19	132.4
San Diego	42	28	CL	23	17.0	17	92.6
Anaheim	48	27	CL	32	16.9	18	118.5
Oklahoma	41	21	CL	30	15.6	24	76.3
Keller	25	11	CL	34	18.5	14	115.0

MDUW maximum dry unit weight, *OMC* optimum moisture content, *SSA* specific surface area, *USCS* unified soil classification system

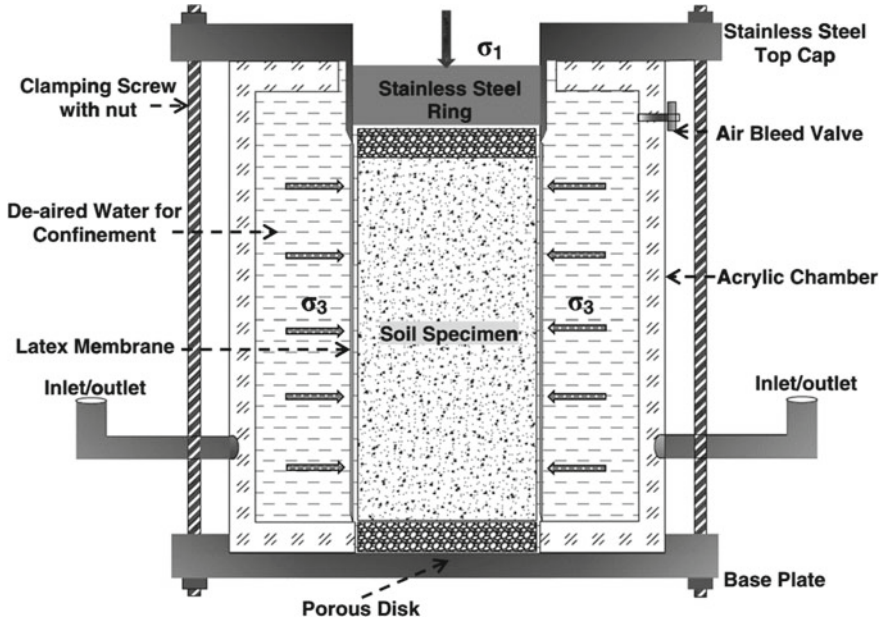


Fig. 1 Schematic of 3D swell strain test setup designed for the study

Table 2 Volumetric swell strains obtained from experimental studies for different soil specimens at 95% MDUW at different confining pressures

Soil	Volumetric swell strain, ϵ_{vol} (%)		
	7 (kPa)	50 (kPa)	100 (kPa)
Grayson	11.65	8.76	7.67
Colorado	9.29	7.55	6.30
San Antonio	9.13	7.40	5.74
Burleson	8.03	6.45	4.69
Keller	6.84	5.73	3.71
Anthem	4.80	4.30	2.87
Oklahoma	5.03	3.69	2.69
San Diego	4.52	3.43	2.13

Table 3 shows a summary of MIP test results for eight clayey soils. In MIP technique, the amount of mercury injected into a soil specimen at various pressure points is measured, and these data were used with the theory of cylindrical pore model to determine the pore size distributions and various related porosity parameters [17]. The distribution of pore volumes is also shown in Table 3.

Table 3 Distribution of pore volumes for different soils as obtained from MIP technique

Soil	Cumulative volume of mercury intrusion (mL/g)	Micro-pores (%)	Medium-pores (%)	Macro-pores (%)
Anthem	0.16	18	5	32
Burleson	0.18	15	55	30
Colorado	0.23	10	50	40
Grayson	0.25	23	37	40
Keller	0.13	20	48	32
Oklahoma	0.21	26	54	24
San Antonio	0.16	20	53	27
San Diego	0.16	7	46	47

2.1 Swell Strain Modelling

The primary objective of the research by Pedarla [17] was to propose a new conceptual model that accounts for soil mineralogy and pore size distribution as these properties are known to influence the swell behaviours of test soils. The details regarding the procedure and the assumptions involved are presented by Pedarla [17].

A new hypothetical parameter termed as the total surface area ratio (TSAR) which governs the effects of surface area from clay mineralogy, and pore area in a compacted soil specimen is hence formulated in this modelling. Total surface area ratio (TSAR) is defined as the ratio of total surface area calculated from the clay mineralogy in a soil specimen to the total pore surface area calculated from MIP tests of the same soil specimen [17]. TSAR of a soil represents the fraction of clay minerals that can be exposed to moisture from the interconnected pores within the same soil specimen. TSAR of a soil specimen is mathematically determined from the following equation:

$$\text{TSAR} = \frac{\text{TSA}_{\text{CF}}}{\text{TSA}_{\text{MIP}}} \quad (1)$$

where TSAR is the total surface area ratio; TSA_{CF} is the total surface area of clay mineral present in the soil; and TPA_{MIP} is the total pore area of finer fraction determined from MIP studies. The summary of TSAR values determined at 95% MDUW for different soils is presented in Table 4.

Figure 2 shows the variations of volumetric swell strains at 95% MDUW condition. It was determined that the swell strain is directly proportional to the value of TSAR. The following swell prediction model was postulated by Pedarla [17] by using the boundary conditions of the test conditions:

Table 4 Summary of TSAR values for soil samples compacted at 95% MDUW

Soil	1D swell	3D swell
Anthem	1.887	1.872
Burleson	3.613	3.861
Colorado	5.638	6.030
Grayson	5.817	5.770
Keller	2.312	2.292
Oklahoma	0.775	0.768
San Antonio	4.110	4.076
San Diego	1.066	1.057

$$\epsilon_{\text{swell}(1D,3D)} = a(\text{TSAR}) + b \tag{2}$$

where *a* and *b* are modelling parameters and are dependent on the test-related boundary conditions.

Three TSAR correlations were developed for three individual confining pressure conditions for these tests. The development of additional experimental databases in the future would aid development of more generalized TSAR versus swell strain correlations that account for compaction and test confining conditions. In summary, this study demonstrated a fundamental method using soil internal information that would provide more accurate predictions of the complex swelling behaviour of soils.

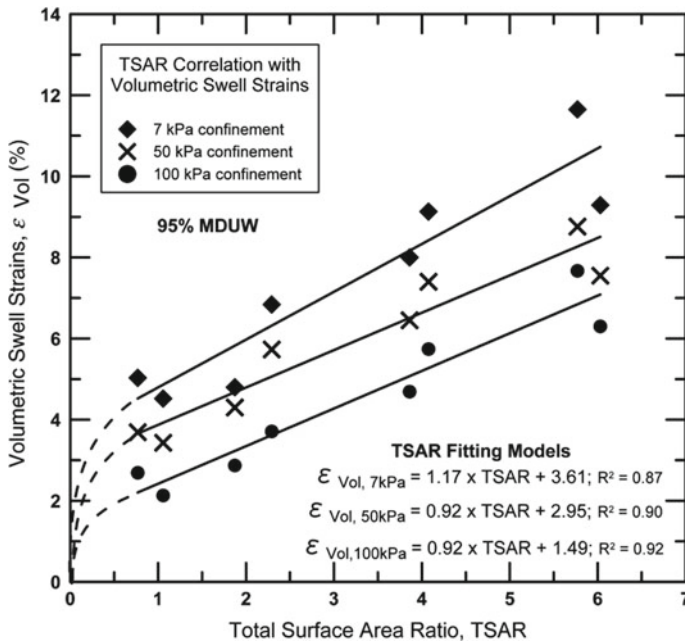


Fig. 2 TSAR correlation with volumetric swell strain for sample compacted at 95% MDUW

3 Diffused-Double-Layer Swell Prediction Model

Diffused-double-layer (DDL) theory, as proposed by Chapman [22], provides a strong basis for the understanding of swell behaviour of a clay specimen. When clay comes in close contact with water, the negative charged clay particles tend to attract the water molecules. The water molecules distribute over the surface area of the clay particles thereby increasing the particle size. The extent to which the clay particles have attraction forces on the water molecules can be termed as diffused-double-layer water. Lu and Likos [7] specified that crystalline swelling or Type 1 swelling which is caused by interlayer absorption of water particles was followed by electrical double-layer attraction forces which is also known as Type 2 swelling. These long-range double-layer attraction forces are the primary concern for the present research and are hence considered and used in the swell prediction model. Researchers have made efforts to develop correlations based on the DDL theory, which have accurately predicted the swelling pressure of bentonite [23]. When the complexities of naturally available expansive clays and the wide distribution of expansive minerals is considered, such a theory was used by Puppala et al. [24], wherein many assumptions were made to address the soil matrix swelling from the fundamental diffused-double-layer influence.

Puppala et al. [24] had selected fourteen naturally available expansive soils for this study (Table 5). The properties such as specific surface area, cation exchange capacity and total potassium of these soils were also determined using methods proposed by Chittoori and Puppala [9]. These experimental results were used to interpret three dominant clay minerals, viz. montmorillonite (MM), illite (I) and kaolinite (K). One-dimensional (1D) swell strain and swell pressure tests were conducted in an oedometer, in accordance with ASTM D4546 (2008). A summary of these test results is presented in Table 6. It is apparent from these tests that there is no direct correlation between plasticity property, plasticity index (PI) and 1D swell strain or swell pressure potentials of the tested soils. This confirms the myths in the PI-based swell characterization methods. Soil swell properties were observed to be dependent on the presence of clay minerals that predominantly attract and hold water molecules. Therefore, a deeper understanding of diffused double layer and its potential thicknesses was expected to provide deeper understanding of the soil swelling behaviour [24].

3.1 *Diffused-Double-Layer Swell Prediction Model*

The model is based on the double-layer water attraction capacity of individual clay minerals. Pedarla [17] used this concept to develop the diffused-double-layer swell prediction model (DDLSPM). The assumptions for the formulation and development of the DDLSPM were described in detail by Pedarla [17]. As discussed earlier, upon contact with moisture, the clay minerals in soils undergo expansion

Table 5 Soil characterization and mineralogy tests results

Soil	LL	PI	OMC	CEC	SSA	MM (%)	I (%)	K (%)	Classification
Anthem	48	27	18	118.5	71.7	25.3	24.5	50.8	CL
Burleson	55	37	19	132.4	100.1	33.8	19.6	46.6	CH
Cleburne	38	21	15	105.8	57.1	20.4	6.3	73.2	CL
Colorado	63	42	19	185.0	91.6	35.8	35.0	29.3	CH
Denton	55	30	19	156.5	41.2	20.4	8.7	71.0	CH
Grapevine	46	26	19	156.5	34.3	18.6	11.5	69.9	CL
Grayson	75	49	24	223.0	116.1	43.0	23.7	33.3	CH
Keller	25	11	14	115.0	60.0	22.0	18.3	59.7	CL
Mansfield	67	38	26	176.4	121.4	42.8	22.1	35.1	CH
Oklahoma	41	21	24	76.3	63.3	19.7	70.0	10.3	CL
Plano	24	12	27	229.3	54.4	29.6	37.7	32.7	CL
San Antonio	67	43	22	192.4	97.4	37.9	30.9	31.2	CH
San Diego	42	28	17	92.60	87.2	26.9	25.3	47.8	CL
Waco	58	34	28	250.1	126.7	50.1	18.8	31.2	CH

Table 6 Summary of the 1D swell strains and swell pressure test results at 95% MDUW

Soil	Notation	PI	1D swell strain (%)	Swell pressure (kPa)
Anthem	AN	27	4.5	94.2
Burleson	BU	37	5.8	112.8
Cleburne	CL	21	3.2	81.1
Colorado	CO	42	8.2	137.7
Denton	DE	30	1.5	65.3
Grapevine	GV	26	1.3	82.7
Grayson	GR	49	9.8	168.4
Keller	KE	11	5.6	98.0
Mansfield	MA	38	3.4	113.6
Oklahoma	OK	21	3.8	63.0
Plano	PL	12	4.7	116.5
San Antonio	SA	43	7.3	137.7
San Diego	SD	28	3.4	50.5
Waco	WA	34	2.2	79.9

with increase in their double-layer water thickness. Hence, the clay minerals are assumed to be stacked in a uniform chain pattern. The compacted soil specimen comprises of soil solids and voids. Among the soil solids, the clay portions contribute to the swelling behaviour. The determination of volume of clay minerals in a soil specimen was determined by dividing the clay portion. Once the number of mineral layer stacks for all three clay minerals are determined, the total

diffused-double-layer thickness or expansion or swell displacement for a given expansive soil is given by Eq. (3).

$$\text{TDDL} = \sum_{i=1}^n N_i \times \text{DDL}_i \quad (3)$$

where TDDL is the total diffused-double-layer-induced swell thickness or displacement, n is the number of clay minerals (i.e. 3) in the soil, N_i is the number of crystal layers pertaining to individual mineral, DDL_i is the diffused-double-layer thickness of an individual mineral. The value of TDDL represents the cumulative thicknesses of DDLs of all the three minerals, and this indirectly represents soil swelling without including internal crystalline swelling. Once the total diffused-double-layer thickness of the soil was determined, it was used to estimate the DDL-induced swell strains of the soil specimens, as noted in the following Eq. (4).

$$\varepsilon_{\text{DDL}}(\%) = \frac{\text{TDDL}}{h} \times 100 \quad (4)$$

where ε_{DDL} is the strain caused by the formation of diffused-double-layer thickness during saturation; and h is the initial specimen height. Table 7 shows the TDDL values and DDL swell strains for all fourteen expansive clays at 95% MDUW conditions. Table 7 presents the total double-layer water-induced strain by each of the soil specimens. The compacted soil specimen has an initial height of 2.54 cm. During the saturation phase of the specimen, the minerals attract the moisture molecules and form a diffused-double-layer water. The specimen strains are calculated based on the initial specimen height and the total double layer formed due to the mineral attraction forces between clay mineral and water molecules. It was evident that Grayson soil formed the largest double-layer water thickness.

Table 7 Swell strain estimated from DDLSPM at 95% MDUW condition

Soil	Notation	TDDL (m)	ε_{DDL} (%)
Anthem	AN	0.0427	168
Burleson	BU	0.0897	353
Cleburne	CL	0.0190	75
Colorado	CO	0.0849	334
Denton	DE	0.0285	112
Grapevine	GV	0.0300	118
Grayson	GR	0.1191	469
Keller	KE	0.0397	156
Mansfield	MA	0.0690	272
Oklahoma	OK	0.0350	138
Plano	PL	0.0493	194
San Antonio	SA	0.1009	397
San Diego	SD	0.0325	128
Waco	WA	0.0370	146

3.2 DDLSPM Correlation with Swell Properties

An attempt was made by Puppala et al. [24] to correlate DDLSPM-based swell strains with those measured from the swell tests. Correlations with the measured 1D swell strains of all soils are presented in Fig. 3a, which correspond to 95% MDUW condition. Figure 3b presents the correlations with measured swell pressure at 95% MDUW condition. From Fig. 3, it is evident that swell potential of a soil is directly proportional to its respective DDL thicknesses and strains. This confirms that the present DDLSPM approach is sound and shows a good correlation between them. The correlation trend in both figures shows a nonlinear trend between DDLSPM swell strains and measured swell characteristics, and hence, a nonlinear formulation is formulated and used in the present analysis. This formulation is presented in the following Eq. (5):

$$\varepsilon_i \text{ or SP} = a \times \varepsilon_{\text{DDL}}^b \quad (5)$$

where ε_i is the swell strain measured at initial compaction condition; SP is the swell pressure of an expansive clay; $\varepsilon_{\text{DDL}}^b$ is the diffused-double-layer-induced swell strain; and a and b are the formulation constants or correction factors. The constants a and b are dependent on many independent soil and test parameters like particle arrangement during compaction, moisture access to the clay particles and direction of particle swelling. a and b are not unique, and they are dependent on the swell property that is correlated with ε_{DDL} . These constants are regarded as potential indicators of the reduction factors of total DDL-based swell strains to measured corresponding swell characteristics. The trends in Fig. 3 show that swell strain and DDL strain show a certain degree of correlation between both parameters. This indicates that the potential use of the DDL theory and the DDL-based swell strain estimation could provide a more fundamental approach to estimate swell properties of compacted clayey soil specimens [24].

4 Resilient Modulus Measurements at High-Suction State

The design of pavement sections built over high-plasticity subgrade soils requires the knowledge of resilient modulus over a wide range of suction to consider the variations in resilient modulus with seasonal and diurnal variation of moisture. An experimental setup adept at performing suction-controlled repeated load triaxial (RLT) tests at high suction (5–600 MPa) has been developed by integrating an automated relative humidity apparatus within a cyclic triaxial setup. Previously, several researchers had examined the fundamental effects of matric suction (s) on M_R of various pavement materials [25–28]. However, most of these studies had been performed by indirectly measuring suction of tested soil specimens in post-test

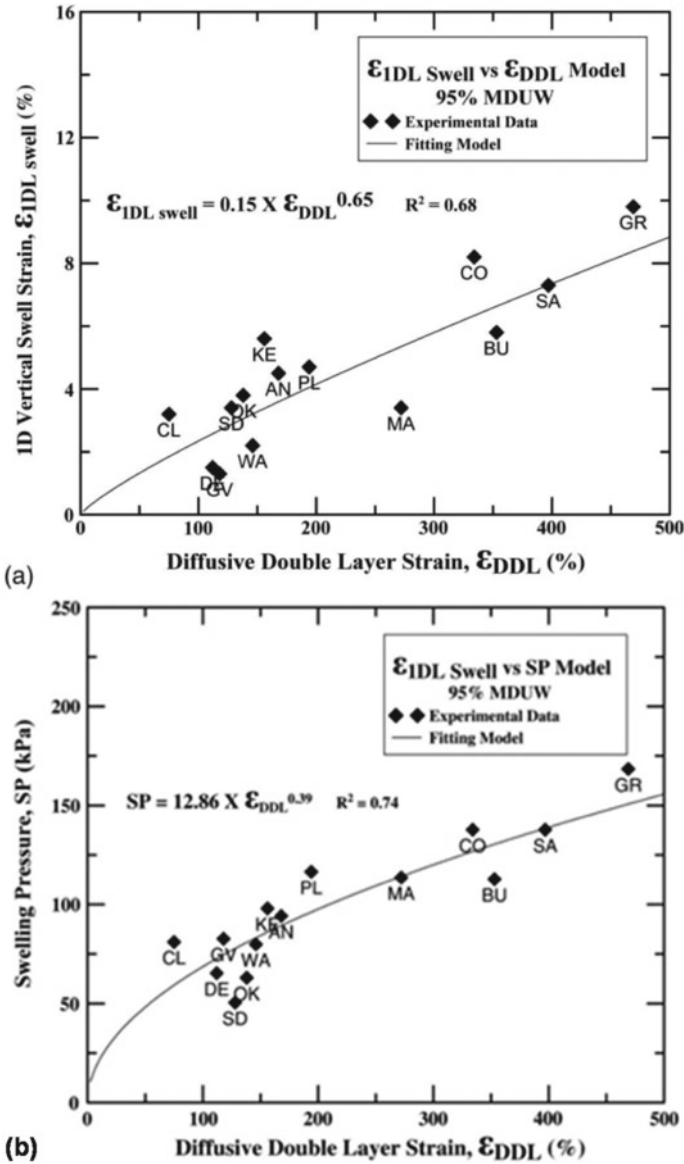


Fig. 3 DDL swell model for a 1D swell strains and b swell pressure at 95% MDUW

conditions by utilizing filter paper techniques, which have been reported to be quite user-dependent and unreliable [29]. In the past, only a limited number of studies have been conducted by performing tests under suction-controlled condition using the axis-translation technique, where low-to-moderate suction levels were

maintained throughout the specimen. However, due to the limitations of the axis-translation technique, which include limitations of ceramic disks and air diffusion, high values of suction cannot be applied, which hinders the applicability of such approaches for a different soil types, most notably fine-grained materials.

Other researchers had documented the performance issues for pavements constructed over high-plasticity expansive soils [30, 5, 3, 31]. In spite of the requirement of advanced setup which is capable of simulating the in situ conditions during extreme climatic conditions and determining the value of M_R in such conditions, such facilities are available [32, 33]. The characterization of expansive soil behaviour is particularly crucial at high values of suction beyond 1 MPa and up to 700 MPa [34]. During the dry season when there is high temperature and low moisture content for long durations high values of suction are induced, which may be well beyond the test range of the conventionally adopted axis-translation technique. To date, suction-controlled RLT tests have not been conducted at high-suction states, and corresponding influences of shrinkage and desiccation cracking on M_R have not been effectively analysed.

A novel testing setup has been developed by integrating a cyclic triaxial testing setup with an automated relative humidity system to conduct RLT tests at suction ranging from 5 to 100 MPa. Figure 4 shows the schematic layout of the RLT test setup. The details regarding the triaxial setup are provided by Banerjee and Puppala [35] and Banerjee et al. [36, 37]. The auto-RH apparatus used in study is capable of applying a constant relative humidity (RH) throughout the specimen gas phase, which induces total suction in the range of 5–600 MPa and beyond.

4.1 Auto-Relative Humidity Apparatus and Suction-Controlled RLT Testing

Vapour pressure control is used to induce high-suction states within the soil specimen. An automated relative humidity apparatus was utilized to induce high-suction states. A similar automated RH control unit was used by Likos and Lu [34] to determine total suction characteristic curves of non-expansive and expansive clays. The study by Banerjee et al. [38] demonstrated the first attempt to integrate an RLT test setup with the automated RH control unit. The auto-RH apparatus comprises of an auto-RH control unit, a desiccating chamber, a gas bubbler, and an RH and temperature probe, along with peripherals such as connecting pipes and read-outs. The aim of this apparatus is to supply a steady stream of moist air at the target RH to control the desired total suction within the soil specimen. Therefore, a steady stream of low-pressure humid air having the target RH is generated by mixing of water vapour saturated air (“wet”) and dry air in different proportions in an environmentally sealed mixing chamber. The details of the working principle are provided by Banerjee [39].

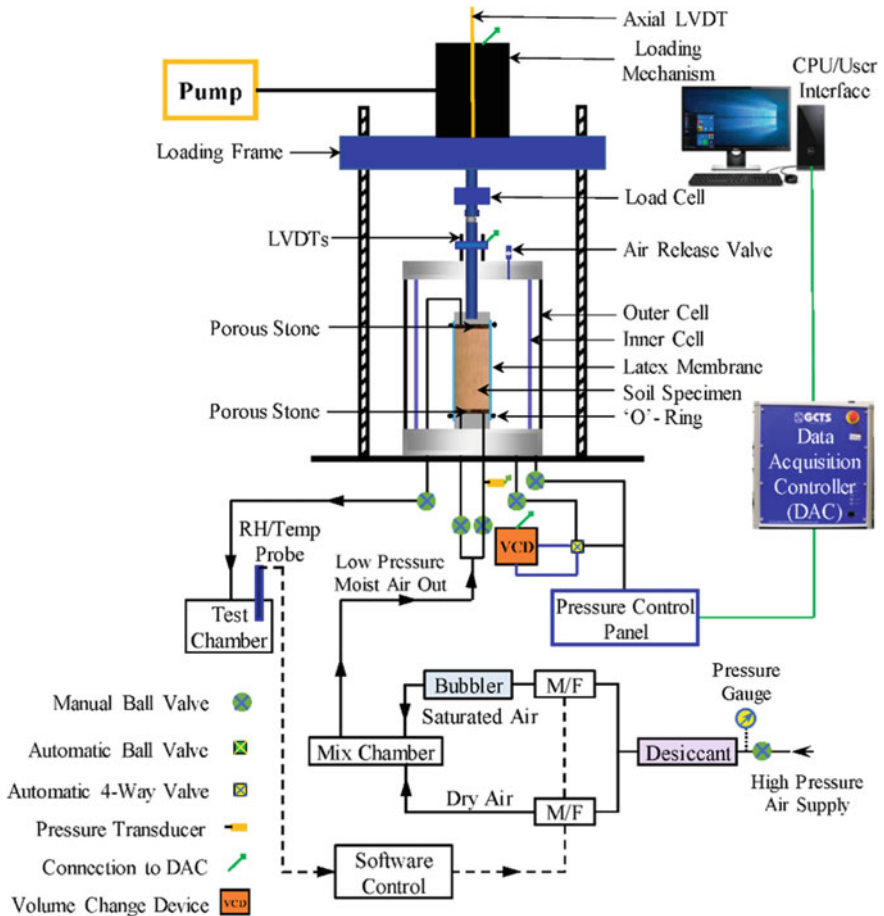


Fig. 4 Schematic layout of the setup for conducting suction-controlled RLT tests on soils under high total suction using auto-RH apparatus

After the pre-conditioning stage, wherein the sample is subjected to the target RH stream of air outside the triaxial cell, the soil specimen is removed and enclosed within the triaxial cell. Humid air at the required RH is routed through the base pedestal of the triaxial cell, which is fitted with a porous stone. The humid air is forced to pass through or around the specimen. The exhaust air from the soil sample is routed out of the triaxial cell via a porous stone housed within the top cap and a semi-rigid pipe to a small cylindrical test chamber. This chamber houses the humidity/temperature probe, which allows direct measurement of the RH and temperature of the exhaust air. The small cylindrical test chamber has a small opening to allow the exhaust air is gradually flow out, thereby providing a continuous flow of air through the system, for a quicker equilibration process.

The feedback from the RH/temperature probe allows the auto RH-control unit to automatically regulate the volumes of dry and wet air streams by using the mass-flow (M/F) valves. The signal from the RH/temperature probe is utilized to compute the induced total suction in the soil specimen which is determined using the Kelvin's equation (Eq. 6, Sposito [40]).

$$\psi = -\frac{RT}{v_{wo}\omega_v} \ln\left(\frac{u_v}{u_{vo}}\right) = -\frac{RT}{v_{wo}\omega_v} \ln(\text{RH}) \quad (6)$$

where ψ = total suction (kPa), T = absolute temperature (K), R = universal gas constant ($\text{J mol}^{-1} \text{K}^{-1}$), v_{wo} = specific volume of water (m^3/kg), ω_v = molecular mass of water vapour (kg/kmol), u_v = partial pressure of pore-water vapour (kPa), and u_{vo} = saturation pressure of pure water vapour (kPa).

In this study, an expansive clayey soil was used to illustrate the performance and utility of the novel integrated triaxial setup at performing the suction-controlled RLT tests at high-suction state. The expansive clayey soil is a mixture of a locally available sandy clay and commercially available sodium bentonite clay comprising the clay mineral montmorillonite. The clayey soil mixture is classified as high-plasticity clay (CH), according to the Unified Soil Classification System (USCS) with a plasticity index of 92%. The clayey soil (CH) specimens were compacted at target dry density of $1.47 \text{ g}/\text{cm}^3$ and moisture content of 24%.

A series of suction-controlled repeated load triaxial (RLT) tests were conducted on clayey soil specimens at high-suction state by Banerjee et al. [38]. Suction-controlled RLT tests were performed at different values of total suction. In order to avoid the influence of Soil Water Characteristic Curve (SWCC) hysteresis, all the soil specimens were prepared at a specific target density and water content and subsequently saturated and then air-dried by applying an alternating 12 h drying and suction equilibration cycles. The auto-RH apparatus was used to equilibrate the suction within the soil specimens, before the specimens were subjected to loading sequences of the RLT test. The equilibrated soil specimens were taken out from the acrylic chamber and were carefully transferred to the triaxial cell. A major advantage of suction control using vapour pressure technique is that since externally air pressure is not applied, net or effective confining pressure is same as the applied cell pressure. Thereby, the same confining pressure is applied by the pressure control panel as recommended by AASHTO T307 [41], which have been listed by Banerjee [39].

A series of suction-controlled RLT tests were conducted at different suction levels of 5, 30 and 100 MPa on soil specimens in suction-controlled conditions using an auto-RH apparatus. M_R was determined for each loading sequence as the average of M_R over the last five cycles (96th to 100th cycles). Figure 5 shows the variation of M_R with deviator stress and confining pressure for specimen subjected to 5 MPa total suction. Figure 5a depicts the variation of M_R with a change in values of cyclic deviator stress for different confining pressures at total suction of 5 MPa, whereas Fig. 5b shows the variation of M_R with a change in confining pressure for different values of cyclic deviator stress at total suction of 5 MPa.

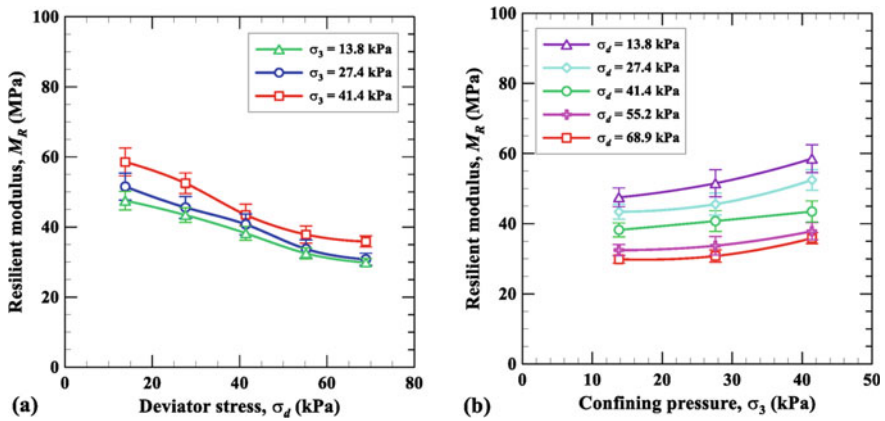


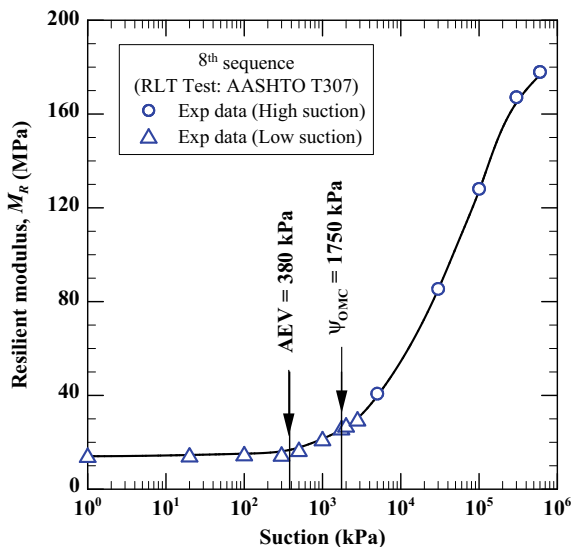
Fig. 5 Variation of M_R with **a** deviator stress and **b** confining pressure of clayey soil specimen at a total suction of 5 MPa

It was noted that the M_R decreased with an increase in the values of cyclic deviator stress for all confining pressure subjected to 5 MPa suction. Similar trends were observed at lower suction state by Ng et al. [25], Ruttanaporamakul et al. [26] and Banerjee [39].

The coefficients of variation (CV) for each sequence for 5, 10 and 30 MPa total suction values were computed. The maximum and average CV for all the suction levels was observed to be around 7.7% and 5.2%, respectively. Since typically these tests are expected to show poor repeatability such low values of CV are deemed to be acceptable.

The same RLT apparatus can be alternatively connected to system to control suction via axis-translation technique. This versatility helps in development of variation of M_R with suction over a wide range. Axis-translation technique may be used till a suction of 1.5 MPa and vapor pressure technique may be used for suction beyond 5 MPa. The gap between 1.5 MPa to 5 MPa may be filled by estimating the water content from the drying SWCC curve and performing an RLT test on an approximately suction-equilibrated soil specimen to determine its M_R value. The variation of M_R with suction for the clayey soil sample is shown in Fig. 6. In a semi-logarithmic scale, it follows a highly non-linear trend. The combination of data using axis-translation and vapor pressure techniques aid in the development of such a trend over wide range of suction values. It can be observed that initially the value of M_R is constant until the suction reaches near a state that lies between the air entry value (AEV) and the optimum moisture content (OMC) condition. Subsequent increase of suction results in a rapid increase in the effect of suction on the value of M_R until the residual state is reached where the influence of suction on M_R is negligible. The development of such a versatile apparatus will aid in the development of M_R —suction models and correlations account for wider range of suction.

Fig. 6 Variation of M_R over wide range of suction of clayey soil specimen



5 Summary and Conclusions

Several essential findings were obtained from the research studies conducted related to unsaturated and expansive soils. These findings have been discussed in this section.

Research into unsaturated soil has witnessed many advancements primarily due to the abilities to better understand micro- and chemico behaviours that can be linked with macro behaviours. In one of studies presented the Swell characterization studies of different clayey soils were conducted at different confining stress conditions. A new analysis method was utilized to determine the pore surface area of clayey particles in soils using MIP data. A new parameter termed as TSAR was defined. A semi-linear relationship between the TSAR value and the swelling behaviour was observed when compared to experimental test results. In future other soils need to be tested and the model presented needs to be validated in order to generalize the swell behaviour of clayey soils.

The development of a novel swell prediction model based on the diffused-double-layer (DDL) theory for expansive soils was also introduced. The model is based on the diffused-double-layer water induced soil swell theory which emphasizes on the attraction of water molecules adhering to the surface of the clay minerals thus resulting in the swelling of soil mass. DDL theory provides a strong foundation for the swell prediction model and shows a good fit of measured swell data for all the eight soils studied in the present research. Two correction factors or constants a and b are introduced in this model which governs the behaviour of the model. The constants available from this model are dependent on many independent parameters like particle arrangement during compaction, moisture access to the

clay particles and direction of particle swelling. The model was validated by comparing the predictions with the experimental soil swell test results. It was observed that some soils with high PI values experienced low swelling, whereas soils with low PIs, experienced higher swelling. This confirms the misconceptions in the PI-based swell characterization methods. In future, the correction factors a and b from DDL model may be standardized by comprehensively studying them at different compaction levels and moisture access theories for different soils.

A fully automated relative humidity apparatus was integrated with a cyclic triaxial setup to conduct repeated load triaxial tests under suction-controlled conditions to compute the M_R at high-suction state. The application of suction using vapour pressure technique and conducting RLT tests at high suction states is the novelty of the study. This integrated setup is applicable for various types of fine-grained soils at different degree of saturation. The results from the series of suction-controlled RLT tests at different high-suction conditions demonstrated the ability of the integrated setup to determine M_R values with high reliability, due to low values of CV. These results along with additional data from other experimental tests on expansive soils can be used for the development and calibration of elaborate prediction models for variation of M_R over wide range of suction for various types of silty and clayey soils, especially for expansive soils.

The advanced models and characterization methods would assist in better prediction of performance of essential civil infrastructures over varying diurnal and seasonal climatic and ground conditions. Thereby, increasing the confidence on the design developed and minimizing the maintenance required during its service life due to better designs.

Acknowledgements The experimental work described in this paper was part of various research projects funded by the National Science Foundation (NSF), including funding from Award # 1031214 (Program Director Dr. Richard J. Fragaszy), Major Research Instrumentation Program (Program Manager: Dr. Joanne D. Culbertson; Award # 1039956) and National Science Foundation Industry-University Cooperative Research Center (I/UCRC) program funded “Center for the Integration of Composites into Infrastructure (CICI)” site (NSF PD: Andre Marshall; Award # 1464489), and their support is gratefully acknowledged. Any findings, conclusions or recommendations expressed in this material are those of the authors and do not necessarily reflect the views of the National Science Foundation. We also acknowledge the support of Texas Department of Transportation’s Research and Technology Implementation (RTI) for their past funding.

References

1. Puppala, A.J., Cerato, A.: Heave distress problems in chemically-treated sulfate-laden materials. *Geo-Strata Am. Soc. Civil Eng.* **10**(2), 28–32 (2009)
2. Katti, R.K., Moza, K.K., Katti, D.R.: Unconventional behavior of expansive soils. In: *Proceedings of the 16th Budapest Conference on Soil Mechanics and Foundation Engineering*, pp. 137–146 (1984)
3. Puppala, A.J., Congress, S.S.C., Banerjee, A.: Research advancements in expansive soil characterization, stabilization and geoinfrastructure monitoring. In: Latha, G.M. (ed.) *Frontiers in Geotechnical Engineering*, pp. 15–29 (2019)

4. Jones, D.E., Holtz, W.G.: Expansive soils—the hidden disaster. In: Civil Engineering, American Society of Civil Engineers, New York, pp. 139–153 (1973)
5. Puppala, A.J., Manosuthkij, T., Nazarian, S., Hoyos, L.R.: Threshold moisture content and matric suction potentials in expansive clays prior to initiation of cracking in pavements. *Can. Geotech. J.* **48**(4), 519–531 (2011)
6. Banerjee, A., Patil, U.D., Puppala, A.J., Hoyos, L.R.: Suction-controlled repeated load triaxial test of subgrade soil at high suction states in unsaturated soils. In: Proceeding of Seventh International Conference on Unsaturated Soils, Hong Kong, pp. 667–672 (2018)
7. Lu, N., Likos, W.J.: Unsaturated soil mechanics. J. Wiley, Hoboken, N.J. (2004)
8. Puppala, A.J., Katha, B., Hoyos, L.R.: Volumetric shrinkage strain measurements in expansive soils using digital imaging technology. *Geotech. Test. J.* **27**(6), 547–556 (2004)
9. Chittoori, B.C.S., Puppala, A.J.: Quantitative estimation of clay mineralogy in fine-grained soils. *J. Geotech. Geoenviron. Eng.* 997–1008 (2011)
10. Puppala, A.J., Manosuthkij, T., Chittoori, B.C.S.: Swell and shrinkage characterizations of unsaturated expansive clays from Texas. *Eng. Geol.* **164**, 187–194 (2013)
11. Chakraborty, S., Nair, S.: Impact of curing time on moisture-induced damage in lime-treated soils. *Int. J. Pavement Eng.* **21**(2), 215–227 (2020)
12. Chakraborty, S., Nair, S.: Impact of different hydrated cementitious phases on moisture-induced damage in lime-stabilised subgrade soils. *Road Mater. Pavement Des.* **19**(6), 1389–1405 (2018)
13. He, S., Yu, X., Banerjee, A., Puppala, A.J.: Expansive soil treatment with ionic soil stabilizer. *Transp. Res. Record: J. Transp. Res. Board* (2018)
14. Pedarla, A., Puppala, A.J., Hoyos, L.R., Chittoori, B.: Evaluation of swell behavior of expansive clays from internal specific surface and pore size distribution. *J. Geotech. Geoenvironmental Eng.* **142**(2) (2016)
15. Carter, D.L., Mortland, M.M., Kemper, W.D.: Specific surface. In: Klute, A. (ed.) *Methods of Soil Analysis*, 2nd edn. ASA and SSSA, Madison, WI, pp. 413–423 (1986)
16. Cerato, A.B., Lutenegeger, A.J.: Determination of surface area of fine grained soils by the ethylene (EGME) method. *Geotech. Test. J.* **25**(3), 315–321 (2002)
17. Pedarla, A.: SWCC and clay mineralogy-based models for realistic simulation of swell behavior of expansive soils. Doctoral Dissertation, Department of Civil Engineering, University of Texas at Arlington, Arlington, Texas (2013)
18. Likos, W.J., Wayllace, A.: Porosity evolution of free and confined bentonites during interlayer hydration. *Clays Clay Miner.* **58**(3), 399–414 (2010)
19. Zhou, H., Fang, Y.-G., Gu, R.-G., Zeng, C.: Microscopic analysis of saturated soft clay in Pearl River Delta. *J. Cent. South Univ. Technol.* **18**(2), 504–510 (2011)
20. Cui, Z.D., Tang, Y.: Microstructures of different soil layers caused by the high-rise building group in Shanghai. *Environ. Earth Sci.* **63**(1), 109–119 (2011)
21. Mitchell, J.K., Soga, K.: *Fundamentals of Soil Behavior*, 3rd edn. Wiley, Hoboken, NJ (2005)
22. Chapman, L.A.: Contribution to the theory of electrocapillarity. *Philos. Mag.* **25**(148), 475–481 (1913)
23. Schanz, T., Tripathy, S.: Swelling pressure of a divalent-rich bentonite: Diffuse double-layer theory revisited. *Water Resour. Res.* **45**(5) (2009)
24. Puppala, A.J., Pedarla, A., Pino, A., Hoyos, L.R.: Diffused double-layer swell prediction model to better characterize natural expansive clays. *J. Eng. Mech.* **143**(9) (2017)
25. Ng, C.W.W., Zhou, C., Yuan, Q., Xu, J.: Resilient modulus of unsaturated subgrade soil: experimental and theoretical investigations. *Can. Geotech. J.* **50**(2), 223–232 (2013)
26. Ruttanaporamakul, P., Rout, R.K., Puppala, A.J., Pedarla, A.: Resilient behaviors of compacted and unsaturated subgrade materials. In: *Geo-Congress 2014 Technical Papers: Geo-Characterization and Modeling for Sustainability*, pp. 1396–1405 (2014)
27. Salour, F., Erlingsson, S.: Resilient modulus modelling of unsaturated subgrade soils: laboratory investigation of silty sand subgrade. *Road Mater. Pavement Des.* **16**(3), 553–568 (2015)

28. Han, Z., Vanapalli, S.K.: Relationship between resilient modulus and suction for compacted subgrade soils. *Eng. Geol.* **211**, 85–97 (2016)
29. Ng, C.W.W., Menzies, B.: *Advanced Unsaturated Soil Mechanics and Engineering*. CRC Press (2014)
30. Petry, T.M., Little, D.N.: Review of stabilization of clays and expansive soils in pavements and lightly loaded structures—history, practice, and future. *J. Mater. Civ. Eng.* **14**(6), 447–460 (2002)
31. Das, J.T., Banerjee, A., Puppala, A.J., Chakraborty, S.: Sustainability and resilience in pavement infrastructure: a unified assessment framework. *Environ. Geotech.* 1–13 (2009)
32. Puppala, A.J.: *Estimating Stiffness of Subgrade and Unbound Materials for Pavement Design*. NCHRP Synthesis 382, Transportation Research Board, Washington, DC (2008)
33. Salour, F., Erlingsson, S., Zapata, C.E.: Modelling resilient modulus seasonal variation of silty sand subgrade soils with matric suction control. *Can. Geotech. J.* **51**(12), 1413–1422 (2014)
34. Likos, W., Lu, N.: Automated humidity system for measuring total suction characteristics of clay. *Geotech. Test. J.* **26**(2) (2003)
35. Banerjee, A., Puppala, A.J.: Influence of rate of shearing on strength characteristics of saturated and unsaturated silty soil. In *Proceedings of the 50th Indian Geotechnical Conference*, Pune, India (2015)
36. Banerjee, A., Puppala, A.J., Congress, S.S.C., Chakraborty, S., Likos, W.J., Hoyos, L.R.: Variation of resilient modulus of subgrade soils over a wide range of suction states. *J. Geotech. Geoenviron. Eng.* **146**(9) (2020)
37. Banerjee, A., Puppala, A.J., and Hoyos, L.R.: Suction-controlled multistage triaxial testing on clayey silty soil. *Eng. Geol.* **265** (2020)
38. Banerjee, A., Puppala, A.J., Hoyos, L.R., Likos, W.J., Patil, U.D.: Resilient modulus of expansive soils at high suction using vapor pressure control. *Geotech. Test. J.* **43**(3), 720–736 (2020)
39. Banerjee, A.: *Response of Unsaturated Soils under Monotonic and Dynamic Loading over moderate Suction States*. Doctoral Dissertation, Department of Civil Engineering, University of Texas at Arlington, Arlington, Texas (2017)
40. Sposito, G.: *The thermodynamics of soil solutions*. Oxford University Press, New York (1981)
41. AASHTO. AASHTO T-307: *Determining the Resilient Modulus of Soils and Aggregate Materials*. American Association of State Highway and Transportation Officials, Washington, DC (2012)

Recent Advances on Dynamic Load Testing of Bored Piles and Other Cast-in-Situ Piles



E. Anna Sellountou and Brent Robinson

Abstract Dynamic testing was initially developed as a reliable way to estimate static capacity of driven piles in lieu of static tests that require significant time and money. However, principles of dynamic testing can be applied and have been successfully applied over the last 40 years in estimating static capacity of bored piles and other cast-in-situ piles. Challenges associated with bored piles, like knowing the as-built shape of the shaft or taking accurate force measurements in the top of the shaft, can be addressed by modern techniques and other recent technological advancements. The use of a force transducer at the top of the bored pile (or an instrumented hammer) can help with the collection of accurate force measurements especially on large diameter piles where excessive built-up or excavation would be required otherwise. The use of thermal wires or ultrasonic pulses type devices can address the unknown shape of boreholes. In this paper, advances in the dynamic load testing techniques as applied to bored piles and other cast-in-situ piles are presented.

Keywords Dynamic testing · Dynamic pile testing · Bored piles · Thermal integrity profiling

1 Introduction

Continuously increasing structural loads and increased demands on the performance of deep foundation elements have made load testing a necessity in today's construction world. Static load testing and dynamic load testing, or the combination of both, are the most common capacity verification methods. Whether we test for safety (allowable load verification) or for optimization of pile design (measuring the

E. Anna Sellountou · B. Robinson (✉)
Pile Dynamics, Inc., Cleveland, OH, USA
e-mail: BRobinson@pile.com

E. Anna Sellountou
e-mail: ASellountou@pile.com

ultimate geotechnical resistance), pile load testing has become crucial in today's practice. Improving and understanding static and dynamic testing, and understanding their differences and limitations become a necessity.

Dynamic load testing of deep foundations was introduced in the early 70s as a reliable way to estimate static capacity of driven piles in lieu of static tests that require significant time and money. More specifically, in 1964, a research project funded by the Ohio DOT, to develop new technologies of pile testing began at Case Western Reserve University in Cleveland, Ohio, that resulted in the Pile Driving Analyzer[®] (PDA), an electronic device that would display, for each hammer blow, the bearing capacity of a pile based on fundamental stress wave theory. After its first appearance in the early 70s, the PDA has changed the status quo of testing of driven piles. Today, dynamic testing is extensively and successfully used to test driven piles for capacity and integrity all around the world. The same principles are also applied to the testing of bored piles and other cast-in-situ piles. It is likely that most dynamic testing performed around the world today is performed on bored piles.

When applying dynamic load testing principles to bored piles, certain challenges like knowing the as-built shape of the shaft or taking accurate force measurements in the top of the shaft should be addressed. In order to address these challenges, testing agencies now use of a force transducer at the top of the bored pile or an instrumented hammer) to measure the impact force, embedded instrumentation to check resistance distribution and testing methods to determine shaft geometry. Moreover, testing recommendations specifically developed for bored piles or ACIP piles have been published [1, 2] as well as numerous case studies of dynamic testing on bored piles [3–6].

Top transducers speed up the testing procedure, especially on large diameter piles where excessive build-up or excavation would otherwise be required and collect of accurate force measurements can be challenging. Supplemental testing and analysis techniques such as the use of thermal wires or ultrasonic pulses type devices can address the unknown shape of boreholes and further improve load testing interpretation.

2 Load Transducers and Instrumented Hammers

Strain gauges are most commonly used during a dynamic load test event to determine the load applied at the top of the pile. Strain gauges obtain unit deformation readings that are multiplied by the area of the pile and its elastic modulus to yield the measured pile force. For a steel pile, the elastic modulus is well known, but for concrete piles the elastic modulus may vary from mix to mix. For driven concrete piles, the elastic modulus can be calculated based on two conditions: (a) the arrival time of the impact stress wave at the pile top after reflection at the pile toe and (b) the proportionality of strain and velocity during a short loading period with the wave speed being the proportionality factor. Calculating then the wave

speed from arrival time and/or proportionality yields the dynamic elastic modulus, E . However, for bored piles and other cast-in-situ piles obtaining a clear toe response may not be that simple due to the potentially high levels of side friction in the soil or rock socket. Assuming a wave speed value or calculating it based on concrete strength and/or age is not sufficiently accurate. Using a top load transducer or instrumented ram avoids the use of a concrete elastic modulus for pile top force determination. The force calculated from the steel top transducer is also the force applied to concrete pile top. Therefore, a transducer minimizes the effect of an inaccurate wave speed assessment on the dynamic test results and reduces the force calculation inaccuracy.

Another advantage of using a top transducer or instrumented ram is the elimination of pile top extension or the excavation around the pile top. Sensor attachment is recommended to 1.5 diameters or more below the top of the pile to minimize bending and end effects. On-site preparations to attach strain gages to a smooth surface are also eliminated. The placement of the accelerometers that measure the motion of the pile only need to be placed a few inches from the pile top and are much less sensitive to local concrete quality and surface properties compare to strain gauges. It is recommended to place the main cushioning on top of the transducer and a very thin cushion below the transducer to avoid stress concentrations due to unevenness of the pile top surface. Small differences between the force measured in the transducer or from the instrumented ram and the force measured from pile top instrumented with strain can be accounted for by acceleration measurements on the transducer. A thin shell pile build-up is recommended for the pile top to confine the concrete during the high loads that will be applied on the pile.

Pile top transducers are generally fabricated from thick-walled, high-strength steel pipe sections, designed to withstand the given maximum impact force required to mobilize a given resistance. To minimize the effect of deformations during the impact, eight strain sensors are monitored at orthogonal measurement points inside and outside the pipe. The signals from the eight sensors are reviewed by the testing engineer and averaged to determine the pile top force. Thick steel plates are attached to the top and bottom of the transducer to distribute the impact force over the pile top and minimize the effects of eccentric impacts by the ram. If necessary, additional, larger diameter steel plates can be reduce local pile top stresses due to significantly different transducer and pipe diameters. Figure 1 shows an example of a top transducer prior to attachment of external strain sensors and placement on to the pile top for testing. The pipe is 400 mm in diameter with a 37.5 mm wall thickness; the circular top plates are 600 mm in diameter.

As described in Robinson et al. [3], pile top force can also be calculated by instrumenting a single mass drop weight with accelerometers. The accelerometers measure the ram's deceleration, which when multiplied by the ram's mass yields the force applied to the pile top. Assuming the ram's area is sufficiently similar to the pile top area, additional load distributing plates or helmets are also unnecessary. This system requires some low pass filtering to remove potential stress wave effects developed inside the ram. Figure 2 shows a 7 ton ram instrumented with accelerometers, just prior to loading a pile top.

Fig. 1 A 13.5 MN top transducer



Fig. 2 A drop weight instrumented with accelerometers



3 Embedded Instrumentation

The signal matching program CAPWAP®, which was developed at Case Western Reserve University [7], is used to analyse PDA testing datasets in order to estimate the total pile capacity, as well as the side friction distribution and end bearing, and to identify additional dynamic and static resistance parameters such as soil damping and soil stiffness. The calculated resistance distribution (percentage of shaft resistance versus end bearing) depends on a good estimate of the overall wave speed in the pile. So although the pile top force can be correctly measured by the top

transducer without reliance on an assumed pile top wave speed, the overall wave speed is an important dynamic quantity. If a clear toe response is observed from the measurements, the wave speed is readily known. In the absence of a clear toe response, the use of embedded instrumentation, particularly near the pile toe, yields an accurate wave speed.

Embedding instrumentation in bored piles of other cast-in-situ piles can be done by attachment of resistance strain gauges to either a centre bar or reinforcement cage using instrumented sister bars. With known distance between the top of the piles and the sensors and time between impact and wave speed arrival at the sensors determined from the measurements, the wave speed of concrete can be calculated. A correct wave speed interpretation improves not only the estimates of side friction distribution, but also the pile and soil resistance stiffness. This is important when calculating the simulated static load–displacement curve from the dynamic test results. With today’s multichannel data acquisition systems and declining cost of embedded instrumentation, these improvements in measurement and analysis procedures become feasible and cost effective and therefore can become standard practice.

Signal matching allows for estimating the forces at different pile elevations, even without measuring the forces at points below the pile top. Changes in the pile section area and uncertain local elastic modulus values may generate errors in estimated pile forces, limitations similar to those known for embedded static pile instrumentation. Modern techniques like ultrasonic pulse-type devices or thermal integrity profiling (TIP) help access the shape of the borehole or the shape of the finished pile, respectively, greatly improving this way the signal matching modelling process and results. Knowing the pile shape during signal matching analysis will considerably improve the estimated skin friction distribution, localized embedded forces, etc. Alvarez et al. [8] describe the use of strain gauges and accelerometers installed near the pile toe to improve side friction estimations.

4 Recommendations on Drop Weight, Cushion Selection and Permanent Pile Displacement When Testing Bored Piles and Other Cast-in-Situ Piles

Robinson et al. [3] present general recommendations to be used for bored piles regarding ram weight, W_r . The ram weight must be chosen depending on the magnitude of the required pile bearing capacity, Q , as shown below:

$W_r/Q \geq 1\%$ for piles embedded in hard cohesive soils or bearing on rock

$W_r/Q \geq 1.5\%$ for friction piles in general

$W_r/Q \geq 2\%$ for bored piles with end bearing in coarse-grained soils

Larger drop weights with smaller drop heights are generally preferred over smaller drop weights with higher strokes. Larger weights have the advantage of wide pulses and therefore lower compression and tension stresses in the piles for a

similar applied energy. Stresses should not exceed the allowable values during a dynamic test. In the case of higher than the allowable stress generation, more cushioning must be used in order to reduce the magnitude of force versus time. Cushions, placed on top of the transducer, are normally made of plywood. A minimum thickness of 40 mm (1.5 in.) is advisable, but thicker cushions are sometimes needed to reduce stresses. Heavy cushioning is a disadvantage for signal matching analysis due to the wider pulses described above. Less cushioning generates a sharper response which helps determine a more accurate skin friction distribution. Total capacity prediction will not be affected as long as sufficient displacement occurs.

AASHTO [9] recommendations for regularly reinforced precast concrete piles should be followed for the calculation of allowable compression and tension stresses. More specifically, compression stresses should be less than 85% of the concrete compressive strength, f'_c . Tension stresses should be less than 70% of the steel yield strength, f_y , times the degree of reinforcement (reinforcement cross sectional area divided by pile cross-sectional area).

Wave equation analyses can be used to select the drop heights and cushioning based on the available drop weight, allowable dynamic stresses and required capacity.

Dynamic load testing in bored piles and other cast-in-situ piles are typically performed by applying few hammer drops with increasingly larger stroke until a cumulative displacement greater than or equal to the toe diameter, D , divided by 60 has been achieved [10]. When pile toe is tipped into sand layers where higher end-bearing activation is desired, larger cumulative sets may be necessary. In the presence of plastic clay formations at the pile toe, high displacements could generate undesired dynamic resistance effects creating a potential for overestimation of the static pile resistance. In this case, sets per blow not exceeding $D/90$ are recommended.

5 Shaft Geometry Evaluation

A major challenge associated with evaluating load tests of bored piles and other cast-in-situ elements is the lack of ability to inspect them prior, during and after the casting process and to confirm the as-built geometry of the finished product. Knowing the geometry of the finished pile makes dynamic testing data processing easier and more accurate. Traditional techniques such as concrete volume records combined with modern and more powerful techniques that are now available such as thermal integrity profiling (TIP) and electronic callipers allow the determination of the excavated shape and as-built cross-sectional area of the finished pile.

TIP uses the hydration temperature of the shaft concrete during the hydration of the cement to assess the geometry of the shaft. Thermal wires (equipped with thermal sensors evenly spaced approximately every 300–500 mm) are attached to the reinforcing cage prior to casting the shaft and collect temperature data during the curing process of the shaft concrete. Based on the heat signatures, a profile of the as-built pile shape can be generated by TIP, as shown in Fig. 3.

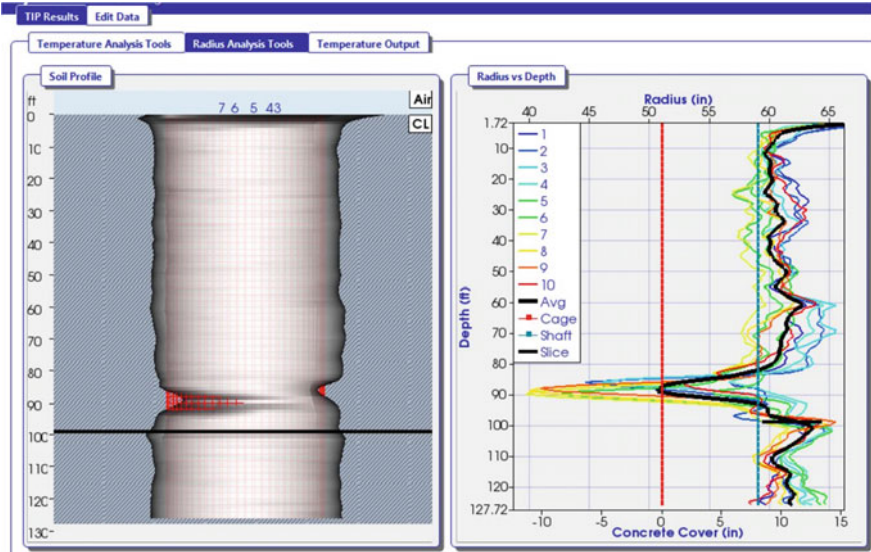


Fig. 3 TIP radius results and 3-D model from a pile with an inclusion

Electronic callipers of ultrasonic signals are often utilized to determine the excavated borehole shape and verticality, in the wet cast installations. Electronic callipers measure the radius with depth using ultrasonic pulses. One or more transmitters or transceivers send signal through a foundation excavation filled with water or slurry. A receiver records the timing of the signal’s reflection off the sidewall or casing. These measurements are repeated as the device is lowered or

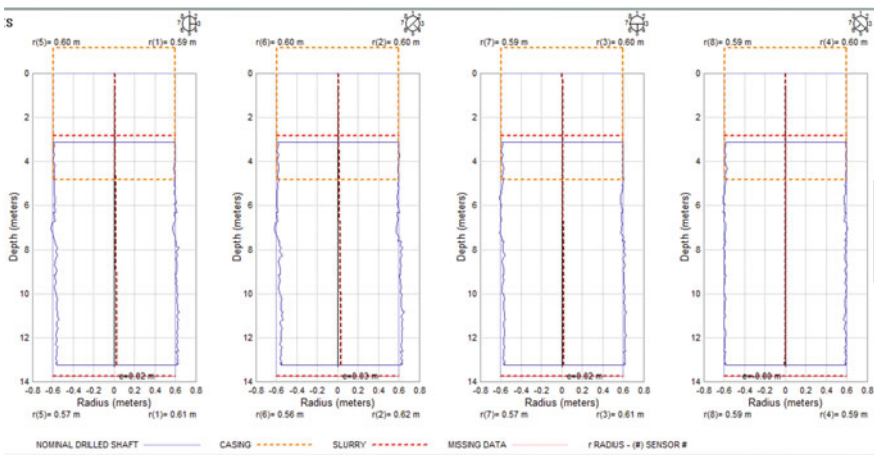


Fig. 4 Electronic calliper data for a uniform shaft

raised in the excavation, and the distance is calculated by initial or continuous calibration of the wave speed in the drilling fluid. An example is shown for a uniform shaft in Fig. 4. This type of data can also be used to obtain information about the pile shape that helps the processing and analysis of dynamic testing data.

References

1. Vaidya, R., Likins, G.: Guidelines for successful high strain dynamic load tests & low strain integrity tests for bored piles. In: Proceedings of the Indian Geotechnical Conference. Kakinada, India (2014)
2. Alvarez, C., Sellountou, A., Rausche, F.: State of the art dynamic load testing of ACIP piles in the Americas. In: 10th International Conference on Stress Wave Theory and Testing of Deep Foundations, San Diego (2018)
3. Robinson, B., Rausche, F., Likins, G., Ealy, C.: Dynamic load testing of drilled shafts at national geotechnical experimentation sites. In: O'Neill, M., Townsend, F. (eds) An International Perspective on Theory, Design, Construction and Performance, Geotechnical Special Publication, American Society of Civil Engineers, vol. 116, Orlando (2002)
4. Conroy, R., Mondello, B., Hussein, M., Gissal, R.: Drilled shafts load testing; made easy and inexpensive. *Foundation Drilling Magazine*, pp. 53–57, June/July (2010)
5. Beim, J., de Gracia, C.: Dynamic pile testing of three drilled shafts on the bridge over the Changuinola River in Panama. In: Iskander, M.I., Laefer, D.F., Hussein, M.H. (eds.) Contemporary Topics in Deep Foundations, Selected Papers from the 2009 International Foundation Congress and Equipment Expo, Geotechnical Special Publication, American Society of Civil Engineers, vol. 185, pp. 607–614, Orlando (2009)
6. Hussein, M., Bullock, P., Rausche, F., McGillivray, R.: Large-scale dynamic high-strain load testing of a bridge pier foundations. In: 8th International Conference on the Application of Stress-Wave Theory to Piles, pp. 371–377, Lisbon (2008)
7. Goble, G.G., Rausche, F., Likins, G.E.: The analysis of pile driving—a state of the art. In: International Seminar on Stress Wave Theory on Piles, pp. 131–161. Stockholm, Sweden (1980)
8. Alvarez, C., Zuckerman, B., Lemke, J.: Dynamic pile analysis using CAPWAP and multiple sensors. In: GEO Congress, ASCE, Atlanta, Georgia (2006)
9. AASHTO: LRFD Bridge Design Specifications, 4th edn. American Association of State Highway and Transportation Officials, Washington, DC (2006)
10. Rausche, F., Likins, G.E., Hussein, M.H.: Analysis of post-installation dynamic load test data for capacity evaluation of deep foundations. In: Laier, J.E., Crapps, D.K., Hussein, M.H. (eds.) From Research to Practice in Geotechnical Engineering, Geotechnical Special Publication, American Society of Civil Engineers, vol. 180, pp. 312–330. Reston, Virginia (2008)

Recent Advances in Geotechnical Infrastructure



Bindumadhava Aery

Abstract Recent developments in geotechnical engineering are increasing steadily commensurate with development in digital engineering along with advancement in construction equipment. This paper presents recent advancements in three-dimensional geological models and its benefits to infrastructure projects with case histories. Three-dimensional geological models are increasingly being used to characterize the world of ground engineering. Soil, rock, geological structures such as faults, rock fall zones and slips are often best examined in 3D. In addition, geomorphology of materials above, below or surrounding project sites must be well understood by design and construction teams to optimize both safety and costs. This is especially true for large, complex or unsafe sites or for forensic investigations in both terrestrial and offshore settings. 3D geological models are more suitable for large projects or projects that have potentially complex ground or hazardous site conditions.

Keywords Infrastructure projects · 3D geotechnical models · Digital geotechnics · Photogrammetry · Laser Scan

1 Introduction

Recent advances in digital devices, which are easily available like digital camera, drone, smart phones, tablets and apps, have changed data collection system. This transformation in collection and recording of field data considered to be this decade advancement. In exploring the possibilities for the use of digital tools, it has been found that there are several areas where they may be applied in geotechnical engineering. Traditionally, geotechnical data collection is done by hand, which is both time-consuming and expensive. Digital techniques may offer improvements in efficiency and quality. Ranging from the use of tablets and web-based applications

B. Aery (✉)
Aurecon, Brisbane, QLD, Australia
e-mail: Bindumadhava.Aery@AureconGroup.com

for slope assessments, to the use of virtual reality to view site survey information in 3D, these digital tools are both practically useful and exciting. Digital geotechnics is developing rapidly in many different applications and forms. Much of the development appears to be heading towards a virtual reality (VR) output or end use. Recently, Rose et al. [1] and Ross et al. [2] demonstrated benefits of geotechnics for infrastructure projects. This paper presents benefits of three-dimensional geotechnical model and slope assessment using digital technology.

2 Three-Dimensional Geotechnical Model: Benefits

Generally, most of infrastructure projects can be enhanced using three-dimensional (3D) geotechnics, not all are suitable and may not require use of this technology. Rose et al. [1] provided a guide to assist where and when these applications may be best used:

- where sites contain geological complexity that cannot be adequately represented on 2D sections,
- specific areas where complexity and risk are high, however geological processes must be recognized and understood,
- on forensic projects where a tight drilling pattern is needed to help identify issues,
- there is sufficient drilling density and other data (seismic, topographical, etc.) to build a meaningful model,
- the effects of geomorphology and depositional patterns if recent depositional processes need to be well defined,
- projects where the works methodology will vary with the ground conditions such as dredging in mainly soft ground with potential for the presence of hard rock or dense materials such as gravels.

3D geotechnical model is not suitable/not necessary for following cases:

- where sites are geologically simple, i.e. contain a single uniform layer,
- specific areas where complexity and risk are low and ground conditions very well understood,
- when there is insufficient drilling density and other data (seismic, topographical, etc.) to build a meaningful model,
- in projects that may be faulted or contain slip surface and there is not a good understanding of the geological processes involved,
- projects where the works are not sensitive to the ground conditions.

3 3D Models

3D geological model can be generated using conventional investigation data (exploratory boreholes/CPT/seismic survey) or data collected using photogrammetry and laser scan models. Following paragraphs illustrated each type with a case history.

3.1 *Photogrammetry and Laser Scan*

With the increasing availability of affordable Unmanned Aerial Vehicles (UAV/drones) on the market, there is a huge opportunity to use them for engineering projects. Drones can be used to “visit” places otherwise not easily accessible or inherently unsafe on foot and can in many cases be used to undertake inspections of cliff faces without the need for scaffolding or roped access. The key limitation being that one can only see the rock without being able to touch it, but often this may not be that important. Photogrammetry techniques enable accurate 3D digital models to be developed from the photographs taken from UAVs. The process uses readily available commercial software, and when combined with traditional survey or laser scanning data, the models can be just as accurate as traditional survey techniques but with far more detailed coverage; see Fig. 1.

The major limitation of photogrammetry for use in slope stability applications is vegetation; however, with the increasing ability of artificial intelligence, already

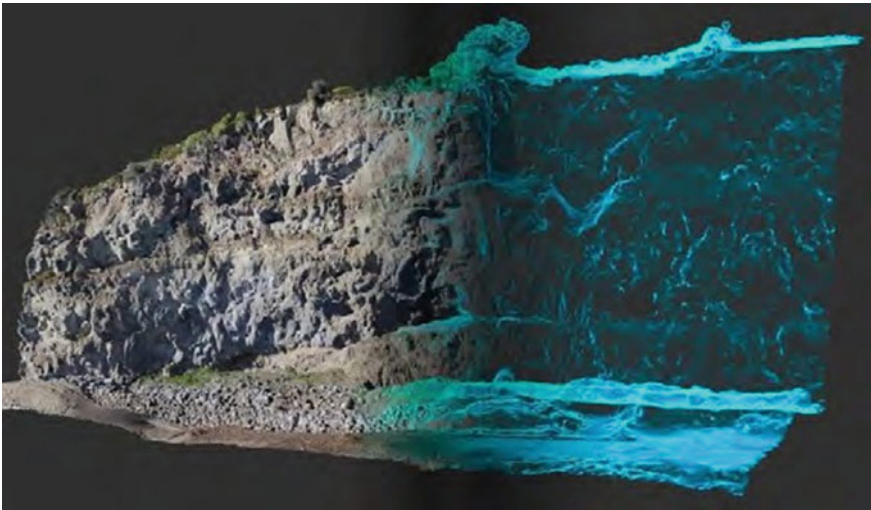


Fig. 1 Combined photogrammetry and laser scan model (left) transitioning to the laser scan model only (right) (after Rose et al. [1])

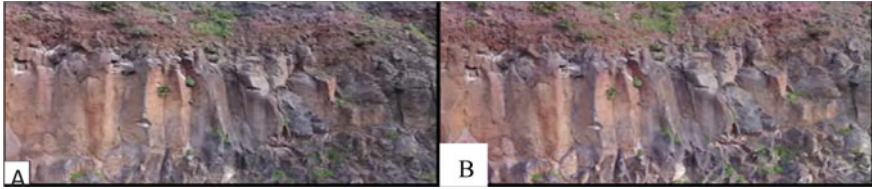


Fig. 2 Comparison of a real photograph (a) and a screenshot of photogrammetry model (b) (after Rose et al. [1])

standard photogrammetry software is including tools to automatically identify isolated objects within the models to aid in “cleaning-up” models. For slopes with limited vegetation however, the quality of the data is nearly indistinguishable from a real image of the site (Fig. 2). Models comprise a point cloud where each point has its own x -, y - and z -coordinate. Recent models have a point every 3 mm across a site that is hundreds of metres in size. This level of detail is often unnecessary for some applications; however for engineering geological applications, the data can be incredibly valuable.

Currently, slope stability models are typically undertaken on an assumed profile, or perhaps a detailed cross section may comprise a surveyed point every 500 mm, but this is only undertaken by providing the surveyors with a specified line to measure. If a more critical section is discovered later, then ideally the survey crew should be sent out to site again to measure the new section. A photogrammetry or laser scan model negates this requirement, providing an accurate model across the entire site and if a new cross section is required, then it is a case of simply extracting the data from the 3D model. This technique has been used to extract very accurate cross sections of a cliff on which to then run 2D rockfall analyses.



Fig. 3 2D rockfall analysis undertaken on cross section re-imported back into the 3D (after Rose et al. 2008)

The results of the 2D analyses can then be brought back into the 3D environment. An example of this is presented in Fig. 3; the rockfall modelling was used to manage health and safety on a seismically active site in Christchurch, New Zealand.

4 Westgate Tunnel Project, Melbourne, Australia

This is another case history of 3D geotechnical modelling to resolve tunnelling project as presented by Rose et al. [1]. The West Gate Tunnel Project comprises 2.8 and 4 km tunnels beneath Yarraville in Melbourne. The complex geology encountered within the tunnel alignment includes existing fill embankments, Holocene soft clays, Quaternary alluvium and infilled palaeochannels, high strength basalt of the Newer Volcanics, Tertiary clays and sands of the Brighton Group and Newport Formation, deeply weathered basalt of the Older Volcanics and underlying Tertiary clays and lignite of the Werribee Formation, often appearing as interflow deposits within the Older Volcanics.

During the development of engineering solutions, two key features of the 3D geological model became apparent; the infilled palaeochannel beneath the existing freeway near the inbound south portal and the weathering profiles within the Older Volcanics.

The Stony Creek palaeochannel is infilled with Holocene soft clays and is overlain and partially displaced by predominantly coarse, granular fill (gravels and cobbles) placed around 50 years ago as part of the construction of overpass embankments for the West Gate Freeway. The development of the 3D model for the infilled palaeochannel used a combination of the available borehole information (four sections containing moderately spaced boreholes across the palaeochannel), historic aerial photographs of the former creek and drawings for the construction works as there was, quite reasonably, insufficient investigation information to fully delineate the palaeochannel based on interpolation from boreholes alone. Sections cut at 40 m centres along the 400 m length of palaeochannel were used to develop the 3D geometry of the palaeochannel around the bends of the former creek alignment.

The 3D geological modelling (Fig. 4) of the weathering within the Older Volcanics presented a different challenge in that the variably weathered material may range from a residual soil to an extremely high-strength, fresh basalt over short distances. The uncertainty and ambiguity associated with modelling non-continuous, variable surfaces between sparse borehole information along the tunnel alignment and extrapolation of this away from the tunnel alignment can become difficult to represent in a 3D model.

A beneficial outcome that was observed during the modelling is that the development of the model strongly encouraged 3D thinking based on ‘Geo-logic’ and clearly identified gaps in the available information and understanding.

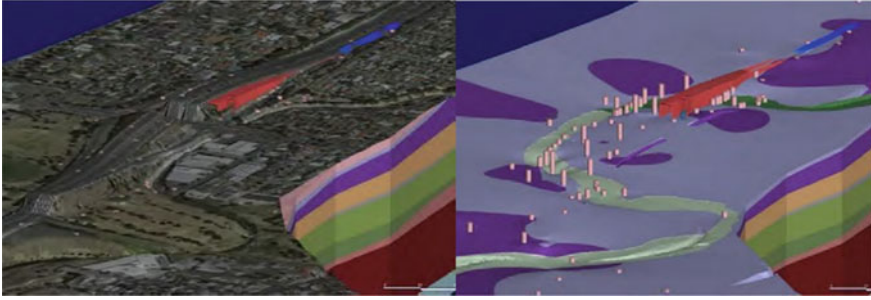


Fig. 4 Development of 3D geological model for Stoney Creek palaeochannel (after Rose et al. [1])

5 Slope Assessment Using Digital Technology

Aurecon South Africa (Pty) Ltd has demonstrated (Ross et al. [2]) use of web-based app to assess the hundreds of slope for South African National Roads Agency SOC Ltd (SANRAL). This includes the visual assessment of all high cuts and fills along the national and some regional routes in the Western, Northern and Eastern Cape Provinces of South Africa; a total of more than 4500 slopes—a monumental task. Figure 5 illustrates a typical rock cut assessed.



Fig. 5 Rock cuttings at Ecça Pass, located on the R67 north of Grahamstown, Eastern Cape, South Africa, were assessed using the Aurecon Field Force App (after Ross et al. [2])

The SANRAL Slope Management System was used to assess the slopes and is based on work done by Hall and Knottenbelt (1992), and later further refined by SANRAL. This rating system is summarized in a form which is completed following a visual inspection of each slope. The assessment requires assessing various aspects of the slope including slope height, slope angle, geology, drainage, signs of distress, record of past incidents and anticipated stability measures. GPS location and road chainage are recorded, and photographs are taken. General notes and observations are also recorded. The main objective of the rating system is to identify potentially problematic slopes, for which remedial measures may be designed and implemented.

Prior to the advent of smart devices and web applications this work would have involved vast amounts of paper work, manual input of data and long lead times before any information would be available for review. One can only imagine the reams of paper required to produce some 4500+ individual slope inspection reports. Although not new technology, an inhouse web-based application called the *Aurecon Field Force App* was developed to not only speed up the process, but also to save a lot of paper.

The *Aurecon Field Force App* allows the user to input the slope assessment data, as required by the rating system, into a tablet or smart phone on site, digitizing the data from the onset and avoiding manual data entry later. The application allows data entry in the form of simple drop-down menus to select ratings, and the built-in formulas immediately calculate the final rating of a slope. As a secondary function, the *Aurecon Field Force App* also allows the user to record a voice note with more detail, which could be used as a tool to relay unofficial but valuable information for a slope. Photographs are taken in the application, and the GPS location is recorded by the click of a button. A naming convention based on the road name, section and chainage was proved convenient.

The slope angle and height of the slope were estimated more accurately using a secondary application which utilizes the angle of the mobile phone or tablet camera to the horizontal. Traditionally, a slope would have to be surveyed to determine its height, but, by using the mobile device camera's focal length and measured angles, the height of a slope can be estimated less subjectively. This was an important facet of the project as only slopes with heights more than 5 m were to be assessed.

Once all the data is entered into the *Aurecon Field Force App* and the inspector is satisfied, the assessment can be uploaded. This can be done via cellular data or, in remote areas where cellular reception issues are encountered, the day's assessments can be uploaded over Wi-Fi later. All assessments are stored on the mobile phone or tablet's memory. The Aurecon Field Force App input screens are shown in Fig. 2. As part of the assessment the user inputs values for slope height, slope angle, surface water drainage, slope length, geology, seepage debris and history of incidents, which are as per the SANRAL risk rating methodology.

When accessing the application from a web browser, in the office, the map view gives the user an overview of the reviewed slopes which are colour coded according to their ratings. Green indicates a stable slope, orange minor problems, red major problems and black indicates an unstable slope. Filtering and sorting of potentially

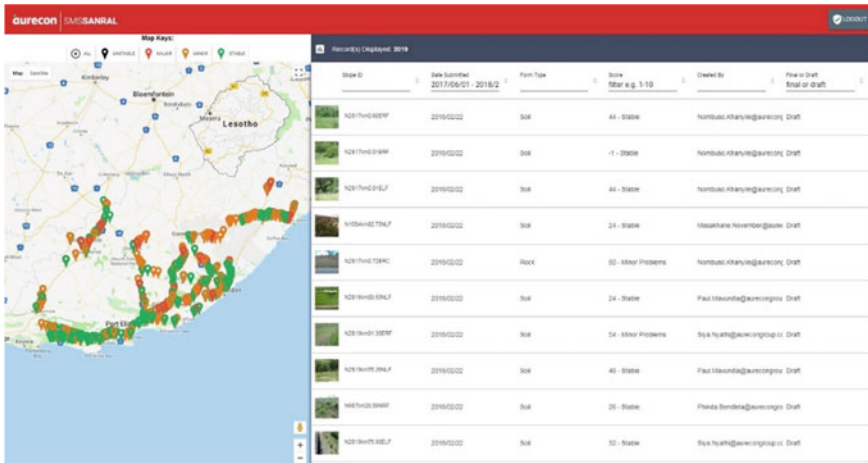


Fig. 6 Screenshot of *Client Viewer* (after Ross et al. [2])

problematic slopes and displaying them spatially on a map allows the user to plan mitigative works more efficiently. In addition, the user can easily filter the data enabling them to view specific routes or sections.

Once approved, the individual reports are generated and exported to PDF by the click of a button. Data can also be exported in Microsoft Excel format for further manipulation and statistical analysis. Other benefits include the ability to track the progress of the work as multiple teams are uploading inspection reports and a *Client Viewer* that allows the client, or other external parties, to see the progress of the work in the field. Data is reviewed and accepted internally before being displayed in the *Client Viewer* (Fig. 6).

6 Conclusions

Designing and presenting in three dimensions using 3D geological models are becoming common practice. This powerful tool allows designers, stakeholders and clients to see ‘The same thing’ in terms of geological and engineering complexity below the ground prior to design and construction.

The modelling process can also play a part in guiding where data in the form of boreholes, mapping, etc., is targeted. In order to achieve the best outcome in terms of a 3D geological model, usefulness users might consider the following process which is similar to the Baynes et al. (2005) discussion and the C25 model proposed by Parry et al. [3]. This is essentially a three-staged process with hold points for review and is also potentially iterative by returning to the conceptual model phase (Fig. 7). Conceptual (Stage 1) and Observational (Stage 2) stages are where the geologist/engineering geologist, assisted by the engineer is seeking out “truth in

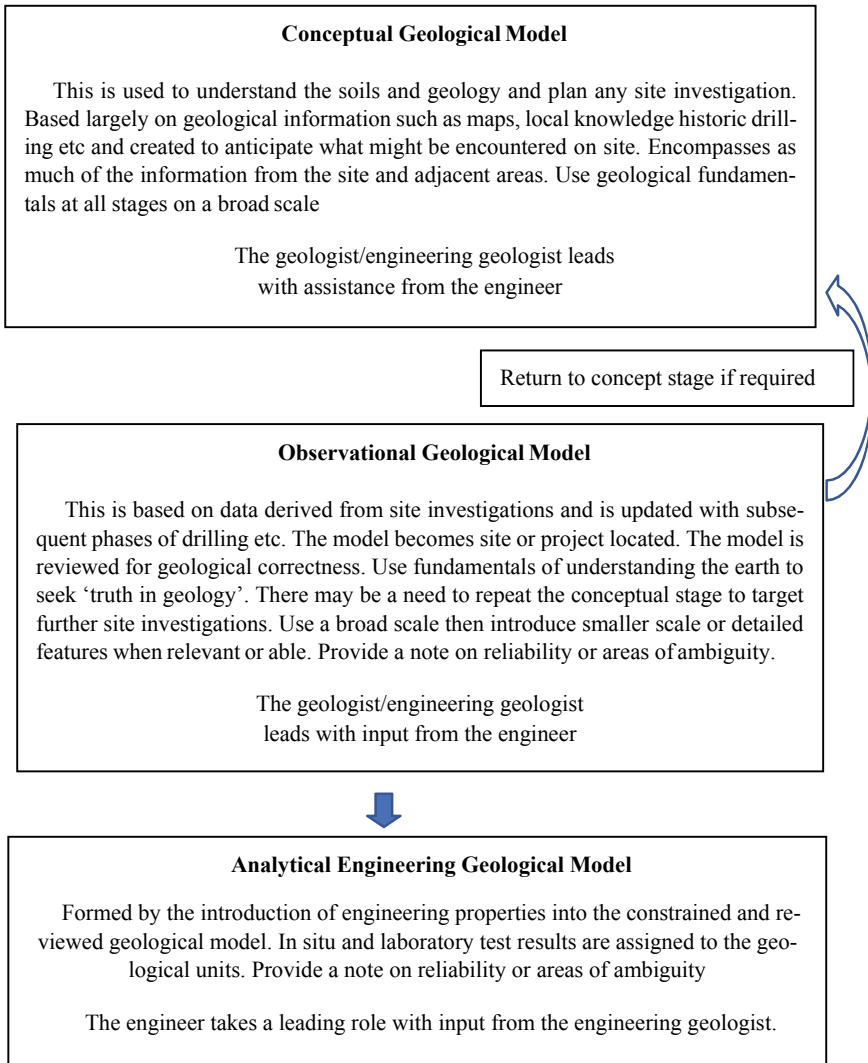


Fig. 7 Suggested geological modelling process (after Parry et al. [3])

geology and geomorphology” or at least the closest possible approximation of the facts. The third stage (Analytical) is where the engineer takes a leading role and is assisted by the geologist/engineering geologist following the introduction of engineering parameters into the model for design and construction purposes.

The effective use of a web-based application to facilitate data entry, review, management and storage of data associated with the visual assessment of a large number of cut slopes and fills has significantly improved the efficiency of the work and increased the quality of the output generated. Now that the visual assessment is

complete the application serves as a database and can be maintained for future work. This shows that geotechnical engineering is not unaffected by the digital advances around us.

Acknowledgements Author would like to thank Aurecon to provide me an opportunity to share their work and Graham Rose and Drian Ross, and lead authors paper for their permission to reproduce their work.

References

1. Rose, G., Kirk, P., Gibbons, C., Lander, A.: Three dimensional geological models in ground engineering: when to use, how to build and review, benefits and potential pitfalls. *Aust. Geomech.* **53**(3), 79–88 (2018)
2. Ross, D., Kruger, D., Damhuis, R.: Slope assessment in digital age—a case history. *Aust. Geomech.* **53**(3), 51–60 (2018)
3. Parry, S., Baynes, F.J., Culshaw, M.G., Eggers, M., Keaton, J.F., Lentfer, K., Novotny, J. Paul, D.: Engineering geological models—an introduction: IAEG Commission 25. *Bull. Eng. Geol. Environ.* **73**, 689–706 (2014)

Forensic Geotechnical Investigation of Settlement Failure of Pile Group Supporting Columns of Conveyor Belt



C. N. V. Satyanarayana Reddy and M. Nagalakshmi

Abstract Forensic geotechnical investigation has gained significance among civil engineering professionals as majority of the failures of structures originate from substructure or foundation soil. The forensic studies enable establishing the exact causes for failures and to take up remedial measures to stabilize the structures where ever feasible and help in avoiding similar failures in future constructions by overcoming the deficiencies in geotechnical design of foundations and improving the ground prior to construction if found necessary. The findings of forensic geotechnical investigations of failures of structures are enabling the geotechnical engineers to advise more efficient and safe foundations in different soil conditions and to suggest the post construction care if any to be taken up. The forensic geotechnical investigations not only address the remedial action for overcoming the failures but also provide useful information with regard to causes for failures and the steps to be taken to avoid such failures in future constructions in similar soil conditions. The present paper describes various steps involved in forensic geotechnical investigation and illustrates the same through analysis of settlement failure of a pile group supporting columns of conveyor system at one of the locations of material handling in Visakhapatnam port. The investigation revealed the causes for settlement failure of pile group as inadequate soil exploration, insufficient pile length and negative skin friction drag force on pile from soft clay layer. Based on the forensic geotechnical investigation carried out, remedial measures are suggested.

Keywords Settlement • Pile group • Load capacity • Bored cast in situ pile • Soil investigation • Forensic investigation • Negative skin friction

C. N. V. Satyanarayana Reddy (✉)
Department of Civil Engineering, College of Engineering, Andhra University,
Visakhapatnam 530003, India
e-mail: cnvsreddy@gmail.com

M. Nagalakshmi
College of Engineering, Andhra University, Visakhapatnam 530003, India
e-mail: nagalakshmi20.bec@gmail.com

1 Introduction

Forensic geotechnical engineering deals with the investigation/analysis of geotechnical/soil-related failures of the structures that occur during/after construction. The forensic study is carried out to identify distress in the structure, the cause of failure and suggest suitable remedial technique for rectification of the problem/failure. The distresses in the structure include cracks, tilts, lateral movement and excessive settlement of structures. The common causes of geotechnical failures are lack of detailed soil investigation, sudden/unexpected changes in ground water profile, inappropriate construction methods adopted in the site, etc. [1, 2] Investigation of these kinds of failures is important to address similar issues and prevent possible failures in future. Apart from conventional geotechnical tests, non-destructive tests are also required to conduct forensic geotechnical investigation. A well-planned forensic investigation includes the following heads [3].

(a) Compulsory Tasks

Before establishing cause of failure, it is necessary to investigate the condition of the site immediately after failure and record the preliminary observations (Reconnaissance Survey) in order to arrive at the cause of failure. Original soil investigation reports, analysis and design of the structure should be verified and the engineers involved in planning, design, construction and performance monitoring are to be investigated in order to know the design methods and specifications of the material used for construction.

(b) Optional Tasks

In case of certain complex engineering failures, standard geotechnical testing alone is sufficient to evaluate the cause of distress. In such cases, additional investigations such as non-destructive testing of the structural elements is conducted to evaluate quality of construction materials.

(c) Analysis and Evaluation of Data

The distress in a structure occurs due to underestimation of loads, lack of sufficient soil investigation data, improper design and construction methods. Certain field and laboratory tests are conducted to characterize the ground and assess the cause of distress in the structure.

The data required for the investigation include topography of the site, geological formations such as folds, faults, joints, etc. at the site, seismicity of the region, stratification of soil layers, alterations in ground water table, results of field and laboratory studies, etc. The load deformation history of the soil is reestablished by conducting data analysis based on mobilization of shear strength, liquefaction potential, critical void ratio of soil existing at the site, limit conditions and partial factors of safety.

(d) **Conclusions**

Conclusions indicate the cause of failure and suggest suitable recommendation.

(e) **Report**

All the data collected during investigation is documented in an easily retrievable format. The report includes all the findings of investigation with supporting documents such as soil investigation reports, meteorological conditions before and after the failure, interviews of persons involved in construction of structure right from planning to the execution stage. It comprises data analysis, investigation methodologies along with their results and conclusions indicating the cause(s) for failure and remedial techniques to be adopted.

The present paper deals with forensic investigation of settlement failure of pile group that occurred during construction phase of conveyor belt system in one of material handling plants at Visakhapatnam Port. The case study illustrates the above-described methodology of forensic geotechnical investigation.

2 Details of Failure

One of the Material Handling Firm at Visakhapatnam Port has planned for new storage facility by laying new conveyor belt. The conveyor belt supporting system comprised of RCC Columns erected on pile cap laid on a group of four bored cast-in-situ piles and a horizontal framework for supporting conveyor belt is laid over the columns. The piles used are of 450 mm diameter and 15.5 m length based on soil investigation report issued by a private agency. The piles are terminated at 15.5 m depth considering presence of rock based on bore log of nearby area. During the execution of the work, two columns supporting the framework of conveyor belt at a location settled by about 100 mm due to self weight as shown in Fig. 1, prior to installation of conveyor belt.

The Material Handling Firm has approached Andhra University to investigate into the problem and to provide technical advice. A site visit has been made to inspect the effected columns, and it is observed that the area is stacked by coke up to 4.0 m high over a large extent. Further, it is observed that the location is in close proximity to a drain which is 3–4 m deep. It is understood during the interaction with the concerned officials that the problem of pile group settlement started after stacking of coke material in that area. It is also observed that no exploratory borehole is located within 100 m distance from affected area. From the scrutiny of the design documents, it is noticed that the design load on each pile is 650 kN. Initial and routine pile load tests are not performed to check the design load of piles.

Based on the collected information, fresh soil investigation is carried out at the affected pile group location to establish the subsoil information and to estimate allowable load capacity of adopted piles based on termination depth.



Fig. 1 Settled columns supporting conveyor structure

3 Details of Soil Investigation

The exploratory borehole used in the forensic study is of 150 mm diameter in soil and 65 mm diameter in rock and terminated at 26.5 m length in rock strata after advancing borehole in rock stratum by 4 m. The Standard Penetration Tests are conducted at every 0.75 m interval up to 3.0 m depth and thereafter at every 1.5 m intervals up to rock stratum. The Standard Penetration Tests are performed as per IS 2131-1981 [4]. The laboratory tests are carried out on undisturbed, disturbed and SPT samples as per relevant IS codes of practice [5]. The bore log (Table 1) is prepared using field data and laboratory test results of soil samples collected during investigation. The engineering properties of soil at different depths are presented in Table 2.

The bore log revealed that foundation soil at the location consisted of filled up soil (clayey sand with gravel) in top 0.5 m depth, soft marine clay, clayey gravel, weathered rock/SDR, highly fractured rock, weathered rock/SDR followed by hard fractured rock. The ground water table is observed at a depth of 2.3 m below the ground surface.

Table 1 Bore log of affected location

Location : Visakhapatnam port Depth of GWT: 2.3 m		Bore hole no : BH-1 Depth of bore hole: 26.5 m Type of boring : Rotary Diameter of boring: 150 mm							
Layer depth (m)	Description	Type	Depth (m)		N	CR (%)	RQD (%)		
			0-15 cm	15-30 cm				30-45 cm	
0.0-0.5	Filled up soil (gravelly clayey sand)	DS	0.0	0.5					
0.5-10.0	Soft marine clay	DS	0.5	3.0					
		SPT	3.0	3.45	01	02	03		
		DS	3.45	7.5					
		SPT	7.5	7.95	02	02	04		
10.0-13.4	Clayey gravel	DS	7.95	10.0					
		SPT	10.5	10.95	09	14	23	37	
		DS	10.95	13.0					
		SPT	13.0	13.4	30	42	Refusal	>100	
13.4-19.0	Soft disintegrated rock (SDR)	DS	13.4	14.5					
		SPT	14.5	14.54	Refusal	-	-	>100	
		SPT	16.0	16.45	24	30	35	65	
		SPT	17.5	17.58	Refusal	-	-	>100	
19.0-22.0	Highly fractured rock	DS	17.58	19.0					
		SPT	19.0	19.01	Refusal	-	-	>100	
22.0-22.5	Weathered rock	RCS	19.01	22.0			26.6	0	
22.5-26.5	Fractured hard rock	DS	22.0	22.5					
		RCS	22.5	24.5				26.4	10.5
		RCS	24.5	26.5				32.8	14.6

DS: Disturbed sample, SPT: Standard Penetration Test, N: Standard Penetration Resistance, RCS: Rock core sample, RQD: Rock quality designation, CR: Core recovery

Table 2 Engineering properties of soil at bore hole

Depth (m)	Description of strata	ISC	Type of sample	Grain size analysis			Plasticity characteristics				ρ (g/cc)	NMC (%)	FSI (%)	C (t/m ²)	ϕ (Deg)
				G (%)	S (%)	F (%)	w _L (%)	w _p (%)	I _p (%)						
0.0-0.5	Filled up soil (Gravelly clayey sand)	SC	DS	20	38	42	34	21	13	-	-	-	-	-	
0.5-10.0	Soft marine clay														
0.5-3.45	-do-	CH	SPT	01	30	69	63	32	31	2.02	65.5	60	1.6	12	
3.45-7.5	-do-	CH	DS	00	25	75	58	28	30	-	-	-	-	-	
7.5-10.0	-do-	CH	SPT	00	22	78	60	28	32	2.01	61.6	50	1.8	10	
10.0-13.5	Clayey gravel	GC	SPT	43	32	25	43	24	19	2.28	25.8	35	1.2	29	
13.5-19.0	SDR														
13.5-14.5	-do-	-	DS	29	48	23	32	20	12	2.22	20.7	-	-	-	
14.5-14.54	-do-	-	SPT	Sample inadequate for analysis											
16.0-16.45	-do-	-	SPT	20	52	28	31	19	12	2.20	15.8	10	-	-	
17.5-17.58	-do-	-	SPT	No sample recovered											
17.58-19.0	-do-	-	DS	25	55	20	28	19	09	-	-	-	-	-	
19.0-22.0	Highly Fractured Rock														
19.0-19.01	-do-	-	SPT	No sample recovered											
19.0-22.0	-do-	-	RCS	Rock cores recovered with CR 26.6% and RQD = Nil											
22.0-22.5	Weathered rock	GC	DS	59	13	28	30	19	11	-	7.5	-	-	-	
22.5-26.5	Fractured Hard Rock														
22.5-24.5	-do-	-	RCS	Rock cores recovered with CR = 24.4% and RQD = 10.5% with unconfined compressive strength of 3210 t/m ²											
24.5-26.5	-do-	-	RCS	Rock cores recovered with CR = 32.8% and RQD = 14.6% with unconfined compressive strength of 3450 t/m ²											

G: Gravel, W_L: Liquid limit, ISC: Indian Standard Soil Classification Symbol, S: Sand, W_p: Plastic limit, ρ : In situ density, C: Cohesion, F: Fines, I_p: Plasticity Index, NMC: Natural water content, ϕ : Angle of internal friction

4 Analysis of Pile Settlement Problem

The pile load capacity of used pile of 450 mm diameter and 15.5 m length to support the columns of conveyor belt is determined based on established subsoil properties at affected location as per IRC 78-2014 [6]. As SDR strata is observed to have varying stiffness and consistently refusal is also not observed, skin friction contribution from clayey gravel overlying the SDR layer is also considered in load capacity evaluation. Load capacity in skin friction from clayey gravel is determined as per IS 2911 part 1 (Section 2)—2010 [7].

Allowable load capacity is determined as

$$Q_a = (R_e/3) + (R_{af}/6) + (R_s/2.5) \quad (1)$$

where R_e = ultimate capacity in end bearing = $9C_{ub} \cdot A_b$

R_{af} = ultimate capacity in side socket shear = $C_{us} \cdot A_{s2} + r_s \cdot A_{s1}$

R_s = ultimate capacity in skin friction in clayey gravel

C_{ub} = average shear strength below base of pile over a depth of 2 times diameter of pile

C_{us} = ultimate shear strength along socket length

r_s = ultimate skin friction resistance in clayey gravel

A_{s1} = surface area of pile in clayey gravel layer

A_{s2} = surface area of pile in SDR stratum.

In SDR layer, N value is considered as 60 and accordingly shear strength or cohesion of SDR is taken as 400 kN/m² as per IRC 78-2014. The ultimate skin friction resistance (kN/m²) in clayey gravel is determined as “2N”. In marine clay, the ultimate skin friction resistance is determined as 0.9 times undrained cohesion (kg/cm²) of soil, which is taken as 1/16th of ‘N’ value (= 3). The ultimate skin friction resistance (r_s) in clayey gravel and soft marine clay has been taken as 74 kN/m² and -17 kN/m² respectively. A factor of safety of 2.5 has been used to arrive at allowable skin friction resistance in clayey gravel. Deduction for downward drag due to negative skin friction of soft marine clay is made in evaluation of load capacity of pile. The details of load capacity estimation are presented in Table 3. Downward drag force is determined by multiplying ultimate skin friction resistance in soft clay layer with corresponding surface area of pile.

Table 3 Details of load capacity estimation of affected pile

Soil layer	Thickness (m)	Allowable load capacity in	
		Skin friction/side socket shear (kN)	End bearing (kN)
Soft marine clay	10.0	-240.3	–
Clayey gravel	3.5	146.5	–
SDR	2.0	188.6	190.9

The allowable load capacity after accounting for downward drag from soft marine clay is determined as 286 kN as permanent liner is not provided around the piles. Ignoring downward drag from soft marine clay, the allowable load capacity of piles with PVC casing in soft clay zone is about 526 kN. Since dumping of material is done at the area, the downward drag force developed on the pile surface which resulted in low allowable load capacity of 286 kN against the required design load capacity of 650 kN. Hence, the settlement of pile group occurred.

5 Remedial Action

In view of the prevailing situation, it is advised to install new piles to support the columns of conveyor belt by terminating the piles in fractured hard rock available at 22.5 m by maintaining a minimum socketing length of ' d ', where ' d ' is the diameter of pile. Hence, pile length of 23 m is considered.

5.1 Allowable Load Capacity of Suggested Pile

Ultimate load capacity of pile with termination in fractured hard rock is determined as

$$Q_u = R_e + R_{af} = k_{sp} \cdot q_c \cdot d_f \cdot A_p + A_s \cdot c_{us} \quad (2)$$

Allowable load capacity of pile is determined as $Q_a = (R_e/3) + (R_{af}/6)$

where K_{sp} is an empirical constant = 0.3 for $(CR + RQD)/2 = 0.3$

q_c = average unconfined compressive strength of rock below base of pile for a depth of twice the diameter of pile = 3200 t/m²

d_f = depth of factor = $1 + 0.4 \times (\text{length of socket/diameter of pile})$ with a maximum value of 1.2

c_{us} = ultimate shear strength of rock in socket length in Mpa = $0.225\sqrt{q_c}$

For socketing length of " d ", depth factor is determined as 1.2. For unconfined compressive strength of rock, $q_c = 32$ MPa, ultimate side socket shear resistance in rock is determined as 1.27 MPa. Ultimate side socket shear resistance in SDR is taken as 66.7 kN/m² corresponding to $N = 60$. Side socket shear contribution is considered over " $6d$ " length (= 2.7 m) of pile above tip.

The details of allowable vertical compression load capacity estimation of 450 mm diameter and 23.5 m length pile at location are tabulated in Table 4.

The allowable load capacity of suggested pile is more than the required design pile load capacity of 650 kN. Hence, it is adequate for supporting the columns of conveyor belt system.

Table 4 Details of load capacity estimation of suggested pile

Soil layer	Thickness (m)	Allowable load capacity in		Allowable load capacity	
		Skin friction/ side socket shear (kN)	End bearing (kN)	Considering negative skin friction effect	With usage of Permanent casing
Weathered rock	2.25	212.2	–	717.6	957.9
Fractured hard rock	0.45	134.7	611		

6 Conclusions

Based on the present forensic investigation of affected pile group supporting columns of conveyor belt, the following conclusions are drawn.

1. The settlement failure of pile group is due to inadequate subsoil investigation and termination of pile in weathered rock of varying stiffness instead of fractured hard rock.
2. Downward drag on pile surface from soft clay due to stacked coke has resulted in settlement of pile as permanent liner is not placed around the pile.
3. Routine pile load tests at the affected location where proper soil investigation is not done could have helped in modifying pile size/length and avoided the failure.
4. The need for extending soil exploration beyond 3 m depth into rock is realized as there can be thin layers of fractured rock sandwiched in weathered rock material, particularly in sites adjacent to natural drains.
5. Conduction of initial tests and routine tests is mandatory in projects where large numbers of piles are used.
6. The fractured hard rock at the affected location is available at 23 m depth below ground surface from fresh soil investigation carried out.
7. The columns of the conveyor belt are to be supported on fresh bored cast-in-situ piles of 450 mm diameter and 23.5 m length.

References

1. Anirudhan, I.V.: Types of distress in geotechnical structures. In: Proceedings of Indian Geotechnical Conference IGC 2005, Ahmadabad, pp. 165–168 (2005)
2. Leonards, G.A. : Investigation of failures. J. Geotech. Eng. Div. ASCE **108**(GT2), 187–246 (1982)
3. Rao, V.V.S., Sivakumar Babu, G.L.: Forensic geotechnical engineering. In: Proceedings of International Society for Soil Mechanics and Geotechnical Engineering TC 40, Oct 2009

4. IS 2131-1981: Method of test for standard penetration test, Bureau of Indian Standards, New Delhi
5. IS 2720 Relevant parts: Methods of test for soils, Bureau of Indian Standards, New Delhi
6. IRC 78-2014: Standard specification and code of practice for road bridges Section-VII (foundations and substructure)
7. IS 2911 Part 1 (section 2)—2010: Code of practice for design and construction of pile foundations, Concrete Piles- Bored cast in situ piles, Bureau of Indian Standards, New Delhi

Field Application of High-Strength Deep Mixing Method for Waste Water Pipeline in Soft Ground



E. C. Shin, J. K. Kang, Y. K. Rim, and J. J. Park

Abstract Recently, the high-rise residential buildings are being constructed in soft ground along the coastal area. Several infrastructures such as road, bridge, drinking and waste water supply lines and necessary to meet the basic requirement by the residents at the apartment complex. In this paper, the field application of high-strength deep mixing method (HDCM) is presented for reconstruction of collapsed waste water supply line with the diameter of 1000 mm in soft ground. Soil samples were obtained for various laboratory tests which were used for the numerical analysis of settlement for foundation soil of waste water supply line. The excessive settlement of waste water supply line was occurred due to the disturbance of the soft soil layer under the pipeline during the pull-out of sheet pipe walls. When the HDCM was applied as a ground improvement method to reinforce the foundation soil for waste water supply pipeline, the bearing capacity was increased greatly and the settlements was occurred as 37.6 and 48.5 mm, respectively, which is much less than the allowable settlement of 100 mm.

Keywords Waste water pipe line · Ground settlement · Soft ground · Braced-cut

1 Introduction

The land reclamation from the sea has been very popular method to obtain the required land for the construction of industrial complex, harbour facilities and residential area in the past 40 years. In the last end of land development project, the various utility lines such as drinking and waste water supply and collection pipelines as well as electrical cable should be installed underground at the unfavourable soil ground condition. A number of braced-cut systems were adopted secure the stability of temporary braced-cut walls such as sheet pile wall, H-pile

E. C. Shin (✉) · J. K. Kang · Y. K. Rim · J. J. Park
Department of Civil and Environmental Engineering, Incheon National University,
Incheon, South Korea
e-mail: ecshin@inu.ac.kr

with soil-cement wall, deep mixing column and jet grouting with bracing system under the soft ground.

In general, the deep cement mixing (DCM) column improving the soft clay ground by mixing chemical stabilizer which consisted of cement and lime at the original site is used for the infrastructure construction. Deep cement mixing is used to reduce the generation of waste during soft soil improvement and achieve low noise in a short period of time. The fundamental improvement principle of the deep mixing process is in the formation of a rigid hardened body produced by the hydration reaction between the stabilizer and water. The chemical reaction (pozzolanic reaction) between the product by the hydration reaction and the marine clay material improves the soft ground [1].

Deep mixing method started to be developed from a research work by the Research Institute of Harbor Technology belonged to the Ministry of Transport of Japan since 1976. At the same time, lime column was developed and used by now in Sweden which is method of mixing soil in underground as injecting the powder of quick lime into the ground through the air pipe with high pressure. In domestic study about deep mixing, since the special earth concreting (SEC) method with which cement is used as hardening agent was introduced from Japan in 1985. It has been applied mainly to a retaining wall, foundation for building, foundation of seawall or quay as a harbour construction. In the related research, Bergado et al. [2] studied recent developments of ground improvement in soft Bangkok clay. Kim et al. [3] conducted a reliability analysis of the external stability of the quay wall installed in the deep mixed soil. Park et al. [4] studied reliability analyse with respect to external stability of quay founded on deep mixing ground. Lee et al. [5] studied with respect to formation shape of cement mixing bulb with construction condition of deep mixing method. Han et al. [6] studied about strength of cement mixing bulb by construction condition of deep mixing method. Chon [7] studied about compressive strength characteristics for deep mixing method. Kim et al. [8] analysed the effect of the deep ground mixing and sand treatment method on the application of the lower ground and retaining line. Recently, DCM lift injection method has been applied in Incheon coastal area [9].

The purpose of this study was to analyse the cause of deformation and differential settlement during the installation of waste water pipeline around a natural river and to propose a countermeasure through stability analysis.

2 Earth Pressure During Excavation on Soft Ground

The active thrust on the bracing system of open cuts can be estimated theoretically by using trial wedges and Terzaghi's general wedge theory (1941). Triangular distribution earth pressure theory used in the design of retaining wall is significantly different in case of retaining wall in soft ground. The larger the deformation behaves the smaller the earth pressure.

When determining the construction depth of the retaining wall and the cross section of the self-supporting sheet pile, the earth pressure mainly used for Rankine–Resal earth pressure calculation is mainly used. In the case of assuming that the background of the retaining wall is horizontal, ignoring the wall friction angle with the wall, the main earth pressure and the passive earth pressure at the bottom of the excavation are expressed by the following Eqs. (1) and (2), respectively.

$$P_a = \gamma_t z_w + \gamma'(z - z_w) + qK_A - 2c\sqrt{K_A} \tag{1}$$

$$P_p = \gamma_t z_w + \gamma'(z - z_w) + qK_P - 2c\sqrt{K_P} \tag{2}$$

where P_a is the main earth pressure at the depth of z , P_p is the passive earth pressure at the depth of z , γ_t is the wet unit weight of the soil, γ' is the unit weight of the soil in water, z is the depth to any point on the surface, z_w is the depth from the surface to the groundwater surface, q is the surface load on the surface, and ϕ is the internal friction angle of the soil.

Experimental earth pressure distributions are presented based on actual field measurements, and Peck’s (1969) empirical earth pressure distribution is the most used. These diagrams for cuts in sand, soft to medium clay, and stiff clay are given in Fig. 1.

The transverse earth pressure starts from the stationary earth pressure. When the wall is pushed to the excavation side, the earth pressure decreases to the main earth pressure. If it is pushed to the back side, the earth pressure continues to increase but the manual earth pressure can’t be increased. In other words, the minimum and

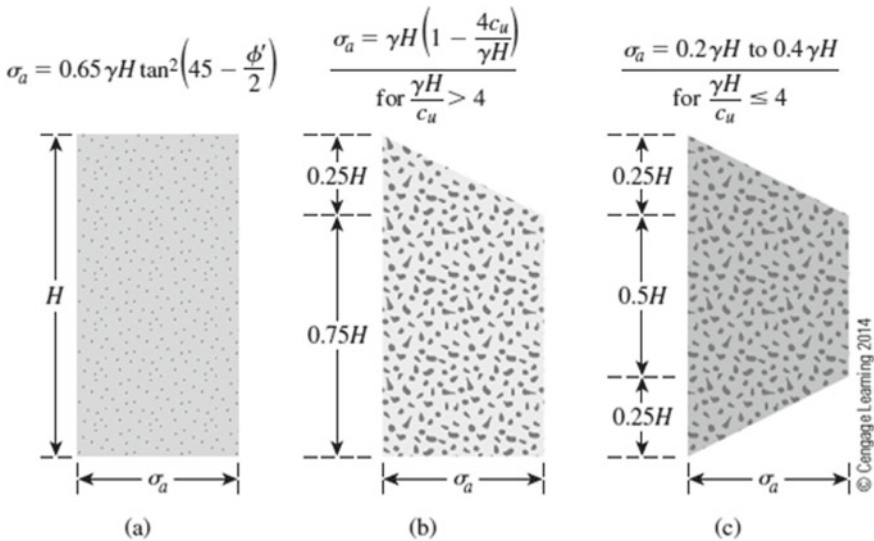


Fig. 1 Pressure diagram for cuts in sand (a), soft medium clay (b) and stiff clay (c) [12]

maximum earth pressure limits are set. The ground modelling is simulated by a spring, and the basic equation of carbon spring is given by the following Eq. (3).

$$E_w I_w \frac{d^4 y}{dz^4} + \frac{A_p E_p}{L_p} y = p_i \pm k_h y \tag{3}$$

where E_w, L_w are elastic modulus and moment of inertia of the earth retaining wall and A_p, E_p, L_p are cross sectional area, elastic modulus and length of the supporting structure, respectively. p_i is initial at rest earth pressure (σ_0), k_h represents the horizontal reaction force coefficient.

Using Eq. (3) in SUNEX ver. w6.16 [10] and EXCAV ver. 2.51 [11], which are currently used as commercial software, stability of the wall is analysed. The lateral displacement of the wall at each step, the shear force and moment acting on the wall, and the axial force acting on the support are obtained. Figure 2 shows the analysing model using the equation.

3 Subsurface Exploration on Soft Ground and Soil Characteristics

The total length of this construction is 7.9, and 3.55 km is overlapped with natural river construction. A total of three investigations were conducted on the design subsurface exploration of the waste water pipeline. In this study, the existing ground surveys were combined and re-confirmed the soft ground layer through additional drilling of 5 holes. The sample was mostly fine-grained soil which is over 50% passing of sieve number 200. It was carried out water washing method and hydrometer distribution test. As a result of particle size analysis by unified classification method, the soil type of KG-1 to KG-3 was CL, and KG-4 was identified as ML.

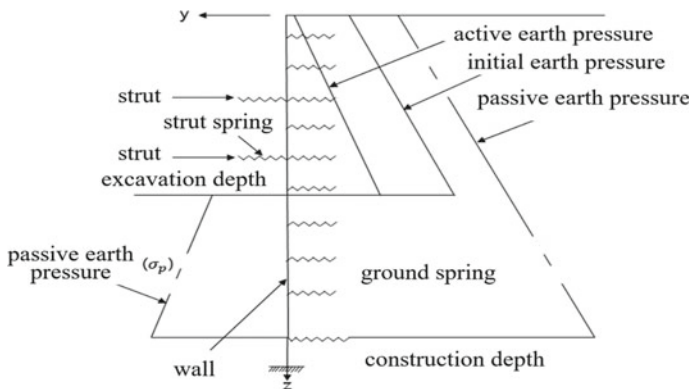


Fig. 2 Schematics of elastic beam model

The preliminary consolidation load was 79.36–101.40 kPa, the compression index was 0.302–0.4337, Moisture unit weight of soil was 17.18–18.09 kN/m³, and the initial void ratio was 1.162–1.420. Overconsolidated ratio was about 1.0 as a normally consolidated soil. In situ test was performed. Cohesion of soil was measured with a field vane tester in order to confirm the undrained shear strength of undisturbed state and disturbed state.

The test results showed that the boring depth was about 3.5 ~ 5.0, cohesion of undisturbed sample with depth was 21.4 ~ 23.3 kPa, cohesion of disturbed sample was 2.6 ~ 3.5, and the sensitivity ratio of each boring was 7.15 ~ 8.23. On the design, cohesion was similar with additional survey as 22.0 ~ 35.3, but sensitivity was not considered. Soil samples of KG-1, KG-2, KG-3, KG-4 were very sensitive. Therefore, it is expected that the ground has large deformation or the settlement possibility is high due to the ground disturbance during excavation. Table 1 shows the results of the consolidation test on the undisturbed samples taken from the boring and field vane shear test.

4 Estimation of Soft Ground Soil Property

Cohesion and internal friction angle were compared and examined by Dunham, Terzaghi-Peck, Meyerhof, Osaki, Schmertmann and Hisatake using empirical formulas based on SPI-N values. The design constants were calculated as shown in Table 2 based on the laboratory test results of the drilled specimens.

Table 3 shows that the preconsolidation load was 70.6–85.1 kPa, compression index was 0.325–0.522, swelling index was 0.06–0.124, consolidation coefficient was 1.96e-3 cm²/sec to 8.09e-3 cm²/sec, and initial void ratio values were 1.032–1.311. It was applied in the design of sewer pipeline construction.

In this study, consolidation data was revised using additional boring and existing boring data for the soft ground settlement sections. The average value showed little bit larger than that of design value. The revised soil property was shown in Table 4.

After STA. No. 50 + 18.0, there is a pressure pipeline along the waste water pipeline in the adjacent area, and the overburden load is expected to increase due to the embankment construction in the future. Also it was found that the depth of soft ground layer was deeper than that of original design from STA. No. 69 + 4.0 to STA. No. 125 + 4.0.

Table 1 Test results of consolidation test and field vane shear test

No.	Consolidation test (ASTM D2435) [13]									
	Preconsolidation load, P_c (kPa)	Compression index, c_c	Swelling index, c_s	Unit weight, r_t (kN/m ³)	OCR	e_o	c_u (undisturbed, kPa)	c_{ur} (disturbed, kPa)		
KG-1	82.92	0.41	0.11	18.09	1.04	1.42	22.9	2.8		
KG-2	80.32	0.43	0.07	17.18	1.09	1.30	23.3	2.8		
KG-3	79.36	0.39	0.06	17.66	1.08	1.19	21.4	2.6		
KG-4	101.40	0.30	0.05	18.05	0.95	1.16	28.4	3.5		

Table 2 Soil property of shear strength for each layer in soft ground

Soil type	Unit weight, r_t (kN/m ³)	Cohesion, c (kPa)	Internal friction angle (°)
Reclaimed layer	19.0	10.0	20
Accumulation (clay, $N \leq 4$)	17.0	17.0	5
Accumulation (clay, $4 < N \leq 10$)	17.6	40.0	5
Accumulation (sand)	18.0	5.0	25
Weathered soil	19.0	20.0	30
Weathered rock	20.0	30.0	33
Soft rock	23.0	100.0	33

Table 3 Soil property on design around waste water pipeline

Boring no.	Preconsolidation load, P_c (kPa)	Compression index, c_c	Swelling index, c_s	Consolidation coefficient, c_v (cm ² /sec)	Initial void ratio, e_o
BH-1	70.6	0.522	0.124	1.96E-03	1.311
BH-2	77.1	0.347	0.06	4.44E-03	1.032
BH-3	85.1	0.325	0.063	8.09E-03	1.195

5 Comparison with Numerical Analysis

5.1 *Elasto-Plastic Modelling for Temporary Earth Wall*

Structural analysis was carried out a beam on elasto-plastic foundation model. It is similar to the beam on winkler foundation used to design piles with a foundation or horizontal load. The wall stability at the final stage was evaluated from the stepwise excavation analysis. It is assumed that the stress is redistributed due to the empirical earth pressure over time after the excavation is completed. The stability of the earth retaining walls and support materials to the earth pressure is evaluated.

Soft soil property was revised using the additional ground survey of 5 boring data, the subsurface exploration data of basic and detailed design of the sewer pipeline and the subsurface exploration data of the basic and detailed design of the natural river improvement project. As a result, the soft ground layer was deeper than the original design ground survey with a maximum of 12 m, and the ground layer also changed. Based on the revised plan, three weakest section sites were selected. EXCAV and SUNEX were used to evaluate the stability of the pipeline by prefabricated wall.

Table 4 Revised soil property around sewer line on this research

Division	Boring no.	Preconsolidation load, P_c (kPa)	Compression index, c_c	Swelling index, c_s	Consolidation coefficient, c_v (cm ² /sec)	Initial void ratio, e_0
No. 8 + 0 ~ No. 50 + 18.0	KG-1	82.9	0.410	0.118	3.148E-03	1.42
No. 50 + 18 ~ No. 125 + 4.0	BH-3	85.1	0.325	0.063	8.090E-03	1.19

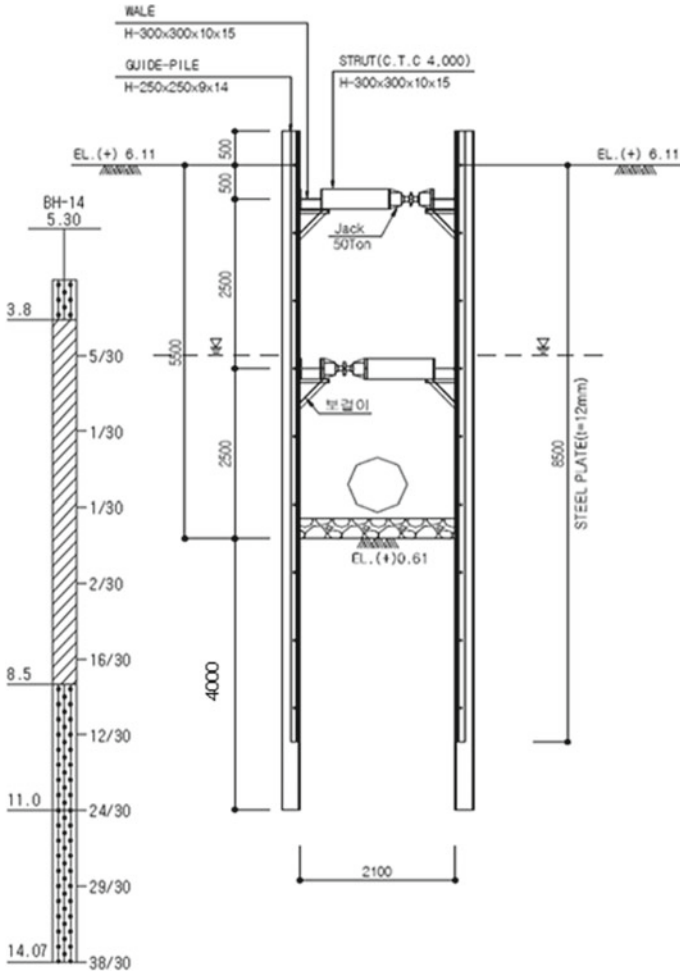


Fig. 3 Braced-cut on the section

5.2 Stability Analysis for Deep Wall After Ground Improvement

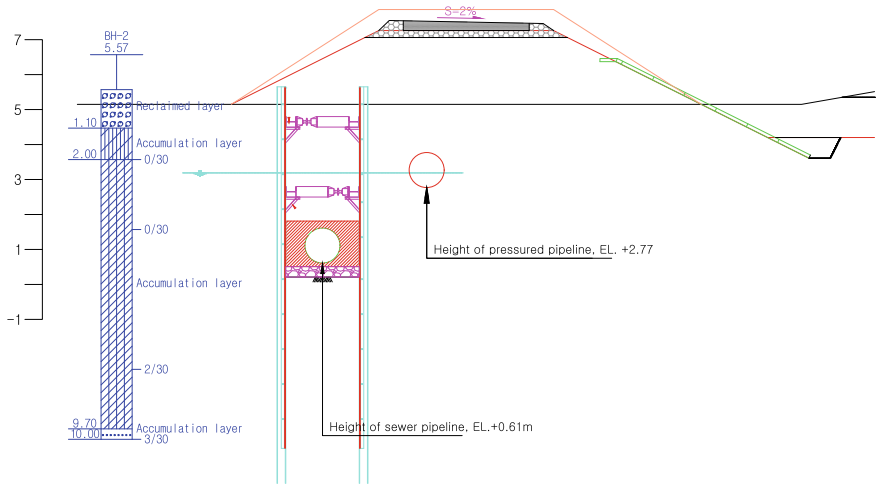
Stability of construction depth of temporary wall was analysed. Figure 3 shows the cross section with braced-cut.

When the construction depth of temporary wall is specific depth at the maximum excavation depth, the safety factor of the construction depth is calculated higher than standard of safety factor 1.2. The results are shown in Table 5.

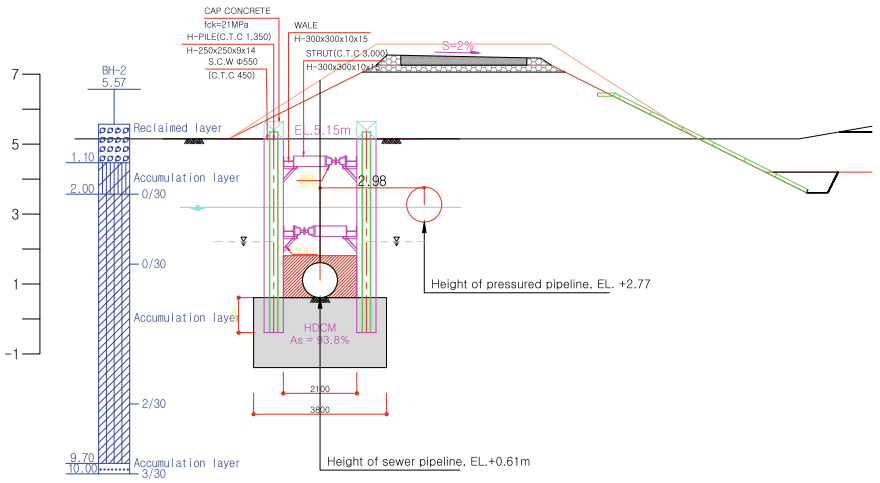
Safety for ground settlement was calculated. Clay Section-A was 7.2 m in the thickness of the soft ground, and no other channel was buried in the vicinity. Clay

Table 5 Results of stability analysis for construction depth of each section

Section	Excavation depth (m)	Construction depth (m)	Safety factor	
			Result	Minimum standard
Soft section-A	5.5	4	2.46	1.2
Soft section-B	5.5	3	1.67	1.2
Soft section-C	5.5	4	1.53	1.2
Soft section-D	7.1	5.9	1.79	1.2
Soft section-E	4.1	7.4	1.83	1.2



(a) Original design section



(b) Reinforced section

Fig. 4 Cross-sectional Clay Section-C with ground improvement

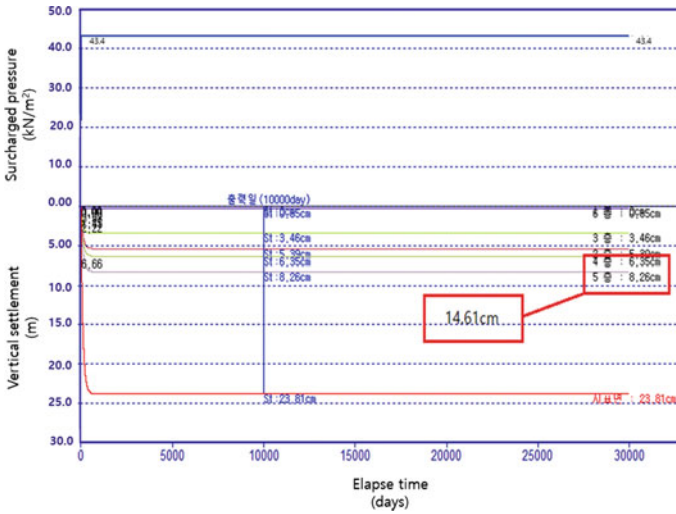


Fig. 5 Ground settlement with elapsed time

Table 6 Estimated settlement of pipeline before and after ground improvement

Section	Diameter of pipe (mm)	Settlement of base (mm)	After ground improvement	
			Result (mm)	Criterion (mm)
Clay section-B	1,000	146.1	37.5	100
Clay section-C	1,000	109.7	48.5	100

Section-B is 8.6 m in thickness of soft ground. An existing line appeared at a distance of 2.98 m from the position where the sewer pipeline is constructed. Clay Section-C was 12 m in thickness of the soft ground, and the soft ground thickness of the three sites was the largest. Figure 4 shows cross section of Clay Section-C as original design section and reinforced section for ground improvement, and Fig. 5 shows the result of settlement with elapsed time.

Before ground improvement, settlement of some area using K-Embank ver. 3 did not satisfy the criteria on the road settlement standard. Table 6 shows the basement settlement of pipeline and allowable settlement after ground improved by using HDCM method.

Table 7 Comparison of safety factor on temporary wall type after soil improvement

Division		Excavation depth (m)	Construction depth (m)	Maximum settlement (mm)	Safety factor	
					Result	Decision
Original design		7.1	5.9	76.47	1.786	O.K
Reduce construction depth (SCW + HDCM)	EXCAV	7.1	1.0	17.19	1.875	O.K
	SUNEX	7.1	1.0	31.34	2.13	O.K
Reduce construction depth (SGP + HDCM)	EXCAV	7.1	1.0	18.88	2.188	O.K
	SUNEX	7.1	1.0	28.89	2.43	O.K
Reduce construction depth (Sheet Pile + HDCM)	EXCAV	7.1	1.0	10.22	2.237	O.K
	SUNEX	7.1	1.0	21.45	2.43	O.K

6 Discussion

As a result of the analysis of the soft ground, it is confirmed that it is highly sensitive soft clay. Therefore, it is suggested to improve the ground using the high-strength DCM method (HDCM). For the construction of sewer pipeline on the deep soft ground, combination methods like SCW, SGP and sheet pile with ground improvement were proposed. The lower part of the pipeline was stabilized by using HDCM. The SCW method is effective in passive earth pressure resistance, forming foundation that resists heaving, and in the reclamation area. The SGP method is capable of forming a foundation that is resistant to heaving, and is inexpensive when buried. The sheet pile has the advantage of being able to increase the effect of passive earth pressure resistance and to form the foundation to resist the heaving. We propose a method to prevent disturbance by using the semi-shield method in the section after Clay Section-C where the soft ground depth is highly deep in the lower part of the basement. Table 7 shows the result of safety review of the construction depth safety of the representative section.

7 Conclusion

This study carried out to find the causes of pipe deformation during the test construction in the overlapping section of the sewer pipeline and natural river construction. It was proposed the countermeasures for the application. In order to clarify the causes of pipe deformation and differential settlement, the present state of soft ground was reviewed by collecting the drill log data. In addition, the distribution and physical soil characteristics of the boring data were examined through laboratory and field experiment test based on the 5 boring data. The results of the causes and countermeasures of pipe damage are presented as follows:

1. In case of high sensitivity, it may cause the settlement due to ground disturbance at the extraction, which may damage the stability of the pipeline. Therefore, it is suggested that the improvement of the soft ground should be done as a way to minimize disturbance to the lower part of the basement.
2. Stability analysis was performed by applying SCW + HDCM and Sheet Pile + HDCM method to Clay Section-B and Clay Section-C sites as the representative sections most vulnerable to subsidence of pipeline.
3. As a result of 2 m strengthening with HDCM method, the soft clay ground was improved and the strength increased and settlement amount decreased. The settling amount satisfies the allowable residual settlement amount, 100 mm.

References

1. Shin, E.C., Kang, J.K., Oh, D.H., Lee, B., Kim, B.H., Jung, S.P.: Effect of chemical improvement by hardening agent on soft soil. In: Proceedings of 2009 Conference Co-Hosted by KISTEC & KGES, pp. 427–432 (2009)
2. Bergado, D.T., Lorenzo, G.A.: Recent developments of ground improvement in soft Bangkok clay. In: Proceedings of the International Symposium on Lowland Technology, Saga University, Japan, pp. 17–26 (2002)
3. Kim, Y.S., Park, O.J., Huh, J.W.: Reliability analysis for the external stability of quay walls constructed on deep-cement-mixed ground. In: Proceedings of Korean Society of Civil Engineering Conference 2005, pp. 2104–2107 (2005)
4. Park, O.J., Huh, J., Kim, Y.S.: Reliability analysis and sensitivity analysis of quay walls constructed on deep-cement-mixed ground. In: Proceedings of Korean Society of Civil Engineers Conference 2006, pp. 2278–2281 (2006)
5. Lee, K.Y., Kwon, S.H., Kim, S.M., Han, W.S.: Shape characteristics of improved soil on construction conditions of deep mixing method. In: Proceedings of Korean Geotechnical Society Conference 2007, pp. 226–223 (2007)
6. Han, W.S., Kwon, S.H., Kim, S.M., Lee, K.Y.: Strength characteristics of improved soil on construction conditions of deep mixing method. In: Proceedings of Korean Geotechnical Society Conference 2007, pp. 923–928 (2007)
7. Chon, S.G.: Compressive strength characteristics for deep mixing method, Ph. D. thesis of L. N. Gumilyov Eurasian National University, Republic of Kazakhstan (2010)
8. Kim, Y.S., Choo, J.H., Cho, Y.S.: Applicability study on deep mixing for urban construction. *J. Korea Academia-Ind. Cooperation Soc.* **12**(1), 500–506 (2011)
9. Park, C.S.: Stability improvement effect of quay wall foundation ground using DCM lift injection method, Ph. D. thesis of Incheon National University, Republic of Korea (2017)
10. Jang C.S.: Elasto-plastic analysis of step underground excavation (SUNEX) manual 13th edition for ver. w6.16., Geogroup Eng. (2015)
11. Oh, J.W.: Program on the design of propped retaining walls for excavation by numerical method (EXCAV) manual ver. 2.51, Korean Geo-Consultants (2004)
12. Das, B.M., Sobhan K.: Principles of Geotechnical Engineering, Cengage Learning (2014)
13. ASTM D2435: Standard test method for one-dimensional consolidation properties of soils. In: Annual Book of ASTM Standards, 04.08, pp. 246–260 (2014)

Sustainable Remediation of a Dumpsite



P. Sughosh, N. Anusree, B. Prathima, and G. L. Sivakumar Babu

Abstract The current practices of containing the waste in dumpsite/landfill are considered as unsustainable due to their negative impact on the environment, society and economy. Remediation of the existing open dumpsite into bioreactor landfills helps in recovering the valuable land area at a faster rate due to the reduction in the time required for waste stabilization process. The problem of leachate treatment can also be addressed effectively during the remediation process. Therefore, remediating an existing dumpsite can be classified as an approach towards achieving the sustainability in landfilling practices. In this study, an approach for remediating an existing municipal solid waste (MSW) dumpsite in Bangalore city is presented by addressing the three major aspects, viz., landfill gas (LFG), leachate and the recovery of air space. Modelling tools are used to estimate the LFG emission and to design the leachate collection and recirculation systems. The methane oxidation potential of the digested MBT waste as a biocover material is evaluated using column experiments. The biocover systems are then designed to mitigate the LFG emissions from the dumpsite.

Keywords Sustainability · Landfill gas · Leachate recirculation · Biocovers

1 Introduction

As per the United States Environmental Protection Agency (US EPA 2008) [1], “Sustainability creates and maintains the conditions under which humans and nature can exist in productive harmony, which permits fulfilling the social, economic and other requirements of present and future generations”. Any process, product or technology can be deemed as sustainable when its impact on the social,

P. Sughosh

Jawaharlal Nehru National College of Engineering, Shimoga, Karnataka 577204, India

N. Anusree · B. Prathima · G. L. Sivakumar Babu (✉)

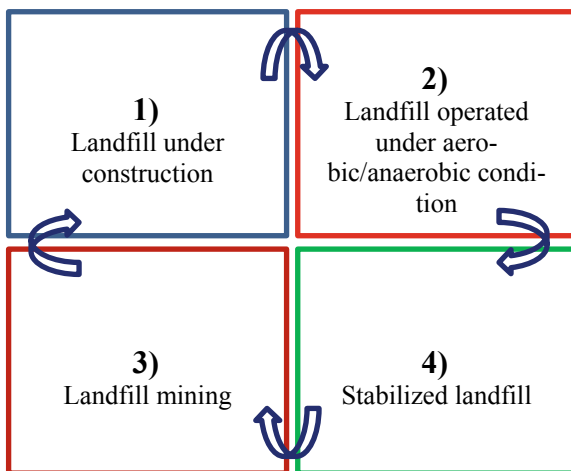
Indian Institute of Science, Bangalore, Karnataka 560012, India

e-mail: gl@s@iisc.ac.in

economic and the environmental aspects is well balanced to create harmony between humans and the nature. The current waste management practices followed in low- and middle-income countries predominantly consist of disposal of municipal solid waste (MSW) in the dumpsites and the landfills [2]. Dumping or land-filling of MSW directly impacts all the three components of the environment, viz., atmosphere (landfill gas emission), hydrosphere (leachate contamination of the groundwater table) and lithosphere (leachate and MSW contaminate the soil) and can be deemed as unsustainable practice. Such practices also ignore the economic value of the waste as the energy and nutrient content of the MSW remain generally untapped. Improvement in the overall sustainability of the landfilling process can be attained by addressing the three major aspects, viz., mitigation of landfill gas (LFG), leachate treatment and the recovery of air space. The above features can easily be incorporated in a new MSW treatment facility consisting of a bioreactor landfill. From the sustainability perspective, bioreactor landfills are preferred to the open dumpsites and conventional landfills due to the social, economic and environmental considerations [3, 4]. In bioreactor landfills, provisions are made for leachate collection through under drainage system, leachate recirculation and collection of landfill gas from the inception stage itself. The schematic representation of the sustainability concept in landfill engineering is shown in Fig. 1. In this concept, the waste treatment facility primarily consists of four bioreactor landfills operating at different waste stabilization phases. After complete stabilization of waste, the biomining activity is carried out before repeating entire process again. Additionally, all the other features which minimize the impact on environment are incorporated in this approach.

The open dumpsites lack the features of bioreactor landfills, and adopting the same for the existing dumpsites would not be possible. Alternatively, open dumps can be retrofitted by providing vertical or horizontal wells to collect and recirculate

Fig. 1 Sustainable landfilling approach



the leachate and by designing biocover systems to mitigate the landfill gas emissions.

The MSW management rules of 2016 have mandated for the remediation of the existing dumpsites in the country which is in turn a step towards achieving the sustainability in waste management practices. With this in perspective, the sustainable remediation of existing dumpsites for the Indian context is explored in this study. The overall objectives of the study are given below.

- Suggest a remediation plan for an existing MSW dumpsite of Bangalore city by providing an approach for the design of the,
 - Leachate collection and recirculation system,
 - Biocover system for controlling landfill gas emission.

2 Methodology

2.1 Site Description

Several dumpsites are being used by the Bangalore municipality for the disposal of MSW generated from the city. Based on the observations made during the site visits, it can be concluded that the problems encountered at these dumpsites are of the same type. Therefore, the approach suggested in this study is also applicable to most of the other dumpsites in Bangalore. In this study, a typical landfill of 4 acres in area and 10–20 m in depth with the liner system is considered. Total unsegregated municipal solid waste of around 1,00,000 tons is assumed to be dumped during the active landfilling phase (between the year 2017 and 2018). The site description for Bangalore dumpsite considered in this study is given in Table 1.

The problems associated with the dumpsites that were observed during the site visits are as follows. Majority of the landfills in Bangalore do not have the leachate or the gas collection systems. The landfill site considered in the study does not have a cover system, but a proper liner system is present at the bottom. The waste is dumped directly on the liners and is not compacted to achieve the target density of

Table 1 Site description for Bangalore dumpsite

Features of study area	
Year of start	2017
Year of closure	2018
Average waste intake (tones/year)	50,000
Area (acres)	4
Average height (m)	10–20
Precipitation (mm)	905

MSW. The provision for the leachate or the landfill gas collection systems is absent. Therefore, the waste contained in the landfill gets saturated during the rainy season and thus increases the risk of groundwater contamination. High leachate head was observed during the site visit (almost up to the surface). The LFG emissions are not controlled, which may cause fire hazards and contribute to global warming.

2.2 Sustainable Approach

The goal of the sustainable approach is to remediate/operate the dumpsite in a way that reduces the human and environment risk in a cost-effective manner. The sustainability approach suggested in this study includes:

- Landfill gas emission control,
- Leachate collection system,
- Leachate recirculation system,
- Biomining and land space recovery.

2.3 Landfill Gas Emission Control

LandGEM model version 3.02 developed by USEPA is used to estimate the total landfill gas emissions from landfill site. The model parameters required for the estimation of LFG generated are the waste intake time duration, capacity of the landfill, methane generation rate (k , year^{-1}), methane generation capacity (L_0 , m^3/Mg) and waste acceptance rate [5]. The MSW composition affects the values of methane generation rate and methane generation capacity. The MSW composition of Bangalore and the derived composition of the MSW used for estimation of ultimate methane yield are given in Tables 2 and 3 respectively.

Table 2 MSW composition of Bangalore [6]

Waste type	Composition in percentage
Fermentable	72
Paper and cardboard	11.6
Cloth, rubber, PVC, leather	1.01
Glass	1.43
Polythene/plastics	6.23
Metals	0.23
Dust and sweeping	6.53
Others	–

Table 3 The composition of waste along with the moisture content and ultimate methane yield of each MSW fractions

Waste category	Percentage composition (% wet weight basis) ^a	Moisture content (%) ^b	Ultimate methane yield L ₀ (m ³ CH ₄ /dry Mg refuse) ^c
Paper	11.6	10	132.8
Textile	1.01	20	14.8
Compostable	72	45	145.1

^a% composition from Chanakya et al. [6]

^bMoisture contents from IPCC Guidelines for National Greenhouse Gas Inventories [7]

^cLo (m³ CH₄/dry Mg refuse) based on values from Staley and Barlaz [8]

2.4 Methane Oxidation Experiment in Biocovers

Cover system in landfills aids in reducing odour, vectors, flies and helps in the control of storm water and leachate. In addition to these, biotic system helps in converting methane gas into carbon dioxide by oxidation when landfill gas is passed through it. This process is achieved by the action of a group of microorganism known as methanotrophs [9]. The most widely used biotic systems are biofilters, biowindrows and biocovers. Column studies were conducted in laboratory to explore the potential of the mechanically biologically treated waste as an effective biocover material.

The MBT waste used for experiments was collected from Mavallipura landfill site and was anaerobically digested for 470 days. The details pertaining to waste sampling, characteristics and anaerobic treatment are given in Lakshmikanthan [3]. The methane oxidation studies were carried out in a PVC column of 15.4 cm diameter and 100 cm in height. The schematic diagram of the setup is shown in Fig. 2.

A gravel bed of 100 cm was placed at the bottom of the column which acted as a support and as the gas distribution layer. A geonet layer was placed above this, and the media was filled in five layers of 5–10 cm thick. 99.95% CH₄ gas was fed to the bottom of the column, and a constant flow rate of 13.6 mL/min was maintained by using rotameter. At the top headspace of the column, a humidified air flow of 100–300 mL/min was maintained to simulate the atmospheric boundary condition. Both the methane and air flow rates were periodically checked by using bubble flow meters. The experiment was conducted at room temperature. A provision for collecting the gas sample for the column was made with the help of a septa arrangement connected to a narrow 1-mm-diameter pipe embedded in a fine cloth to filter the dust particles. This arrangement was placed all along the depth of the column. The gas samples were analysed using gas chromatograph for CO₂, O₂, N₂ and CH₄ concentration. The quality of gas was measured by manual injection of the sample into a portable gas chromatograph (Make–Mayura Analyticals, BGA-Model) with thermal conductivity detector and hydrogen as the carrier gas (30 mL/min flow rate). The HayeSep-A and molecular sieve columns were used in

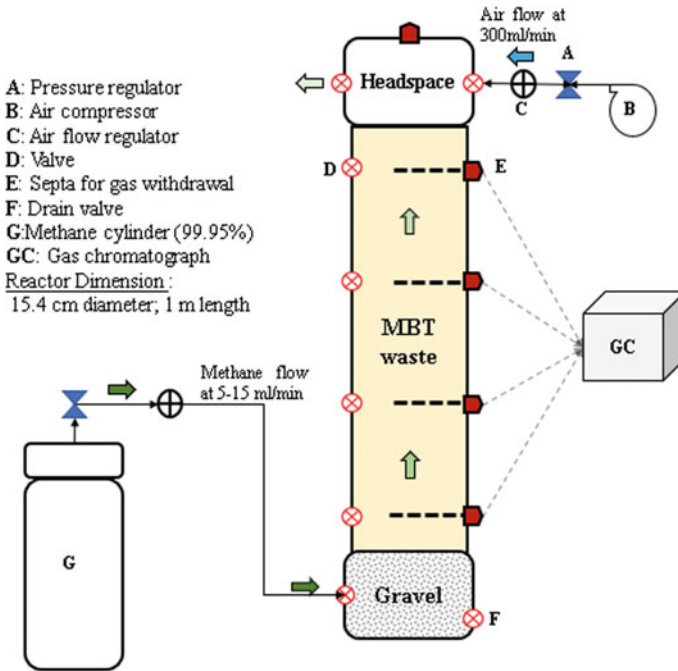


Fig. 2 Schematic diagram of column experiment for methane oxidation in biocovers (Reprinted from sughosh et al. [10]. With permission from ASCE)

series to get a clear separation of CO_2 , O_2 , N_2 and CH_4 gases. Calibration using the standard biogas mixture was performed before each test. The chromatographs were analysed using Peak ABC software.

2.5 Leachate Collection and Recirculation System

Quantification of leachate generated

Visual Hydrologic Evaluation of Landfill Performance (HELP) model developed by US Army corps is used to estimate amount of leachate generated in landfill site. It is quasi-two-dimensional hydrologic model of water movement across, into, through and out of landfills. Landfill systems including various combinations of vegetation, cover soils, waste cells, lateral drain layers, low permeability barrier and geomembrane liners can be modelled. The average head above the liner and the volume of leachate generated was estimated for the existing site condition. The input data for Bangalore weather conditions are used from the repository of the software. The bulk density and field capacity of the waste were 521 kg/m^3 and 0.3, respectively. Table 4 shows the three different conditions considered for analysis in HELP model.

Table 4 Conditions used in the HELP Model to estimate the leachate quantity

Layers considered in HELP model	Run 1—existing site condition	Run 2—leachate collection and removal	Run 3—leachate collection and 50% recirculation	Thickness of each layer (m)
Surface water settings	Bare soil	Bare soil	Bare soil	
1. Vertical percolation layer	Loamy fine sand	Loamy fine sand	Loamy fine sand	0.3
2. Vertical percolation layer	Municipal solid waste	Municipal solid waste	Municipal solid waste	15
3. Lateral drainage layer	Gravel without drainage	Gravel with drainage	Gravel with drainage and 50% recirculation to layer 1	0.3
4. Geomembrane layer	HDPE	HDPE	HDPE	0.001
5. Barrier soil liner	Clay	Clay	Clay	1.0

Horizontal trenches were considered for the design of leachate recirculation system (LRS). Hydrus 2D was used to estimate the number and the spacing of trenches in the landfill. The properties of fresh waste such as hydraulic conductivity and unsaturated properties were taken from Reddy et al. [11] and Wu et al. [12], respectively.

3 Result and Discussion

3.1 Landfill Gas Generation

The maximum total landfill gas and methane flux calculated are 5.266×10^5 and 2.633×10^5 m³/year, respectively. The output of the LandGEM model is given in Fig. 3.

Biocover

Biocovers are used to reduce the potential impact of direct emission of methane to the atmosphere. Biocovers systems are economically feasible and are generally used in place of the gas extraction or flaring systems, especially in the landfills with low methane emission rates.

Figure 4 shows the methane oxidation rates (MOR) calculated from the column experiment as a function of depth. The oxidation efficiency at 20 cm depth was much higher than at the bottom layers. These higher oxidation efficiencies indicated the presence of CH₄-oxidizing bacterial community in the top layers. A decrease in oxidation efficiency was observed with depth and indicated the extent of the oxic zone in the cover material. Maximum oxidation rates of 81.21% were observed in the top layers of the columns where oxygen availability was highest.

The design of biocover system involves determining the methane emission rate at the landfill site and the laboratory-scale studies to estimate the methane oxidation

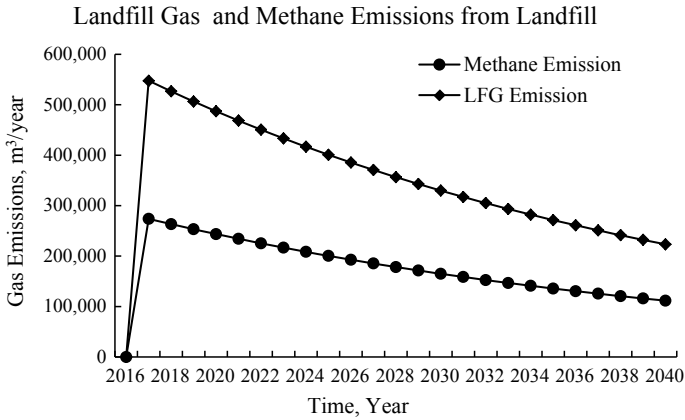


Fig. 3 Total landfill gas and methane gas emission from Landfill (Reprinted from sughosh et al. [10]. With permission from ASCE)

potential of the selected biocover material. From the column studies, the biocover system has a methane oxidation efficiency of 81.21% for a flux rate of 700.35 g/m²/d. Therefore, an area of 848 m² is required to construct a biowindrow system. The digested MBT waste of 0.8 m depth with a moisture content of 30% compacted to a bulk density of 750 kg/m³ is sufficient to oxidize the methane emission from the dumpsite.

Biowindrows of 53 × 53 m × 0.8 m can be provided and will be sufficient to reduce the methane emissions from the entire landfill. Some of the other major factors affecting the performance of such bio windrows at field condition include climatic conditions (temperature, precipitation, etc.), moisture content, landfill gas composition and the gas application rate.

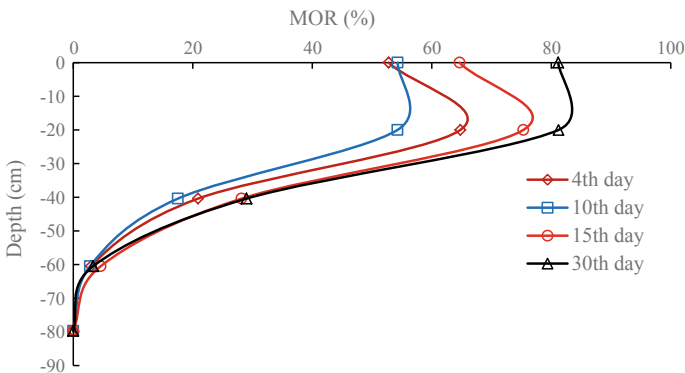


Fig. 4 Methane reduction potential with respect to depth (Reprinted from sughosh et al. [10]. With permission from ASCE)

3.2 Leachate Generation

The Visual HELP model was run and the yearly variation in the precipitation, evaporation, runoff, lateral drainage from layer 3 (lateral drainage layer), recirculation rate and percolation or leakage through layer 5 (barrier soil liner) were analysed for the three conditions stated below.

(a) Existing site condition

Figure 5 represents the analysis result, and the average leachate head by the end of the first year was around 2.28 m against the prescribed limit of 0.3 m (USEPA, 2004). By the end of 10 years, the value reached 15.4 m. These conditions greatly affect the stability and degradation of waste. The potential risk of groundwater contamination is also high under these conditions.

(b) Leachate collection and removal

A drastic decline in leachate head is observed when the leachate is drained from the landfill (Fig. 6). The percolation or leakage through layer 5 reduces in comparison with the previous case. This clearly indicates that draining the leachate out of the landfill decreases the risk of groundwater pollution.

(c) Leachate collection and 50% recirculation

The leachate head increased marginally in this condition but is within the permissible limit. Recirculation of leachate enhances the waste degradation rate and

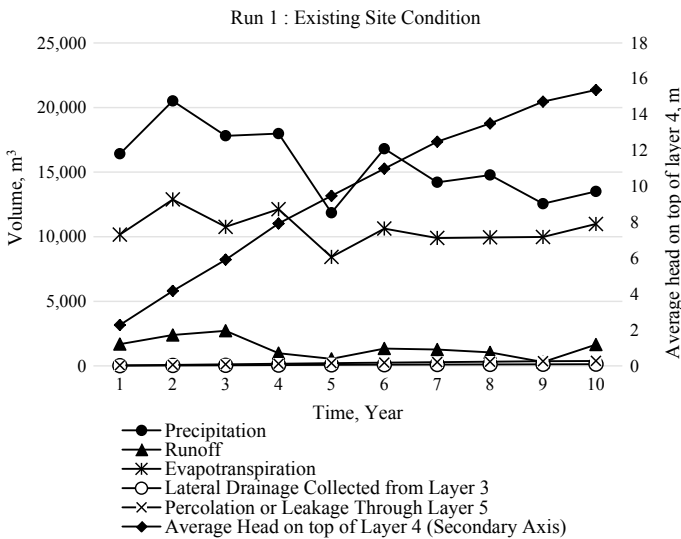


Fig. 5 HELP Model output for existing landfill site condition (Reprinted from sughosh et al. [10]. With permission from ASCE)

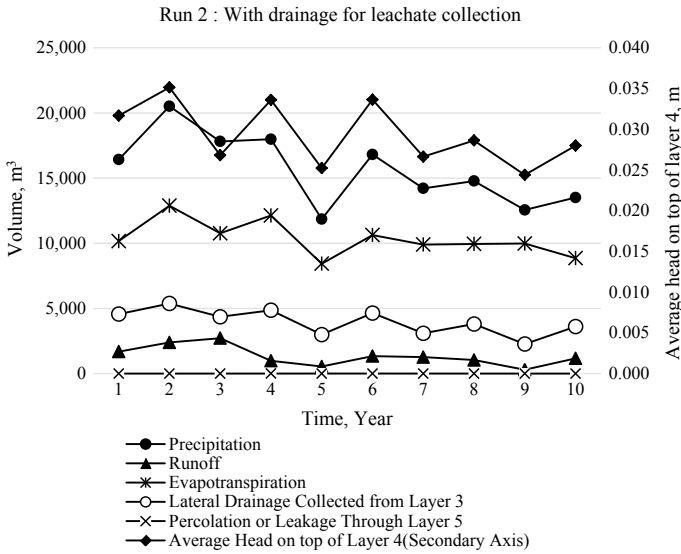


Fig. 6 HELP model output for leachate drainage and collection (Reprinted from sughosh et al. [10]. With permission from ASCE)

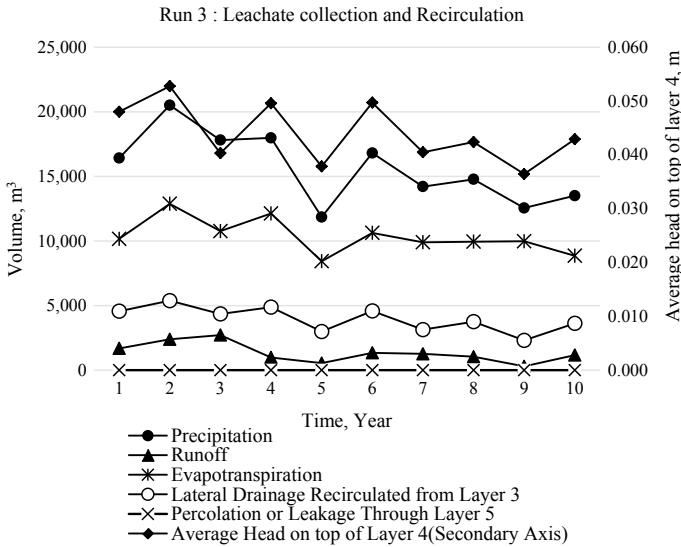


Fig. 7 HELP model output for leachate collection and 50% recirculation (Reprinted from sughosh et al. [10]. With permission from ASCE)

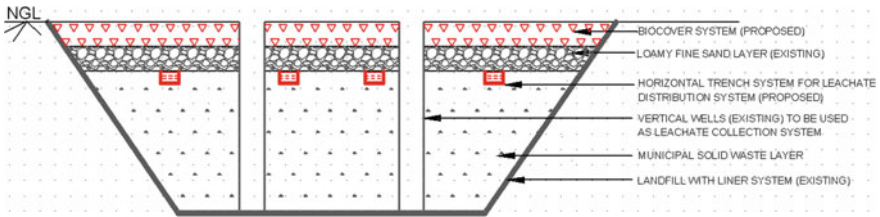


Fig. 8 Schematic diagram for retrofitting an existing dumpsite in Bangalore city (Not to scale). (Reprinted from sughosh et al. [10]. With permission from ASCE)

reduces the time required for stabilization of the waste. From Fig. 7, it is evident that with 50% leachate recirculation, the average leachate head on the liner reduces and, in the process, enhances the biodegradation of waste (Fig. 8).

Design of leachate recirculation system

Hydrus 2D result shows that the horizontal trenches with a recirculation rate of $5.5 \text{ m}^3/\text{day}$ are efficient enough to saturate the waste with a moisture content of 70% up to a distance of 10 m. Therefore, a total of 52 horizontal trenches of $10 \text{ m} \times 0.6 \text{ m} \times 1 \text{ m}$ dimension distributed through the landfill area are sufficient to maintain the required moisture content in waste.

4 Conclusion

The study presents the approach to convert the existing dumpsite into sustainable landfill. This can be carried out by the design of leachate collection, recirculation and biocover systems. The recirculation of the leachate can be achieved by providing 52 horizontal trenches. The landfill gas emission can be prevented by providing bio windrows of size $53 \times 53 \times 0.8 \text{ m}$. Even though the features provided to improve the performance of the landfills are site-specific, the approach presented here can easily be applied to most of the other dumpsites in India with minor modifications.

References

1. US EPA. <https://www.epa.gov/landfills/bioreactor-landfills>. Last accessed 22 Jan 2019
2. Hoomweg, D., Bhada-Tata, P.: What a waste: a global review of solid waste management. Urban development series knowledge papers no. 15. The World Bank, Washington, DC (2012)
3. Lakshmikanthan, P., Sivakumar Babu, G.L.: Performance evaluation of the bioreactor landfill in treatment and stabilisation of mechanically biologically treated municipal solid waste. *Waste Manag. Res.* **35**(3), 285–293 (2017)

4. Sughosh, P., Anusree, N., Sivakumar Babu, G.L.: Life cycle analysis as a tool to assess the sustainability of waste management practices in Bangalore City. *Geo-Congress 2019: Geoenvironmental Engineering and Sustainability 2019*. Reston, VA: American Society of Civil Engineers (2019)
5. Alexander, A., Burklin, C.E., Singleton, A.: Landfill gas emissions model (LandGEM) version 3.02 user's guide. US Environmental Protection Agency, Office of Research and Development (2005)
6. Chanakya, H.N., Ramachandra, T.V., Shwetmala, K.: Towards a sustainable waste management system for Bangalore. In: 1st International Conference on Solid Waste Management and Exhibition on Municipal Services, Urban Development, Public Works IconSWM. Kolkata, India (2009)
7. Eggleston, S., Buendia, L., Miwa, K.: IPCC guidelines for national greenhouse gas inventories. Institute for Global Environmental Strategies, Kanagawa, Japan (2006)
8. Staley, B.F., Barlaz, M.A.: Composition of municipal solid waste in the United States and implications for carbon sequestration and methane yield. *J. Environ. Eng.* **135**(10), 901–909 (2009)
9. Gebert, J., Groenroeft, A.: Passive landfill gas emission—influence of atmospheric pressure and implications for the operation of methane-oxidising biofilters. *Waste Manag.* **26**(3), 245–251 (2006)
10. Sughosh, P., Prathima, B., Murali Arunkumar, Anusree, N., Sivakumar Babu, G.L.: Remediation of typical municipal solid waste dumpsite in Bangalore City. *J. Hazard. Toxic Radioactive Waste.* **25**(1), (2021)
11. Reddy, K.R., Hettiarachchi, H., Parakalla, N.S., Gangathulasi, J., Bogner, J.E.: Geotechnical properties of fresh municipal solid waste at Orchard Hills Landfill, USA. *Waste Manag.* **29**(2), 952–959 (2009)
12. Wu, H., Wang, H., Zhao, Y., Chen, T., Lu, W.: Evolution of unsaturated hydraulic properties of municipal solid waste with landfill depth and age. *Waste Manag.* **32**(3), 463–470 (2012)
13. Tolaymat, T., Kremer, F., Carson, D., Davis-Hoover, W.: Monitoring Approaches for Landfill Bioreactors. National Risk Management Research Laboratory, Office of Research and Development, Ohio (2004)

Micro-structural and Mineralogical Studies to Evaluate the Effectiveness of Industrial Solid Wastes for Stabilization of Expansive Soils



H. N. Ramesh, B. V. Manjunatha, and Madhavi Gopal Rao Kulkarni

Abstract Expansive black cotton soils undergo large volume changes due to swell and shrinkage due to seasonal moisture fluctuations during wet and dry seasons causing severe problems to lightly loaded structures, such as buildings, pavements and pipelines founded on them. Before undertaking any construction activity, the foundation soil should be properly stabilized. The best way to overcome the problems associated with the expansive soil is by stabilization with pozzolanic materials such as hydrated lime and Portland cement stabilization. However, as they may not be economical as well as to reduce the problem of disposal, many industrial and agro-industrial wastes such as rice husk ash (RHA), and bagasse ash (BA) and carbide lime (CL) which resemble the properties of lime and cement can be effectively utilized. While they have reactive silica, they may not have sufficient lime to produce pozzolanic compounds; another waste CL rich in calcium can be amended along with these solid wastes to soil to develop durable strength. Optimization of rice husk ash and bagasse ash contents is determined based on uncompressive strength tests. Strength tests carried out by mixing black cotton soil with various percentages of RHA and BA optimum dosages found are 20% and 15% for RHA and BA, respectively. Both RHA and BA are composed of silica content, and the strength improvement with respect to these additives without CL is marginal due to lack of lime content in them strength, thus enhancing considerably by adding carbide lime. Moulding water content also plays important role in pozzolanic stabilization. A series of strength tests were performed by mixing the black cotton soil with RHA, BA, CL and lime at different water contents and

H. N. Ramesh

Department of Civil Engineering, Bangalore University, Bengaluru 560056, India
e-mail: rheddur@yahoo.com

B. V. Manjunatha · Madhavi G. K. (✉)
Bangalore University, Bengaluru 560056, India
e-mail: madhavit98@gmail.com

B. V. Manjunatha
e-mail: manjunathmbv@gmail.com

Madhavi G. K.
Presidency University, Bengaluru, India

densities compacted with same compactive energy. The strength developed with moulding water content on dry side of optimum condition is more due to the existence of flocculated structure on dry side of optimum condition. The mechanism of strength improvement has been elucidated through microstructural analysis using SEM and XRD studies.

Keywords Bagasse ash · Compaction · Expansive black cotton soil · Minerals · Structure · Unconfined compression strength

1 Introduction

Expansive soils exhibit swell and shrink behaviour along with variation in moisture content owing to the presence of montmorillonite clay with high cation exchange capacity. Thus, structures founded on these soils experience severe damages due to high settlements and low bearing capacity. The problem is particularly severe on structures such as canal lining, pavements and light loads. Improvement of the foundation soil becomes inevitable as the option of replacing the foundation with suitable soil becomes tedious uneconomical and involves huge delay. The most viable and sustainable option is by pozzolanic stabilization. Calcium ions and clay particles react together to form strong cementitious bonds which bind the clay particles and improve the strength and reduce the compression [1]. With lime addition to soil, the swelling potential, liquid limit, plasticity index and maximum dry density of the soil are reduced with increase in optimum water content, shrinkage limit and strength. To conserve conventional stabilizers such as lime and cement and to avoid the disposal solid waste with potential to stabilizers, various materials such as steel slag, mine tailings, carbide lime and rice husk ash can be used alone or as admixtures. Optimization of these additives for effectiveness is important and has been studied in this paper. The solid wastes considered are rice husk ash (RHA), bagasse ash (BA) and carbide lime (CL).

The processing of sugar cane in sugar mills generates about 26% of bagasse and 0.62% of bagasse ash per every tonne of sugar produced [2] and is available in large quantities. Bagasse ash can be utilized in several viable ways [3, 4]. Rice husk ash is produced when rice husk is burnt which is also available in large quantities in agricultural countries such as India. RHA contains high reactive silica, which can be effectively used in the stabilization process as a pozzolanic material, but it cannot be used alone for stabilization due to lack of lime content [5, 6]. Carbide lime (CL) is the bi-product of acetylene gas industry and is formed by hydrolysis of calcium carbide [7], and it resembles the properties of lime as it contains high amount of calcium hydroxide. It is reported that carbide lime-treated soil yields higher strength than the lime-stabilized soils [8]. The application of RHA and CL for the field applications can be economical. RHA has been used as an artificial cohesive non-swelling (CNS) layer for lightly loaded structure such as foundation and soil subgrade [9]. Similarly, CL-stabilized soil subgrade show high bearing

capacity and high resilient modulus than quick lime and more economical than quick lime [10]. In this paper, admixtures of these wastes to impart good strength of expansive soil are studied.

Field density and water content are important variables, and they play important role in the stabilization of soils, particularly in their relationship with compaction compactions parameter. The effectiveness of stabilization at various stabilizers and their admixtures at different water content and densities is studied as function of these parameters at a compactive energy corresponding to Proctor's energy.

2 Materials and Methods

2.1 *Materials: The Source of Soil Collected and Their Characteristics as Well as Those of Admixtures Used Are Presented in This Section*

Black Cotton Soil Expansive black cotton soil was collected from Hosakatti village, 25 kms from Hubli, Karnataka, India, from a construction site by an open excavation at a depth of 2 m below the ground level. The soil passing through 425 micron BIS sieve, air dried and pulverized in the ball mill. Soil is classified as clays of high plasticity (CH) according to Bureau of Indian Standard (B.I.S).

Bagasse Ash (BA) Bagasse Ash is collected from Koppa sugar industry, Mandya district, Karnataka, India. Bagasse ash is collected from conveyor belt of sugar industry, and the organic content bagasse ash is removed by burning in oil-fired furnace at Technomet Solutions, Peenya industrial area at a temperature of 600⁰ Centigrade for 8 h. The ash has a 66% silica, 12% alumina and CaO of 5.6%.

Rice Husk Ash (RHA) Rice Husk Ash was collected from Davanagere District, Karnataka State. Rice husk ash produced from this rice mill is having particle size less than 425 micron and is directly used after oven drying for a period of 24 h. RHA is rich in silica (85%) and low in calcium (CaO of 1%).

Carbide Lime (CL) Carbide Lime used in this study is collected from an oxy-acetylene gas welding plant near Gottigere Hobli of Bangalore urban District in Karnataka State. The carbide lime used in the study is collected from fresh deposit in the disposal region. The physical properties and chemical composition of carbide lime are presented in Table 1. Carbide lime is rich in CaO (83%) and low silica (5.7%).

The commercially available hydrated lime has a minimum assay of 90% of Ca (OH)₂.

The physical properties of soil, BA and RHA are summarized in Table 1.

Table 1 Physical properties of soil, BA and RHA

Property	Soil	BA	RHA
Colour	Black		Grey
Specific gravity	2.65	1.71	1.95
Sand (4.75–0.075 mm) (%)	4	12.0	Nil
Silt (0.075–0.002 mm) (%)	36	66.4	72
Clay (<0.002 mm) (%)	60	–	18
Liquid limit (%)	91	61	
Plastic limit (%)	39	–	
Plasticity index (%)	52	–	
Shrinkage limit (%)	11	–	
Optimum moisture content (%)	32	43	
Max. dry unit weight (kN/m ³)	12.95	10.3	
Unconfined compressive strength (kPa)	180	–	

2.2 Methodology

The test procedures to conduct various laboratory tests are briefly described.

Preparation of Dry Soil Sample The dry samples for various tests have been prepared as per the procedure [11]. The fraction of soil passing through 425 micron has been used for the determination of Atterberg's limits. **Water content** of the soil has been found out as per as per the procedure [11]. **Specific gravity** soil has been found out by density bottle as per as per the procedure [11]. **Atterberg's limits** have been determined as per the procedure [11]. The soil is sieved through 425 micron BIS sieve.

Compaction Test The compaction test has been carried out using mini compaction test apparatus as per the procedure given by Sridharan and Sivapullaiah [12].

Unconfined Compression Test Unconfined compressive strength (UCS) tests are performed as per the procedure [13]. A constant strain rate of 1.25 mm/minute is maintained for the testing of specimens. The tests have been carried out for three similar specimens, and peak stress values reported are the average.

Preparation of samples for determination of un-compressive strength at Proctor's optimum conditions and at different moulding water contents and dry densities

Two series of tests are conducted: (1) to arrive at optimum additive contents and (2) to determine the role of moulding water content and dry density.

For the first series, the soil is mixed with varying additive contents and compacted at Proctor's optimum water content and compacted to maximum dry density and their UCS determined without any pre-curing and after curing for one week and optimum content obtained.

Table 2 Compaction parameters of black cotton soil treated with bagasse ash and lime chosen for strength tests

Mixture	Dry of optimum		Optimum		Wet of optimum	
	Unit weight (kN/m ³)	Water content (%)	Unit weight (kN/m ³)	Water content (%)	Unit weight (kN/m ³)	Water content (%)
B.C soil alone	12.30	26	12.95	32	12.3	38
B.C soil + 15% BA	12.75	30	12.75	33	12.75	35
B.C soil + 15% BA + 4% lime	11.82	28	12.45	35	11.82	41

Table 3 Compaction parameters of BC soil and RHA treated with CL compacted at three significant moulding water contents

Combination	Dry of optimum		Optimum		Wet of optimum	
	Dry unit weight kN/m ³	Moisture content (%)	Dry unit weight kN/m ³	Moisture content (%)	Dry unit weight kN/m ³	Moisture content (%)
BC soil alone	12.30	24	13	32	12.30	40
BC soil + 20% RHA	12.11	28	12.75	34	12.11	40
BC soil + 20% RHA + 8% CL	11.74	30	12.36	36	11.74	42

For the second series, the soil is mixed with optimum amount of additive/admixtures at three different water contents, viz., at optimum, dry side and wet side of optimum and compacted to their respective dry density corresponding to the same compactive effort. Their UCS is determined without any precuring and curing for one week. The moulding water content and density used for this series are given Tables 2 and 3.

3 Results and Discussion

3.1 Bagasse Ash and Lime

Addition of bagasse ash improved the strength of soil marginally without any precuring. Even though the samples were tested without any precuring, a marginal improvement in strength is observed probably due to some time elapsed during mixing and sample preparation before the test is performed by the pozzolanic reaction that would have taken place between reactive silica and free lime content of bagasse ash (5% bagasse ash) present in it as it is reported in case of stabilization of soil with lime alone [14]. Further improvement in strength is observed when bagasse ash is added up to 15%. However, with further increase in BA, reduction in

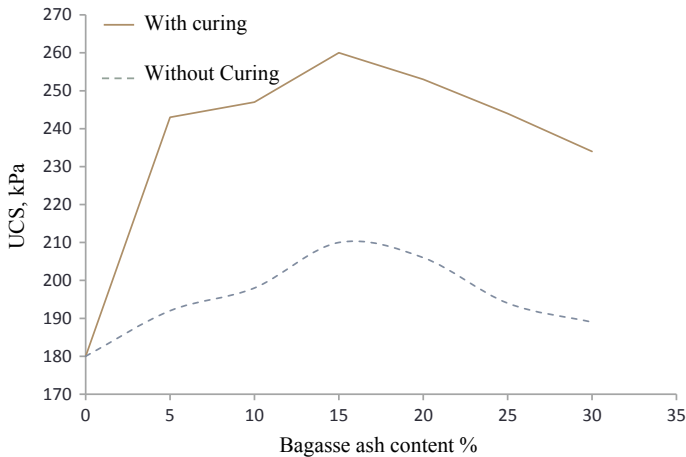


Fig. 1 Variation of unconfined compressive strength of soil with varying bagasse ash contents on without curing and with 7 days of curing

strength is seen as shown in Fig. 1. This may be due to insufficient clay available for reaction with increased amounts of reactive silica and lime [3]. With any BA, content improvement in strength is seen with curing for 7 days of curing period. Even after curing, the strength does not increase beyond 15% of BA addition. Thus, the optimum BA content for the soil used is taken as 15%.

With the addition of optimum dosage of bagasse ash, the strength improvement is not significant; hence, lime is added to soil and bagasse ash mixture to bring about enhanced pozzolanic reaction. In the presence of water, calcium from lime reacts with silica and alumina from bagasse ash and clay, forming cementitious compounds calcium silicate hydrate and calcium aluminate hydrate (CSH and CAH). Due to the formation of these pozzolanic compounds, the strength properties of soils are enhanced. Addition of 1% lime to BC soil–optimum bagasse ash mixture, increase in the strength of 29% is observed on immediate testing as shown in Fig. 2. This is because of formation of C-S-H amorphous compound with an amorphous structure. With the further increase in lime content up to 4%, the strength increased. Beyond 4% lime content, decrease in strength is observed, and this may be due to the insufficient amount of clay particles for complete utilization of pozzolanic compounds formed such as C-S-H gel. Thus, optimum lime content for the soil with 15% of BA is taken as 4%. The lime content at which the predominant formation of C-S-H amorphous compound ceases corresponds to the optimum lime content [15]. After 7 days of curing, further improvement in strength has been observed, and at 5% of lime content, the strength improved fivefolds compared to that of the soil bagasse ash mixture because pozzolanic reactions are time dependent. With the further increase in lime up to 5%, the strength increased and the rate of strength improvement decreased beyond 4% of lime content, and hence, 4% lime is chosen as the optimum dosage in the present investigation.

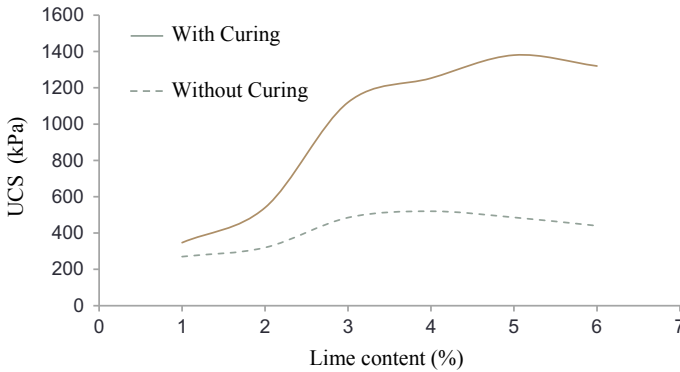


Fig. 2 Variation of UCS of soil and bagasse ash mixture with varying lime content on without curing and after curing for 7 days

3.2 Rice Husk Ash and Carbide Lime as Stabilizers for BC Soil

Studies are also conducted on soil with RHA alone and with CL as admixture.

The type of studies conducted is similar to those conducted with BA and lime except that in this case, instead of commercial lime, CL is used as admixture to supplement calcium ions. The studies revealed that the optimum RHA content with and with CL is 20%. Also, the increase in the strength at any RHA content is more after curing than the samples tested without curing. Addition of CL further increases the strength with or without curing. The optimum CL content is found to be 8%.

3.3 Influence of Moulding Water Content and Dry Density on Strength Properties of Expansive Black Cotton Soil

Strength properties of expansive BC soil treated with bagasse ash and lime compacted at moulding water contents The dry unit weight and water content at dry of optimum, optimum and wet of optimum conditions have been selected based on compaction test results of the respective combinations on either side of the compaction curve. The water contents corresponding to 95% of maximum dry unit weight are selected on the dry side and wet side of optimum, and the corresponding values of water content and dry unit weight values are given in Table 2.

Effect of Bagasse ash and lime on strength properties of Black cotton soil compacted at different moulding water content The strength parameter of expansive soil treated with optimum dosage of bagasse ash is as shown in Fig. 3.

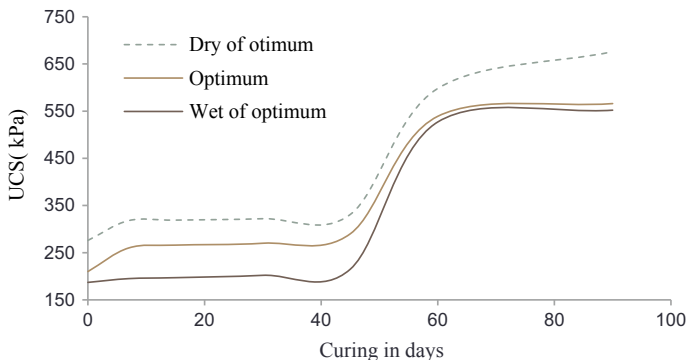


Fig. 3 Variation of strength properties of soil treated with bagasse ash compacted at different moulding water contents with curing period

The strength of black cotton soil, with the addition of optimum dosage of bagasse ash, increased from immediate testing to 90 days of curing period at dry of optimum and at wet of optimum conditions. It can be observed that the strength of black cotton soil–bagasse ash composite on dry side of optimum is more significant as compared to optimum and wet of optimum conditions. This may be attributed to the flocculation of particles which is more significant on dry side of optimum. Flocculation of particles takes place for the soil with the addition of bagasse ash because of the pozzolanic reaction between silica and alumina of soil and bagasse ash mixture and also free lime content present in bagasse ash. Since the unconfined compressive strength will be different at different water contents, to assess an increase in strength due to pozzolanic reaction, the study of strength properties at dry of optimum, optimum and wet of optimum conditions is essential [14].

The strength of expansive soil and bagasse ash mixture treated with lime varied from dry of optimum to wet of optimum conditions without curing. With an increase in curing period up to 90 days, the strength increased for the samples compacted at dry of optimum, optimum and wet of optimum conditions, respectively, is as shown in Fig. 4. This may be attributed to the reaction between reactive silica of soil and bagasse ash mixture and lime producing cementitious products. With further curing up to 90 days, significant improvement in strength of 3.73, 3.7 and seven folds is seen at dry of optimum, optimum and wet of optimum conditions, respectively, which may be attributed to the cluster of cementitious compounds with curing and also pozzolanic reactions which are time dependent.

Effect of Rice husk ash and carbide lime on strength properties of Black cotton soil compacted at different moulding water content Specimens were moulded for three significant combinations of moisture content and corresponding dry unit weight. The dry unit weight and moisture content adopted for BC soil are shown in Table 3. Unconfined compressive strength is determined immediately after moulding and after curing for 7, 30, 60 and 90 days. During the process of curing, specimens were stored in desiccators under relative humidity of 100%.

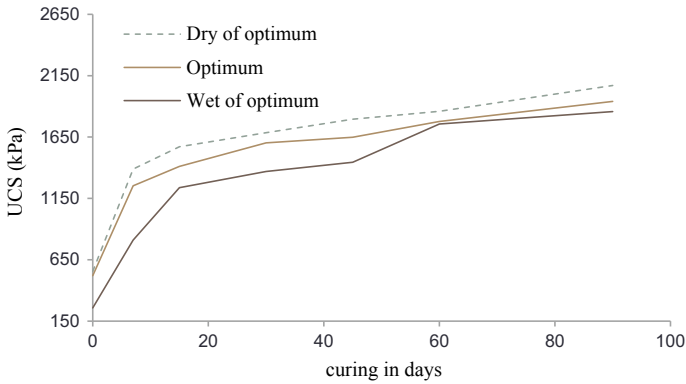


Fig. 4 Variation of strength of soil and bagasse ash mixtures treated with lime compacted at different moulding water contents with curing period

The variation in strength of BC soil stabilized with RHA compacted at different moulding water contents is shown in Fig. 5. The strength of BC soil–RHA mixture, i.e. 20% compacted on dry side of optimum, is higher and varies from 301 to 325 kPa for immediate to that of 90 days of curing period than compacted on optimum and wet side of optimum. Strength at optimum and wet of optimum varies from 274 to 306 kPa and 166 to 236 kPa for immediate to that of 90 days of curing period, respectively. This is due to flocculated structure of composite when compacted on dry of optimum, and also, the effect of curing is negligible in soil mass and RHA mixture [15]. Addition of RHA increases the strength of BC soil, since RHA is an inert material and possesses angular and subangular particles which agglomerates the particle into larger size of the composite by increasing the angle of internal friction of the composite results in increase in the strength [16].

The strength of BC soil stabilized with RHA and carbide lime mixture, i.e. 20% and 8% compacted on dry side of optimum is higher and varies from 393 to 2602 kPa for immediate to that of 90 days of curing period than that of compacted on optimum and wet of optimum. Strength at optimum and wet of optimum varies

Fig. 5 Variation of strength of soil treated with rice husk ash compacted at different moulding water contents with curing period

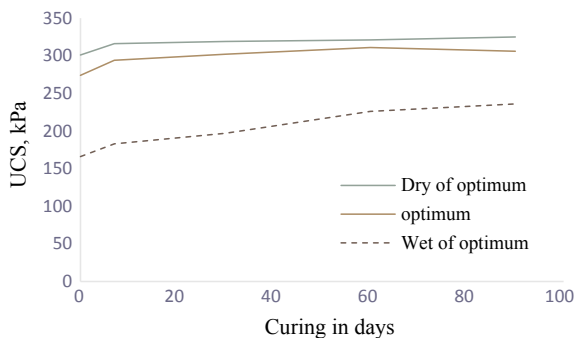
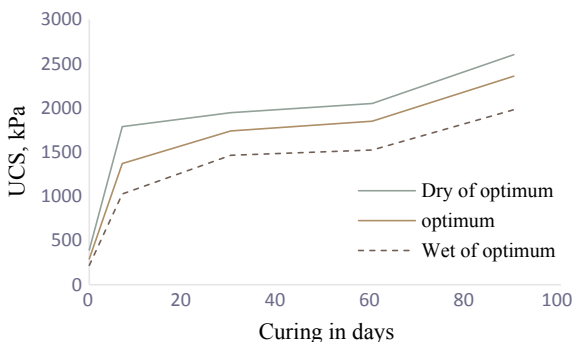


Fig. 6 Variation of strength of soil treated with rice husk ash and carbide lime compacted at moulding water contents with curing period



from 292 to 2359 kPa and 218 to 1980 kPa for immediate to that of 90 days of curing period, respectively. Addition of RHA is only a mechanical stabilization due to the deficiency in the lime content, and to improve strength properties, carbide lime is added. The calcium hydroxide obtained from the hydration of free lime from carbide lime dissociates in water. Hydroxyl ion concentration increases with increase in pH concentration. The increase in pH accelerates the formation of cementitious compounds, which increases the strength of the soil. The alumina and silica from both soil and RHA gradually react with the calcium ions from the hydrolysis of CaO to produce insoluble pozzolanic compounds like calcium silicate hydrate (C-S-H) and calcium aluminate silicate hydrate (C-A-S-H). Formation of these compounds eliminates the void pores in the stabilized soil matrix, and the gel so formed hardens with time, thereby increasing the strength of the soil matrix [17] and [18]. The strength of sample compacted on dry side of optimum is more compared to those compacted at optimum and wet of optimum; this is due to flocculated structure of composite when compacted on dry of optimum, and the results are shown in Fig. 6 [15].

3.4 Mineralogical and Microstructural Studies of Soil Stabilized with Industrial Wastes and Lime

The changes in strength properties of soil with the addition of bagasse ash, CL, RHA, and lime are studied in detail. Variation in strength properties is mainly due to the amount of pozzolanic compounds formed by pozzolanic reaction between soil and additives and microstructural changes. To understand better, the mineralogical, microstructural and chemical composition changes are studied through XRD, SEM and EDAX analyses.

XRD analysis of BC soil stabilized with Bagasse ash and lime The XRD pattern of expansive black cotton soil shows the minerals montmorillonite, quartz and aluminium oxide. Montmorillonite is found at d-spacing of 4.45 Å⁰, 2.56 Å⁰ and

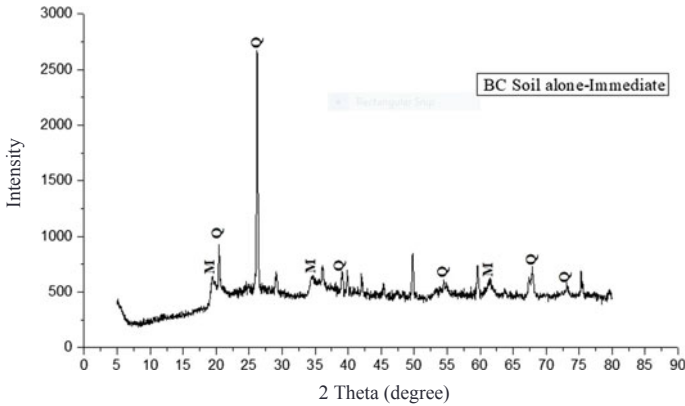


Fig. 7 XRD pattern of soil

1.49 Å⁰ at Bragg’s angle of 19.5⁰, 34⁰ and 62⁰, respectively, and quartz at 4.25 Å⁰, 3.34 Å⁰, 2.81 Å⁰, 1.67 Å⁰ and 1.38 Å⁰ at Bragg’s angle of 20⁰, 37.5⁰, 55⁰, 67.5⁰ and 72.5⁰, respectively, and confirms the presence of montmorillonite, quartz and aluminium oxide, which are the chief clay minerals in expansive black cotton soil as seen from Fig. 7.

The strength of BC soil and bagasse ash mixture treated with lime increased from immediate testing to curing period of 90 days. Enhancement in strength is attributed to the reaction between reactive silica of soil and bagasse ash mixture and lime, producing cementitious products such as CSH and CASH gel products, which is being confirmed by XRD pattern as shown in Fig. 8.

The appearance of the peak at two theta angles of 34.72⁰ and 40.2⁰ with d-spacing of 2.5814 Å⁰ and 2.2376 Å⁰ confirms the formation of CSH compounds. XRD pattern shows the formation of CASH compounds at two theta angles of 59.6⁰ and 67.72⁰ with d-spacing of 1.5498 Å⁰ and 1.3825 Å⁰. As compared to the XRD pattern of black cotton soil, the peaks became very sharp with the addition of bagasse ash and lime which are shown in Fig. 8. The XRD patterns give the strong evidence of the formation of CSH and CASH compounds which plays accounts for drastic boost in strength of BC soil bagasse ash–lime mixtures.

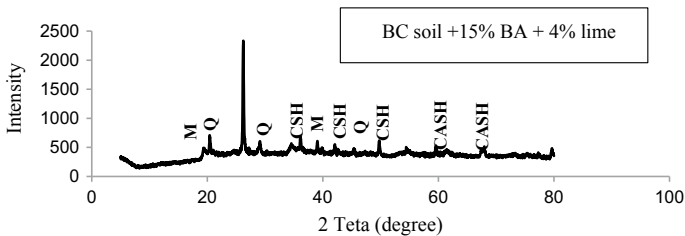


Fig. 8 XRD pattern of soil and bagasse ash mixture treated with lime and cured for 90 days

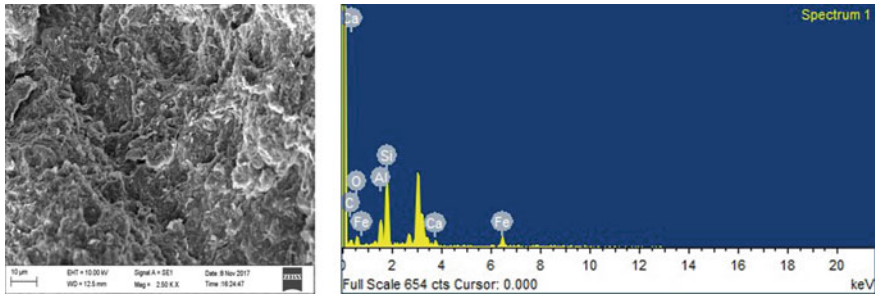


Fig. 9 SEM and EDAX images of soil

SEM analysis of BC soil stabilized with Bagasse ash and lime SEM image of expansive black cotton soil is as shown in Fig. 9, and it is found that the structure of soil is flaky with thin films and the voids in the soil matrix are larger and flakey structure with equal dimensions with thin diagram which again shows that the chief mineral constituent in the soil is montmorillonite due to which it is expansive in nature.

The highly magnified view of the expansive soil–bagasse ash–lime combination of the samples cured for 90 days of curing period is shown in Fig. 10.

The highly magnified image (10,000X) shows the flocculated particles with packets of quartz. The highly magnified image of soil–bagasse ash–lime mixture indicates the formation of C-S-H and C-A-S-H gels which are confirmed by XRD analysis, and these cementitious compounds are in fused state; C-S-H and C-A-S-H

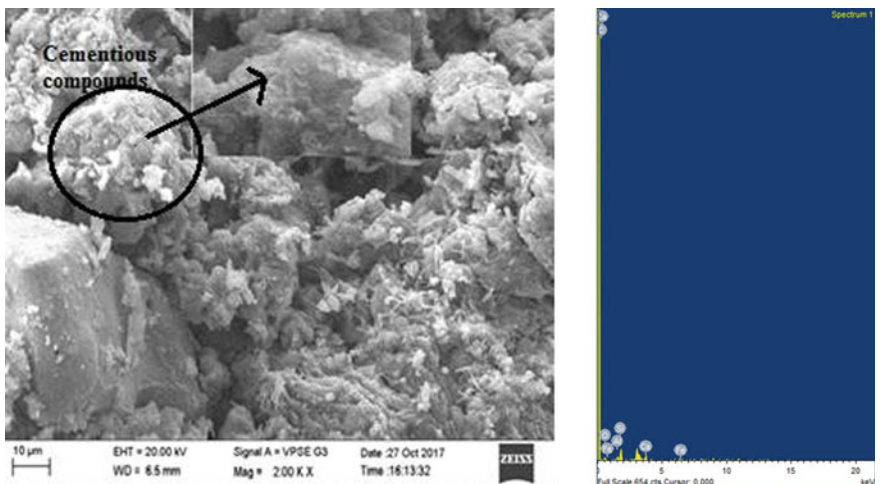


Fig. 10 SEM and EDAX images of soil and bagasse ash mixture treated with lime and cured for 90 days

gels have extended into the pore space and reduced the void spaces. With the addition of lime, more calcium ions are released into the system, and as a result, bagasse ash is dissolved into the system at higher rate, and increased white patches of cementitious products are seen.

XRD analysis of BC soil stabilized with Rice husk ash and carbide lime XRD pattern of BC soil stabilized with RHA at 90 days of curing period is shown in Fig. 11.

The powdered sample of the mixture shows a crystal mineral of montmorillonite (M) at a d-spacing of 4.45, 2.56, 1.69, 1.49 θ and quartz (Q) which are showing at a d-spacing of 3.34, 1.67, 1.38, 1.28, 2.81 θ , respectively. Addition of RHA is a mechanical stabilization, and hence, strength improvement in the stabilizing process is very minimal, and it is due to the agglomeration of soil and RHA particle. Compared to the soil alone, addition of RHA shows more pronounced peak due to the presence of dominant mineral quartz (Q). However, the strength of blended composite is not significantly improved due to the absence of calcium oxide (CaO) content. Hence, the stabilization with the addition of RHA alone is mainly by structural changes.

The changes in microstructural development of soil due to addition of additives play a significant role in enhancing the strength of soils. Addition of RHA in strength gaining process is very limited due to its low calcium oxide content. Introduction of carbide lime to the stabilized BC soil and RHA shows a significant improvement in its strength due to increase in the cohesive property. When the carbide lime is introduced, the CaO of the carbide lime reacts with water and leads to the calcium hydroxide, and the hydroxyl of the solution increases pH and in turn releases more reactive silica resulting in the formation of cementitious compounds such as calcium silicate hydrate (C-S-H) and calcium aluminate silicate hydrate binding the soil particles [19]. The strength of the soil mass also increases due to reduction in the void ratio also. The main cementitious gel formed with the addition

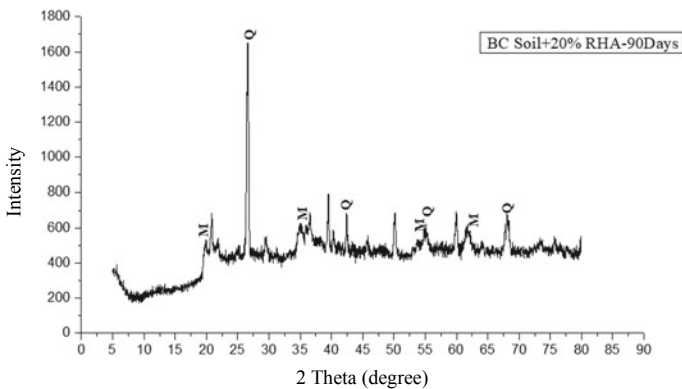


Fig. 11 XRD spectrum for soil + 20% RHA mixture after 90 days of curing

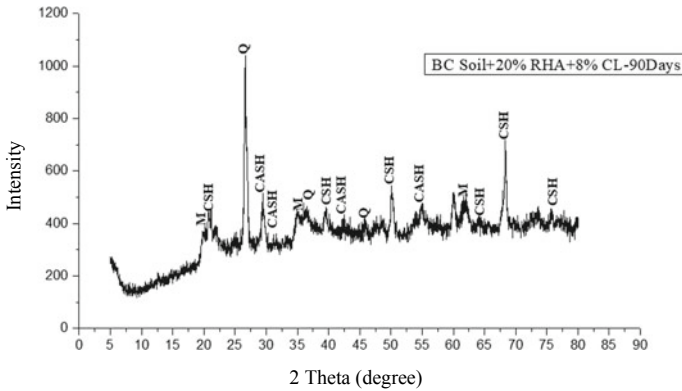


Fig. 12 XRD spectrum for soil + 20% RHA + 8% CL mixture cured for 90 days

of carbide lime with products such as C-S-H and C-A-S-H formed at a d-spacing of 4.07, 2.25, 1.808, 1.451, 1.366, 1.24 θ and 3.05, 2.74, 2.14, 1.66 θ , respectively, is seen in Fig. 12.

SEM analysis of BC soil stabilized with Rice husk ash and carbide lime RHA poses angular and subangular particle, and the addition of RHA leads to increase in the frictional property (angle of internal friction) of the material and decreases the cohesion value of the blend which agglomerates the particle into larger size; thus, there is a slight improvement in the strength which was observed from the UCS results [16]. Addition of RHA into the soil samples is a mechanical interlocking effect which brings changes in the soil structure, as seen from Fig. 13. The images were magnified at 2500x magnification, and it can be observed from SEM images that there is an angular and subangular particle which reduces the pore air void spaces of the sample within the soil and changes the soil structure by agglomeration which increases the marginal improvement of strength of BC soil.

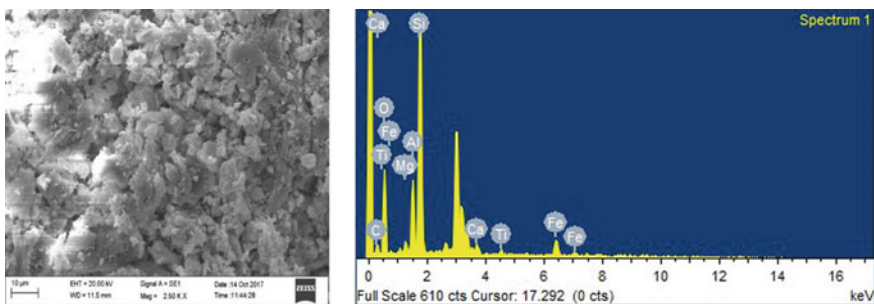


Fig. 13 SEM image and EDX micrograph soil + 20% RHA mixture after curing for 90 days

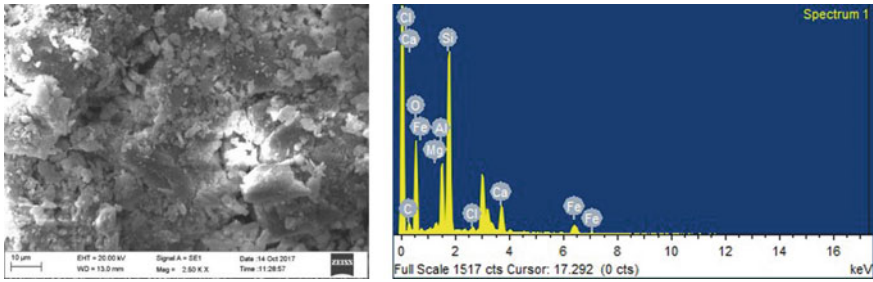


Fig. 14 SEM image and EDS micrograph of soil + 20% RHA + 8% CL mixture after curing for 90 days

Addition of RHA is just a mechanical interlocking effect; in order to improve the strength to a great extent, lime-rich additives are to be added; among one is carbide lime. Addition of carbide lime at an optimum dosage of 8% increases the strength of the blend, and this is due to addition of carbide lime to the soil, and optimum RHA mixture increases the pH dissolving the silica from the composite and reacts with calcium ions from the carbide lime which leads to the formation of gel C-S-H and C-A-S-H which hardens with the time, thus increasing the strength of the mixture, and it is verified from the XRD analysis. The cementitious gel is formed which fills the void spaces within the sample, and this phenomenon occurs due to coating and binding of individual soil particles with cementitious gels resulting in the reduction in migration of ions into the pores resulting in a rigid structure. The morphology of the 90-day samples is shown in Fig. 14.

It is denser than the RHA-treated sample of the 90-day curing period by filling of the cementitious products in the pore space. The denser morphology with curing time leads to strength increase [19].

4 Conclusions

The following major conclusions are drawn for the detailed studies reported:

1. Addition of bagasse ash alone improves the strength marginally. Optimum BA is found to be about 15%. The relatively less improvement with BA has been explained as due to less amount of calcium content of the BA though contains sufficient reactive silica. The strength improves with curing period better with lime.

However, the optimum BA content for uncured and cured samples is almost the same. With the incorporation of different percentages of lime to soil–optimum bagasse ash mixture, the unconfined compressive strength increase on both uncured and cured samples. The optimum lime content is about 4%. The changes are inconsistent with SEM and XRD studies. Thus, it is concluded that CL with sufficient lime content would be highly beneficial.

2. The tests on soil with different amounts of RHA alone have shown that without addition of lime is about 20% with or without curing. However, the strength of soil with RHA and CL is much higher than without BL, but the optimum BA is about the same. This is again due to better production of cementitious compounds in the presence of CL. The optimum CL content for both cured and uncured samples is about 8%. The study clearly shows that CL can be effective replacement for lime.
3. The variation in the strength of soil with optimum contents has shown that the strength mobilization is better when the samples are compacted at water content on dry side of the optimum than at optimum or wet of optimum water content itself. This has been explained as due to flocculation of soil particles on dry side of the optimum water content facilitating better cementation with pozzolanic compounds formed. The study brings out that apart from pozzolanic binding, the fabric soil particles due to variation in the water content even play important role.
4. It is observed that the ratio of strength of soil to the strength soil without additives compacted at water content on wet of optimum with any additive is higher than on soil compacted on dry side of optimum water content as the strength of soil at wet of soil is far less than the soil when is compacted on dry side of the optimum water content. However, the effect of moulding water content and density is much less in the case of RHA s due to its higher pozzolanic reactivity.
5. The variation in the strength of the soil with different additives and admixtures is consistent with pozzolanic compounds formed, but no attempt is made to correlate the strength with pozzolanic compounds formed quantitatively.

References

1. Anggraini, V., Huat, B.B.K., Asadi, A., Nahazanan, H.: Effect of coir fibre and lime on geotechnical properties of marine clay soil. In: 7th International congress on environmental geotechnics: ICEG 2014, engineers, Australia. p. 1430 (2014)
2. Dhengare, Sugar, Amrodiya, Sourabh, Shelote, Mohanish, Asati, Ankush, Bhanwel, Nikhil, Jhichkar, A.K.R.: Utilization of sugar cane Bagasse ash as a supplementary cementious material in concrete and mortar- A review. IJCIET **6**(4), 94–106 (2015)
3. Eberemu, Adrian O.: Evaluation of bagasse ash treated lateritic soil as a potential barrier material in waste containment application. Acta. Geotechnica. **8**, 407–421 (2013)
4. Kharade, Amit S., Suryavanshi, Vishal V., Gujar, Bhikaji S., Deshmukh, Rohankit R.: Waste product 'bagasse ash' from sugar industry can be used as stabilizing material for expansive soils. IJRET **3**(3), 506–512 (2014)
5. Bhasin, N.K., Goswami, M.K., Oli, P., Krishna, N. And Lal, N.B: A laboratory study on utilization of waste materials for the construction of roads in black cotton soil area. Highw. Res. Bull., **36**, 1–11, Irc, New Delhi (1988)
6. Cook, D.J.,Pama, R.P. and Damer, S.A: Rice husk ash as a pozzolanic material. Proc. Conf. On New Horizons in Construction Material, Lehigh university (1976)

7. Jaturapitakkul, C., Roongreung, B.: Cementing material from calcium carbide residue-rice husk ash. *J. Mater. Civ. Eng.* **15**, 470–475 (2003)
8. Kampala, A., Horpibulsuk, S.: Engineering properties of calcium carbide residue stabilized silty clay. *J. Mater. Civil Eng.* **25**(5), 632–644 (2013)
9. Ramana Murty, V., Praveen, G.V.: Use of chemically stabilized soil as cushion material below light weight structures founded on expansive soils. *J. Mater. Civ. Eng.* **20**(5), 392–400 (2008)
10. Dua, Yan-Jun, Ning-Jun Jiangb, N., Liuc, Song-Yu., Horpibulsukd, Suksun, Arulrajahe, Arul: Field evaluation of soft highway subgrade soil stabilized with calcium carbide residue. *Soils Foundation.* **56**(2), 301–314 (2015)
11. Bureau of Indian Standards, New Delhi.: BIS 2720 (Part-II) (1973) Determination of water content, specific gravity, Atterberg's limit of the soil, BIS-2720 (Part II)-1973, (Part-III, sec-I) (1980), (Part V) (1985), (Part V) (1985), 2720 (Part V)
12. Sridharan, A., Sivapullaiah, P. V.: Mini compaction test apparatus for fine grained soils. *Geotech. Test. J.*, **28**(3), 1–20, (2005)
13. BIS 2720 (Part X): Determination of Unconfined Compressive Strength, Bureau of Indian Standards, New Delhi (1973)
14. Viswanath, B.: Role of moulding water content on the strength properties of fine grained soils treated with pozzolanic and non pozzolanic fly ashes and other additives, Ph.D Thesis, Bangalore University (2007)
15. Ramesh, H. N., Sivapullaiah, P. V.: (2011) "Role of moulding water content in lime stabilization of soil". *Ground Improv.*, **164**, 1–5
16. Daimary, N., Bhattacharjee, A., Goswami, R.: Effect of rice husk ash on shear and consolidation of lateritic soil. IGC, December 15–17, Chennai (2016)
17. Ramakrishna, A.N., Pradeep Kumar, A.V.: Influence of compaction moisture content on ucs and cbr of RHA-lime stabilized bc soil. *Indian Geotech. J.* **38**(2), 140–155 (2008)
18. Mcallister, L.D., Petty, T.M.: Leach test on lime-treated clays. *Geotech. Test. J.* **15**(2), 106–114 (1992)
19. Vichan S., Rachan, R.: Chemical stabilization of soft Bangkok clay using the blend of calcium carbide and biomass ash. *Soils Found.*, **53**, 272–281 (2013)

Geotechnical Engineering Accompanied by Risk



Ikuo Towhata

Abstract Geotechnical construction encounters many unexpected troubles, and one of the important reasons for this is the lack of subsurface information and knowledge. This paper calls the troubles “georisk” and exhibits that more subsurface investigations have to be practised in order to reduce this risk. Case history data was interpreted as a collaborative work with several institutions, and it was demonstrated that the risk can be mitigated by allocating more budget to the investigation. Another source of risk is the lack of knowledge, and one needs to pay more attention to the history of troubles that were experienced during projects in the past.

Keywords Georisk · Cost · Soil investigation

1 Introduction

The engineering industries in the second half of the twentieth century were characterized by mass production in which both amount and quality were maintained at high levels. This type of engineering achieved such a great success that people nowadays take the success as normal situation. However, we need to get recalled of the situation in the previous times when most daily goods were produced by hand in a small scale, in response to individual client’s order. Naturally, each client had different orders and the production changed from time to time. Having disappeared nowadays from most fields of engineering, this “make-to-order (MTO)” practice remains universally in construction projects. In the era of mass production, people and the social system are not accustomed to MTO, and many conflicts/inconveniences are induced in construction.

Geotechnical engineering is fully accompanied by MTO obviously because of the following reasons:

I. Towhata (✉)
Kanto Gakuin University, Yokohama, Japan
e-mail: towhata.ikuo.ikuo@gmail.com

- Soil and rock conditions are never uniform in both horizontal and vertical directions. There is no couple of sites with exactly same subsurface conditions.
- Subsurface investigation relies on skill of individual technicians. Different results and interpretation may occur on very similar subsoil. Accordingly, the assessed bearing capacity, stability and deformation change and affect the design details as well as construction procedures.

This situation results in unexpectedly increased cost and longer construction period. This is particularly the case when unexpected subsoil condition is detected during design or construction. This is called “georisk” in this paper. People are not familiar with georisk. From the viewpoint of high-level mass production, they accuse geotechnical engineers of the consequence of georisk.

Georisk is not a new topic. MacDonald [1] stated that the overrun cost was 23% or more in over half of 58 highway projects and showed that more subsurface investigation efforts reduce the overrun more efficiently. It was also shown that only 1/4 of projects kept the overrun within 10%. By referring to this paper, Clayton [2] stated that detailed soil investigation is meaningful in some projects with good returns. It was also pointed out by him that there are other kinds of projects in which the existing information and expert opinion are essential.

Another difference between mass production and civil/geotechnical engineering products is the longer life time of the latter. While cars and electric tools are used for several years only, the latter is used for decades or centuries in which the materials are subject to ageing or deterioration and the external actions may become more serious than expectation. People are not much informed of such negative condition and would tend to feel unhappy against the construction sectors many years after the completion of their structures.

2 Example of Georisk

The most famous example of the consequence of non-uniform subsurface condition is shown in Fig. 1. Although this tower is making a marvellous contribution to the local tourism today, its leaning has been taken seriously by engineers over centuries [3]. Obviously, there was no soil mechanics and subsurface investigation technology when this tower was planned and constructed. Hence, nobody accused of the unexpected leaning of this tower. In contrast, there are more examples of leaning buildings today that have caused safety and financial conflicts between owners and project developers, designers and contractors. Whoever may be responsible for the problem, the unexpected leaning and subsidence are the consequence of insufficient information on subsurface soil/rock conditions. It may be said that more concern on underground uncertainty had been necessary.

The second example is taken from the falling of street surface into ongoing metro tunnelling (Fukuoka City, Japan, 2016). This tunnel was constructed at shallow depth by using the New Austrian Tunneling Method. The official

Fig. 1 Leaning of tower induced by different soil conditions under the foundation



investigation committee concluded that this accident was caused by collapse of an impervious layer above the crown of the tunnel that was locally thin and could not sustain the groundwater pressure above it [4]. Another point was addressed to the insufficient subsurface investigation that could not find the critically thin part of the impervious layer. Furthermore, this site had been known over decades before the accident for the varying thickness of the impervious layer and one of the engineers who used to work there called upon his successors of this risk. It seems, however, that this important information was not transferred after years.

The third example comes from Urayasu City, Japan, where, after the 2011 Tohoku earthquake of $M_w = 9.0$, ground improvement was carried out as mitigation of future liquefaction disaster. During the preliminary stage of jet mixing, unexpected plastic drains (Fig. 2) were encountered and the in situ mixing of cement and soil was prevented. Those drains had been installed during the land construction in shallow water in order to accelerate the consolidation settlement. The existence of those drains had been forgotten afterwards and caused a serious problem in 2017. Although the procedure was improved to overcome this problem, the cost and the construction period increased substantially. The national government decided to provide additional fund to cover the cost increase. However, the elongated construction period was not accepted by the local community, and the size of the project was significantly reduced [5].

These examples indicate the problem of underground uncertainty that has caused and is causing many problems in the construction practice.

Fig. 2 Detected plastic drain that affected procedure of jet mixing



3 Example Problems Caused by Age

It is widely believed that soil has eternal life as a construction material, and this belief has been supported by experience. However, it must be recalled that some kinds of rocks and rock-forming minerals are subject to weathering by which mechanical strength of materials decays with time. Asada [6] collected SPT-N values from residential embankments of different ages and exhibited that the range of SPT-N value decreased with increasing age (Fig. 3). This finding suggests ageing of soil in the embankment. It seems that the same problem occurs in natural slopes and affects the stability of slopes as well as anchors and rock bolts.

Fig. 3 Decreasing of SPT-N value in residential embankment

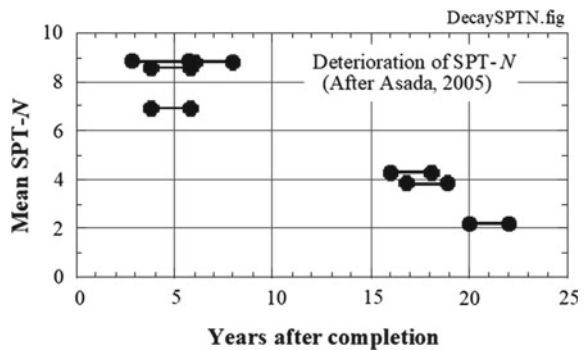


Fig. 4 Collapse of sidewalk induced by deteriorated sewage pipe



Moreover, deterioration of aged infrastructure is often encountered. Figure 4 illustrates one of the examples in which an aged sewage pipe had been broken as shown here, groundwater had flowed into this broken pipe, the backfill soil had been eroded by this water flow, a big cavity had developed, and finally, the sidewalk surface fell down suddenly into the cavity. What is significant in these examples is that one cannot find the ongoing underground problem until the ultimate failure happens.

Deterioration of (geotechnical) structure is induced by the customer's lack of knowledge of nature. At an anonymous place, a small valley was filled with soil. At this moment, the client did not have a clear idea about the future use of this site. Because valley is a place where stream water flows and also groundwater comes in from mountains, the groundwater level in the fill gradually rose. Before the water level became very high, the client decided to use the fill for a factory. The construction project was given to another contractor who was not informed of the history of fill construction. During this phase, the water level reached the critical level and the embankment deformed substantially. The contractor had to install stabilization measures with its own expense, while the client refused to pay, saying that completion of the project was the responsibility of the contractor.

4 Need for More Detailed Geotechnical Investigation

The preceding two chapters indicated that many troubles, which are called georisk herein, have been induced by insufficient subsurface information. Different from manufacturing in modern industries in which materials are subject to quality check, the ground condition is never uniform and has never the quality examined. Moreover, the material cannot be checked by eye inspection due to invisibility of the underground space. In this respect, the number of subsurface investigations is as important as the quality/accuracy of individual investigation.

The Georisk Society in Japan has been organizing annual conferences since 2010, focusing on the importance of subsurface investigation in reducing georisk in a variety of construction projects. Respecting this effort, the author has been collaborating with this society and re-interpreted the case history data. This chapter addresses the findings from this activity.

First, the Georisk Society introduced a successful project of bridge construction (Fig. 5) in which the bridge pier design was improved by detailed subsurface investigation [7]. The bridge connected the Kitakyushu Airport Island with the main Kyushu Island of Japan, having 2.1 km in length with 28 piers underneath. Because the local geological condition was not uniform, the traditional pier design proposed different and substantial depth of end-bearing piles. The traditional design was based on SPT-N value. To reduce the cost, it was attempted to design friction piles with shorter length that were designed either by SPT-N again or additional detailed investigation. Finally, the data from detailed investigation enabled the shortest pile length, and the construction cost was drastically reduced. According to the above-mentioned report, the investigation cost increased from the original US 1 million \$ to 3 million \$, while the construction cost was reduced by 100 million \$. The cost-benefit ratio of $100/(3 - 1) = 50$ was very good.

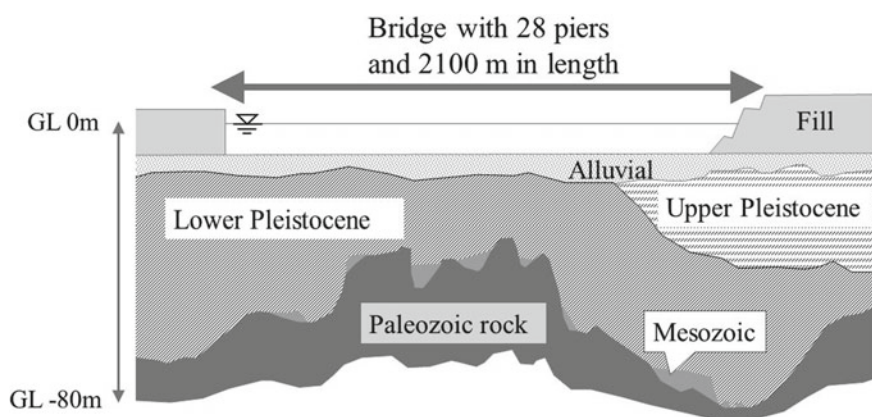
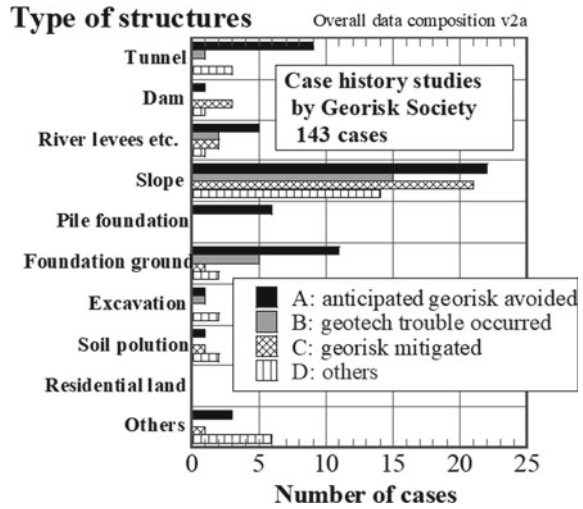


Fig. 5 Kitakyushu Airport Bridge constructed on complicated subsurface condition [7]

Fig. 6 Composition of Georisk Society’s case history study



Second, the composition of the 143 case history data in the Georisk Society’s study (2010–2018) is shown in Fig. 6 where the studied types of construction consist of tunnels, dams, levees, excavation, pollution, etc., while the majority consists of slope instability and foundations. The author found during his comprehensive review that a good number of georisk occurred in cut slopes in which the geological structure (stratum) was normal to the slope surface (opposite dip). Possibly, instability was not cared in such a stratum before cutting, but the material deterioration due to water percolation was found later. It is one of the points to show that geometric investigation was not enough and that subsurface investigation on mechanical properties was needed.

The Georisk Society classified the studied cases into four groups that are namely

- Group A: Original design was over-conservative or risk was found in advance and additional ground investigation helped reduce the cost (59 cases).
- Group B: Risk (trouble) occurred during project and countermeasures increased the total cost (24 cases).
- Group C: Risk was anticipated during early stage of project and mitigation helped avoid the catastrophe (29 cases), and
- Group D: Detail is not clear (31 cases).

The following discussion addresses Groups A–C with more detailed information.

4.1 Group A with Successful Risk Management

This group addresses the successful cases in which the possible georisk was anticipated or measures to remove unnecessary conservatism was found. Hence, more detailed investigation was carried out with additional budget, and the risk was avoided or total construction cost was reduced. It is noteworthy that although cost was reduced, the construction period was scarcely shortened probably because contractors and clients wanted to keep things going as scheduled. Figure 7 compares costs when georisk was (○) or was not (●) avoided by relevant (additional) subsurface investigation, which is otherwise called georisk management. The costs are plotted against the original construction budget that was planned before finding the risk. Evidently, the cost was reduced. Then, the ratio of profit by management is defined by

$$\text{Profit ratio} = \frac{\left[\frac{\text{(Total cost without additional investigation, including damage by georisk)}}{\text{(Total cost after relevant management)}} \right]}{\text{(Costs for additional subsurface investigation, changing design etc.)}} \quad (1)$$

This ratio is plotted against the original construction budget in Fig. 8. There is no clear correlation between the ratio and the budget (size of project). Noteworthy is that the profit ratio may reach 2.0 or more, but that the ratio <1 still contributes to the project by removing the risk and avoiding the catastrophe.

Figure 9 plots the profit divided by the original cost against the worst-scenario cost that would have been increased if georisk had not been managed. The size of the worst disaster does not have a correlation with the plotted ratio. The ratio = 1 means that the entire project was cancelled to avoid the risk. While some projects reveal smaller values of the ratio, it is very possible to attain the ratio >0.5. Finally, Fig. 10 demonstrates the types of additional subsurface investigation after finding

Fig. 7 Comparison of cost with and without successful risk management (Group A)

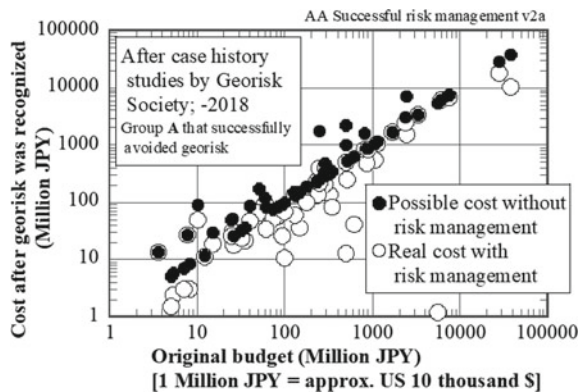


Fig. 8 Profit ratio versus original construction budget (Group A)

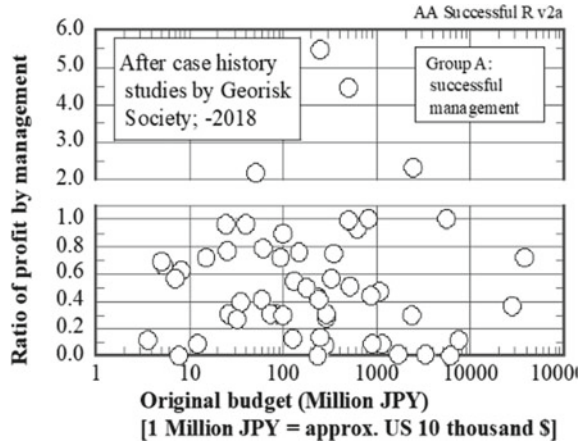
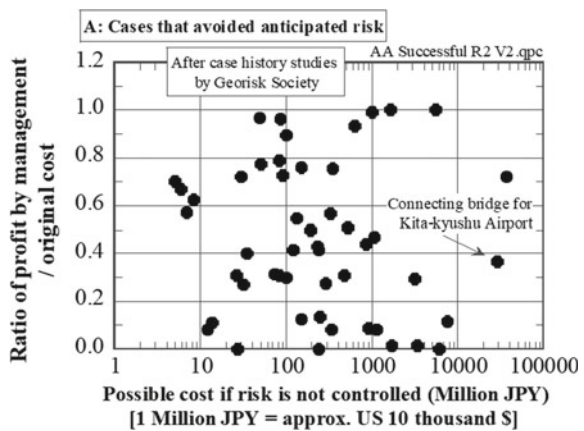


Fig. 9 Ratio of profit and original project budget plotted against total cost after possible risk manifestation (Group A)



the possibility of georisk. The majority is borehole drilling and standard penetration tests partly because of the tradition of the engineering community (SPT is the must in practice) but also because the number of boreholes is considered important in heterogeneous subsoil. Note also that laboratory soil testing is important because, if conducted on samples of good quality, the soil properties can be more directly determined than assessing by means of sounding data (SPT-N, etc.).

4.2 Group B in Which Georisk Was Not Avoided and Cost Increased

This group stands for the failure of georisk management. The risk occurred during the construction, and the needed response resulted in increased cost or elongated

Fig. 10 Types of investigation employed for georisk management (Group A)

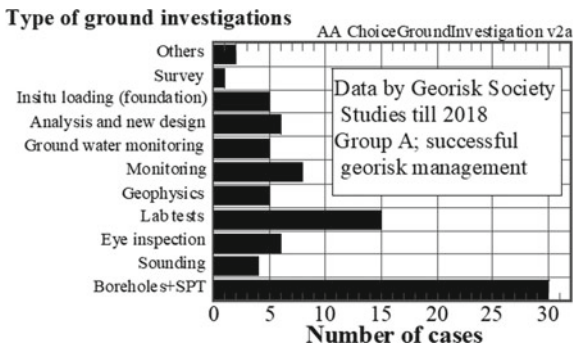
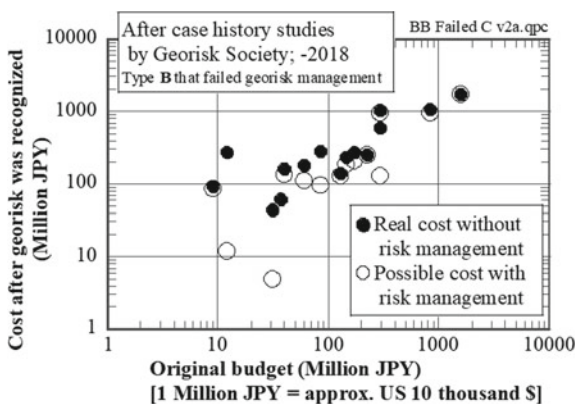


Fig. 11 Comparison of real cost increased by georisk and possible cost reduced hypothetically by missed risk management (Group B)



construction period or both. In this group, it was attempted to assess the hypothetically reduced cost if georisk management had been performed. Figure 11 compares the real cost increased by georisk and the hypothetically reduced cost. Certainly, the former is greater than the latter. The relative difference (ratio) between these costs decreases as the size of the project (original budget) increases possibly because the influence of single individual georisk becomes smaller in bigger projects. The difference between these two costs is defined as the (possible) profit obtained from georisk management, although it did not happen in reality. Figure 12 indicates that the profit/original budget may take the maximum at the intermediate size of the project and decrease afterwards. This again implies that the influence of single georisk is not very large. Figure 13 examines the relative extent of the missed profit either over the total cost increase (real cost–original budget) or the possibly reduced cost if georisk had been reasonably managed. There is no clear trend in this diagram, but there is always a possibility to achieve the high ratio of 0.5 or greater.

Fig. 12 Relative profit and size of project (Group B)

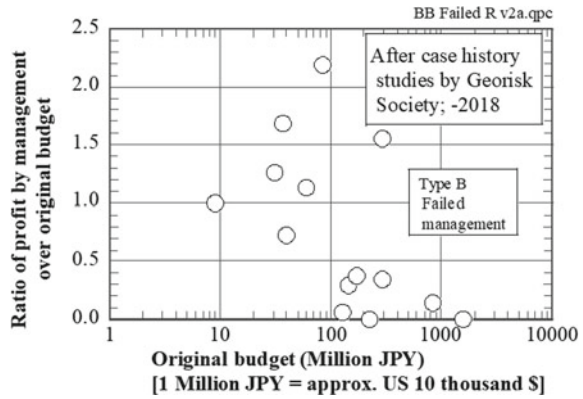
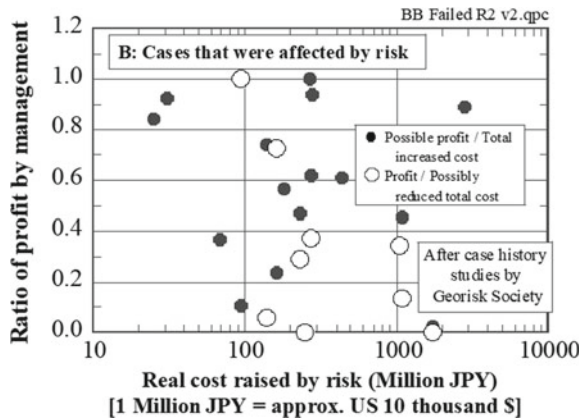


Fig. 13 Ratio of profit over two types of costs versus real cost increased by georisk (Group B)



4.3 Group C in Which Georisk Was Found in the Intermediate Stage of Construction and Was Partially Avoided

Group C is composed of the projects in which georisk was detected after the construction had started. In other words, risk was not fully mitigated, but appropriate management by additional subsurface investigation and changed design reduced the total expenditure to some extent. Thus, Group C is called partial success.

Figure 14 compares two types of cost; the hypothetical cost without risk mitigation and the actual cost that was achieved by mitigation. In three cases, the actual cost was made less than the original budget and successful by risk management,

Fig. 14 Relationship between costs with and without georisk management and the original construction budget (Group C)

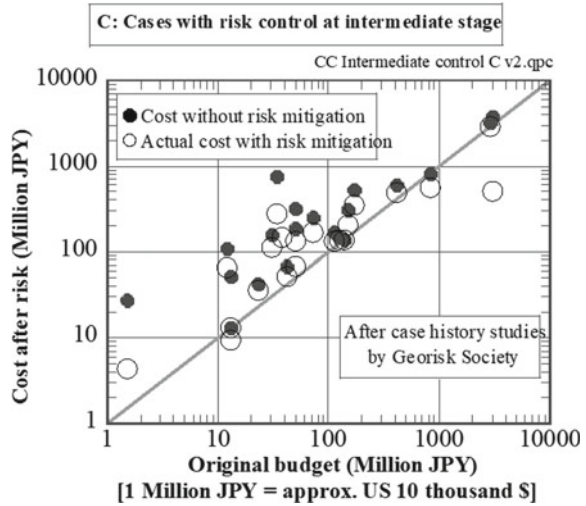
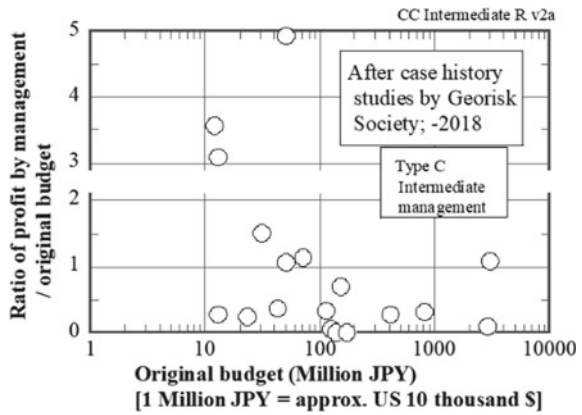


Fig. 15 Ratio of profit in Group C changing with the original budget



although the success remained partial. In the three best cases, the reduced cost was less than the original budget. Figure 15 indicates the ratio of the profit (difference between the worst-scenario cost without management— real cost) over the original budget. It is possible thus to achieve a very good ratio of profit. Figure 16 illustrates that the profit ratio over the hypothetical worst-scenario budget (without management) is not much related with the real cost after georisk management. It is implied that significant cost saving is possible even if georisk is detected during ongoing project (Fig. 17).

Fig. 16 Ratio management profit over total cost without management

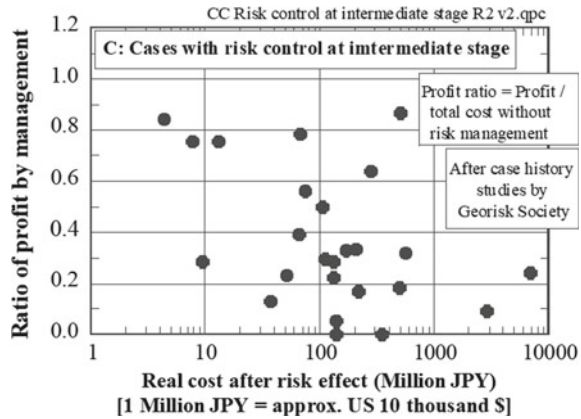
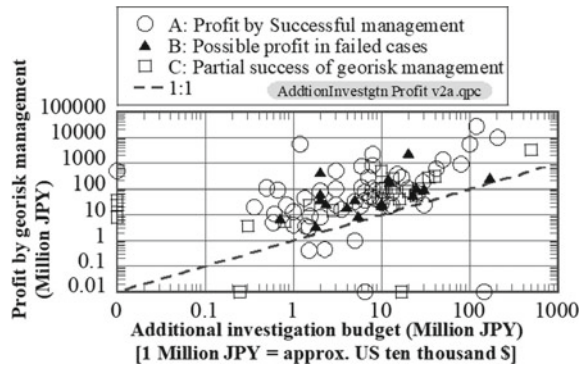


Fig. 17 Overall summary on profit of georisk management changing with cost for additional subsurface investigation (Groups A–C)



5 Complicated System of Nature

This chapter makes a brief remark on georisk of insufficient knowledge on nature. Because the size of construction projects increases in recent times, their impact in nature becomes significant as well. Accordingly, there is a risk that unprecedented catastrophe may occur. Most probably, this risk in future is related with environmental issue.

Melting of glacier is one of the possibilities. Note that the disaster of Mattmark Dam in 1965 was caused by glacier melting [8]; Fig. 18. In the 1960s, melting of glacier was not recognized as risk. Similarly, there may be a future risk about which we are not serious yet.



Fig. 18 Site of fallen glacier at Mattmark Dam site (this photograph was taken in summer, 2010)

6 Conclusion

This paper addresses problems that are encountered in geotechnical engineering projects. At this moment, the most common problem is the one caused by insufficient information about subsurface conditions. By referring to case history studies, the importance of more detailed subsurface investigation was proposed. Moreover, the lack of knowledge on the past projects and nature may cause further unprecedented problems. In this respect, optimism should be refrained from.

Acknowledgements The present study on georisk management was carried out as a collaboration among the Japanese Geotechnical Society, the Georisk Society and the Japan Geotechnical Consultants Association. The case history data was collected by the long-term efforts of the Georisk Society. The author expresses his deepest appreciation to these institutes as well as Prof. T. Watanabe who is the President of the Georisk Society.

References

1. MacDonald, M.: Study of the efficiency of site investigation practices, Transport Research Laboratory, Crowthorne, Berks, Project Report 60, ISSN 0968 4093 (1994)
2. Clayton, C.R.I.: Managing geotechnical risk: time for change? Proc. Inst. Civ. Eng.-Geotech. Eng. **149**(1), 3–11 (2001)
3. Burland, J.B., Jamiolkowski, M., Viggiani, C.: The stabilisation of the leaning tower of Pisa. Soils. Found. **43**(5), 63–80 (2003)

4. Accident Investigation Committee, Public Works Research Institute: Report on street depression at subway construction site. <https://www.pwri.go.jp/jpn/kentou-iinkai/kentou-iinkai.html>. Retrieved on 16 September 2019 (in Japanese) (2017)
5. Towhata, I.: Summarizing geotechnical activities after the 2011 Tohoku earthquake of Japan, 7th Int. Conf. Earthquake Geotechnical Engineering, Ishihara Lecture, Rome (2019)
6. Asada, A.: Assessment of seismic risk in residential areas under future Miyagi-ken-Oki earthquake and its mitigation, Draft report, p. 112 (2005)
7. Tagami, H., Ochiai, H., Yasuda, S., Maeda, Y., Yasufuku, N., Migita, T, and Shirai, Y.: Importance of site-specific plan of ground investigation, 1st Research Meeting on Georisk Management, Tokyo, 29–34 (in Japanese) (2010)
8. Ricciardi, T.: Mattmark, 30 August 1965: A catastrophe that changed Switzerland's perception of Italian migrants. *Rev. Suisse d'Histoire* **66**(3), 401–419 (2016)

Quantitative Assessment of Life Cycle Sustainability (QUALICS): Application to Engineering Projects



Krishna R. Reddy , Girish Kumar , and Jyoti K. Chetri 

Abstract Civil engineering development has advanced dramatically over the years. The unsustainable use of resources in various activities involved in the engineering projects releases undesirable amounts of emissions and other waste streams into the environment causing negative environmental impacts including global warming, resource depletion, eutrophication and acidification among many others. In the past decade or so, considerable efforts have been made to incorporate sustainable practices into the design and construction of infrastructure projects with an aim to minimize the net negative environmental, economic and social impacts of the project. Over the past few years, several researchers have developed project specific tools to aid the practitioners to assess and compare the sustainability of the potential design alternatives in a project. In most cases, these tools focused mainly on the environmental impacts with a minimal (often a qualitative approach) or even no regard to the broader economic and social impacts of the alternative design options in a project. For the true sustainability assessment, it is imperative that the assessment methodology incorporates a quantitative and life cycle approach for the decision-making on the most sustainable design alternative in a project. In this regard, a framework “Quantitative Assessment of Life Cycle Sustainability (QUALICS)” is developed to quantify the overall sustainability of a project/activity and facilitate the decision-making process. The QUALICS framework is not just limited to civil engineering projects but can be used in projects of any engineering domain. The main aim of this paper is to describe the QUALICS framework and demonstrate its application to assess the overall sustainability of design alternatives in a project.

Keywords Sustainability · Climate change · Decision-making · Environmental sustainability · Economic sustainability · Geotechnical engineering · Geoenvironmental engineering · Life cycle assessment · Social sustainability

K. R. Reddy (✉) · G. Kumar · J. K. Chetri
Department of Civil and Materials Engineering, University of Illinois, Chicago, IL, USA
e-mail: kreddy@uic.edu

1 Introduction

Civil engineering has been an integral part of human life since the beginning of civilization. The advancements in civil engineering over the years have led to the development of infrastructure of countries. The buildings are growing taller, foundations are moving deeper, roads are getting wider, and bridges are getting longer. With all these advancements, the amount of raw material consumption, energy usage, waste generation and harmful emissions have increased exponentially. Geotechnical infrastructures, which are a part of civil engineering infrastructures, such as foundations, underground storage tanks, retaining walls, levees and embankments involve significant amounts of natural resource consumption, energy usage, waste generation and harmful emissions. In conventional engineering practice, the design and construction of infrastructure projects are mainly driven by cost and functionality of the technical design with no regard to broader environmental, economic and social impacts associated with various stages of the projects [1]. Recently, American Society of Civil Engineers (ASCE) developed a policy, ASCE Policy 418, promoting sustainability in engineering projects by compelling planners and designers to consider life cycle stages, from raw material acquisition to demolition and material disposal and reuse, in the planning and design process and educating stakeholders about net environmental, economic and social benefits of a project [2].

In recent years, life cycle approach in the engineering design has gained wide prominence. Life cycle assessment (LCA) is one of the tools that involves evaluation of the environmental impacts of each life cycle stage of a project from material acquisition to waste disposal [3]. However, LCA focuses on assessing only the environmental impacts associated with each life cycle stage. Sustainability is not just related to environmental implications; it covers economic as well as social aspects of a project through its entire life cycle, generally referred to as triple-bottom line sustainability. The environmental impacts are generally assessed in terms of energy usage, ozone depletion, global warming, fossil fuel depletion, eutrophication and land use. There are various tools developed to quantify these environmental impacts. On the other hand, economic impacts are quantified in terms of direct costs (e.g. cost of materials, equipment, labour) and indirect costs (e.g. social cost of carbon emission) associated with the project. One of the common methods used to assess direct costs and benefits associated with a project is life cycle cost analysis (LCCA) [2]. A detailed discussion on the economic sustainability assessment and the available tools is presented in Reddy et al. [4]. Social sustainability assessment is a challenging task as there are no defined metrics or tool to quantify the social impacts of a project. However, for a triple-bottom line sustainability assessment, social sustainability is equally important as environmental and economic sustainability. One of the semi-quantitative tools to assess social sustainability is social sustainability evaluation matrix (SSEM) developed by Reddy et al. [5].

Overall sustainability is achieved by the holistic integration of the environmental awareness, economic equity and socially viable aspects into engineering designs. Although there are several tools available to assess the environmental, economic and social sustainability individually, there is no tool that integrates the three pillars of sustainability and quantifies the overall sustainability by normalizing the multivariate impacts into a common scale which can be used to compare the sustainability of design alternatives in a project.

QUALICS is a new framework that integrates the three pillars of sustainability by using two multi-criteria decision analysis tools: integrated value model for sustainable assessment (MIVES) and analytic hierarchy process (AHP). This paper presents the fundamentals of the QUALICS framework along with its applications to geotechnical and geoenvironmental engineering projects. Two case studies demonstrating the applicability of the QUALICS framework to arrive at the most sustainable option among various alternatives in typical geoenvironmental and geotechnical projects are presented in this paper.

2 Quantitative Assessment of Life Cycle Sustainability (QUALICS) Framework

The framework combines two multi-criteria decision methods, MIVES and AHP [6]. The schematic of overall methodology of the framework is shown in Fig. 1. The framework can be applied for sustainability assessment of any kind of engineering projects/product/activities.

2.1 Steps in QUALICS Framework

An engineering problem can have more than one suitable solution. For example, an earth retaining structure could be a cantilever wall made of reinforced concrete or a mechanically stabilized earth wall, both can be designed to perform the same function. In order to choose the most sustainable solution among the two options, it is important to quantitatively assess the broader environmental, economic and social implications across all the life cycle stages involved in the execution of the project. Therefore, the first step of the QUALICS framework is the selection of potential design alternatives, which can perform the same function, for a project. This step involves complete technical design of each of the alternatives based on the project and site requirements and activities.

The second step of the framework is to define the qualitative and quantitative variables that closely represent the major environmental, economic and social implications of all the design alternatives. The variables are divided into several categories including requirements, criteria and indicators. The variables under

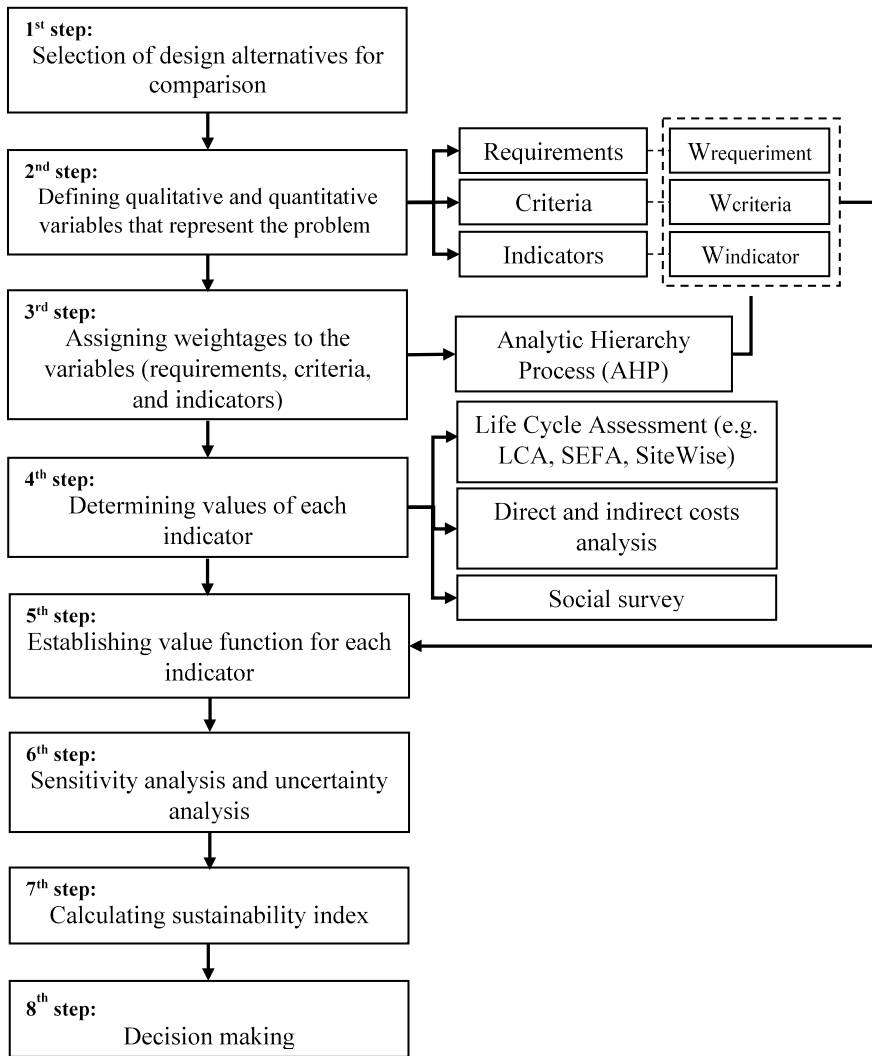


Fig. 1 Schematic of the QUALICS framework

requirement level/category are essentially environmental, economic and social domains. Similarly, each requirement is further subdivided into set of variables categorized as criteria. Furthermore, each criterion is divided into another set of variables categorized as indicators. The variables are project-specific and hence may vary from one project to another. The requirement level variables form the basis of the triple-bottom line sustainability assessment which include environmental, economic and social aspects. The criteria-level variables include the variables which are the subset of the requirement levels. The environmental criteria

include air, water usage and impacts, energy usage, land and ecosystems. Similarly, economic criteria include direct and indirect costs, and social criteria include socio-individual, socio-community, socio-economic and socio-environmental aspects. The variables at indicator level are the ones that represent the impacts that lead to broader impacts at the higher level (e.g. the requirement level).

In the QUALICS framework, the environmental indicators are derived from the impact categories of some of the well-established environmental impact assessment tools such as LCA, Spreadsheets for Environmental Footprint Analysis (SEFA) and SiteWise [6]. The economic indicators include direct costs associated with materials, labour, equipment, transportation and waste disposal as well as the indirect costs such as social cost of carbon emissions. The social indicators may vary depending on the project and the design alternative being assessed. An example of set of variables under requirement, criteria and indicator levels are shown in Table 1.

The third step of the framework involves assigning weightages to the variables of each category. The AHP process is followed to arrive at the weightages of the variables. AHP, a method proposed by Saaty [7], is used to make judgments in an orderly fashion and to identify the priorities among different criteria. The AHP method comprises various steps which include defining the problem and structuring the problem in terms of hierarchy from requirement to indicator level. A pairwise comparison matrix is established to compare the relative importance of one variable against another, e.g. relative importance of environmental aspect against economic aspect for the given project/design alternative. The pairwise comparison establishes the priorities of the variables which is then used to derive the weightages. A simple example of the weightages assigned to each variable is shown in Table 1. The expert knowledge and judgments are used to make comparisons and establish weightages. Detailed explanation on AHP methodology with respect to QUALICS framework can be found in Trentin et al. [6].

The fourth step in the framework is to determine the quantitative values of the variables at the indicator level. The values of environmental indicators are determined using environmental impact assessment tools such as the LCA which considers the life cycle stages from material acquisition to the waste disposal. The values of economic variables can be determined by considering the direct and indirect costs associated with the activity. The direct costs involve the cost of materials, labour, machinery, transportation and waste disposal. The indirect cost involves social cost of carbon emissions. The social impacts are quantified with the help of surveys. The social impact indicators are chosen based on the expert judgment. The survey respondents are chosen based on their experience, knowledge and expertise in the relevant field. The survey results are compiled to arrive at the final scores for each social impact indicator.

The fifth step of the framework is to establish value function for each indicator. The value function normalizes each indicator value in a scale of 0–1 with 0 being a value of minimum satisfaction and 1 being the highest satisfaction. Value function allows comparison of variables with different units of measure. There could be

Table 1 An example of requirements, criteria and indicators and their corresponding weightages used in QUALICS framework

Requirement	W _{requirement} (%)	Criterion	W _{criteria} (%)	Indicator	W _{indicator} (%)
Environmental	33.33	Air	25	Ozone depletion (kg CFC-11 eq)	15
				Greenhouse gas emissions/global warming (kg CO ₂ eq)	20
				Smog Formation (kg O ₃ eq)	15
				Human health-Cancer (CTUcancer)	20
				Human health—non-cancer (CTUoncancer)	15
				Human health—particulate (PM2.5 eq)	15
		Water usage and impacts	25	Acidification potential	50
				Eutrophication potential	50
		Energy	25	Fossil fuel depletion	100
		Land and ecosystems	25	Ecotoxicity	100
Economic	33.33	Direct costs	50	Materials (USD)	50
				Operations (USD)	50
		Indirect costs	50	Social cost of CO ₂ (USD)	100
Social	33.33	Socio-individual	25	Overall health and happiness	20
				Income-generating activities	20
				Contaminant exposure (trespassers, workers)	20
				Accident risk—injury	20
				Effect on recreational activities	20
		Socio-community	25	Appropriateness of future land use with respect to the community environment	17
				Enhancement of commercial/ income-generating land uses	17
				Enhancement of recreational facilities	17
				Degree of “grass-roots” community outreach and involvement	17
				Time for completion of project and access to public	17
				Degree of improvement in aesthetic value	17
		Socio-economic	25	Economic impacts of project on community	20
				Accidental risk and damage to property	20
				Effect on tourism	20
				Disruption of businesses and local economy during construction/ remediation	20
Employment opportunities during construction/ remediation	20				

(continued)

Table 1 (continued)

Requirement	$W_{\text{requirement}}$ (%)	Criterion	W_{criteria} (%)	Indicator	$W_{\text{indicator}}$ (%)
			25	Degree of consumption of natural resources	20
				Degree to which proposed project will affect other media (i.e. emissions/air pollution resulting from	20
				Effects of anthropogenic contaminants at "chronic" concentrations	20
				Degree of protection afforded to remediation workers by proposed remediation	20
				Effects of anthropogenic contaminants at "acute" concentrations	20

various forms of value function varying from linear to S-shaped [5]. The value function used in this study is shown in Eq. 1.

$$V_{\text{ind}} = \frac{\ln\left(\frac{\chi}{\chi_{\text{max}}}\right)}{\ln\left(\frac{\chi_{\text{min}}}{\chi_{\text{max}}}\right)} \tag{1}$$

The sixth step involves sensitivity analysis of the parameters influencing the overall sustainability of the project. It is important to identify the factors which are outweighing the other parameters in the impact assessment. For example, if the negative impacts are predominantly due to transportation across all the impact categories, then the sensitivity analysis can be performed by varying the transportation distance.

The seventh step in the framework is determination of sustainability index. Sustainability index is calculated following the MIVES methodology [7]. In the MIVES methodology, the values of the indicators (V_{ind}) derived from the value function are multiplied with their respective weightages (W_{ind}). The sum total of the products of indicator value and its weightage gives the value for the variables under criterion category (V_{cr}) (Eq. 2). Each criterion value is multiplied by its respective weightage (W_{cr}) and summed to get the value of variables under requirement level (V_{req}) (Eq. 3). The final value (V_{final}) also called the sustainability index is derived from the sum of the products of requirement value and its respective weightage (W_{req}) (Eq. 4).

$$V_{\text{cr}} = \sum_1^n V_{\text{ind}} \times W_{\text{ind}} \tag{2}$$

$$V_{\text{req}} = \sum_1^m V_{\text{cr}} \times W_{\text{cr}} \quad (3)$$

$$V_{\text{final}} = \sum_1^k V_{\text{req}} \times W_{\text{req}} \quad (4)$$

where n , m and k are the number of variables under each category (indicator, criterion and requirement, respectively).

The eighth and final steps in the framework are decision-making. The decision-making process involves comparison of the sustainability index values of each option. The alternative obtaining highest sustainability index value is considered the most sustainable option. The overall sustainability of a project is sometimes subjected to the stakeholders' relative preference of environmental, social and economic aspects. For example, in some projects, social aspects are more important than the environmental and economic aspects. In such case, social requirement is given more weightage during sustainability assessment. A detailed description of the QUALICS framework is presented in Trentin et al. [6].

3 Case Studies

This section describes the use of the QUALICS framework in assessing the sustainability of different design alternatives in geotechnical or geoenvironmental projects. The applicability of the framework is demonstrated using two case studies. A brief overview of the project and site description, potential design alternatives/strategies, the technical design and the results from the sustainability assessment using QUALICS framework is discussed under each case study.

3.1 Case Study 1: Contaminated Site Remediation

The site under study is an 87.52-acre land historically used for agricultural purposes since 1874 which was later transformed to electrical power generating facility in 1969. The site discontinued electricity generation in 2004. During the operation of the plant five spills which included spills of mineral oil, lubricating oil, diesel oil, and fuel oil were documented. The geology of the site is mostly clay deposits with some concrete and fill from the previous site activity. The saturated hydraulic conductivity of the project site soils ranges between 1.26×10^{-5} m/s and 3.17×10^{-6} m/s. The well borings showed that the groundwater table is between 3 and 12 feet below ground level. During the initial site investigation involving 96 soil borings and six groundwater monitoring wells, the site was tested for benzene,

toluene, ethylbenzene and xylene (BTEX) compounds, polychlorinated biphenyl (PCBs), ethylene glycol, volatile organic compounds (VOCs), semi-volatile organic compounds (SVOCs), pesticides and priority pollutant metals. At 7 locations of the 13 locations where samples were taken, the samples had been contaminated with BTEX, PAHs, PCBs, and metals.

A conceptual site model was developed to identify all potential sources of contamination, contaminated media, exposure pathways and receptors. The exposure pathways included incidental ingestion, inhalation of particulates and dermal contact. The potential receptors were identified to be residents and construction workers. The baseline risk assessment for carcinogenic and non-carcinogenic risk for the identified contaminants of concern was conducted, and the preliminary remediation goals for the site were established. Based on the baseline risk assessment, seven hot spots of approximately 100 ft. × 100 ft. were identified for remediation. Feasibility evaluation of different remediation technologies was conducted, and three potential remediation technologies, namely electrokinetic remediation (EKR), excavation and disposal and phytoremediation, were identified. The preliminary design and implementation considerations of the three potential remedial options are presented by Trentin et al. [6]. The three remedial options were further assessed for their relative sustainability using the QUALICS framework using the data derived from the preliminary design of the three remediation technologies.

The environmental impacts of each remedial option were assessed by performing LCA as per the International Organization for Standardization (ISO) standards using SimaPro version 8.5. The details on the scope (system boundary) of the LCA, the life cycle inventory and the impact assessment method used for the LCA in this case study are provided are Trentin et al. [6] 100 ft. x 100 ft. x 4 ft. of contaminated soil (one out of the seven hotspots) was considered as the functional unit for sustainability assessment of the three potential remedial alternatives. Figure 2 shows the results of the life cycle environmental impact assessment of each life cycle stage considered in the EKR option. Similarly, Fig. 3a shows comparison of environmental impacts associated with each remedial options

The economic impacts were also determined by calculating the direct costs (e.g. cost of materials, equipment, labour, transportation) and the indirect costs (e.g. cost of environmental emissions and impacts) at each life cycle stage. The total direct and indirect costs for EKR, excavation/disposal and phytoremediation, respectively are shown in Fig. 3b. Finally, the social sustainability assessment was performed based on the survey conducted using the Social Sustainability Evaluation Matrix (SSEM) developed by Reddy et al. [5]. Figure 3c shows the social sustainability index calculated using MIVES methodology based on the scores obtained in SSEM. The results from these analyses were compiled and used in the value function analysis involving MIVES and AHP method in the QUALICS framework, and the sustainability indices for each remedial alternative considering equal weightages to environmental, economic and social aspects were found to be 0.49, 0.32 and 0.69 for EKR, excavation/disposal and phytoremediation options, respectively (Fig. 3d). A sensitivity analysis with respect to EKR was also

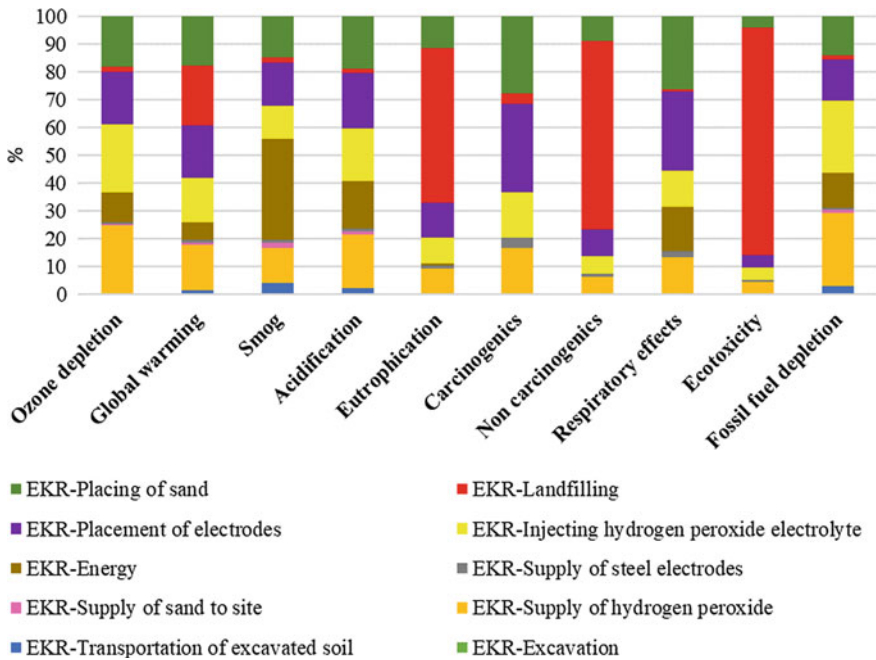


Fig. 2 Environmental impact assessment of each component of the EKR option using TRACI 2.1 V1.01/US 2008 method

performed to evaluate the influence of energy source, distance travelled, materials used for the electrodes and the cost of materials. In addition, the weightages of environmental, social and economic requirements were also varied to identify the sensitivity of stakeholder preferences on the resulting sustainability indices figures not shown.

Phytoremediation option was the most sustainable option with the least environmental and economic impacts. However, the social sustainability of the EKR option was found to be the highest among the three alternatives. Overall, phytoremediation was found to be the most sustainable option irrespective among the three alternatives.

3.2 Case Study 2: Deep Foundation System

This project involved the sustainability assessment of construction of a deep foundation system for a site in Chicago, Illinois, USA. The two deep foundation systems assessed for their overall sustainability with regard to the design and construction were drilled shafts (caissons) and pile foundation. The scope of the assessment was limited to the raw material acquisition, material manufacturing,

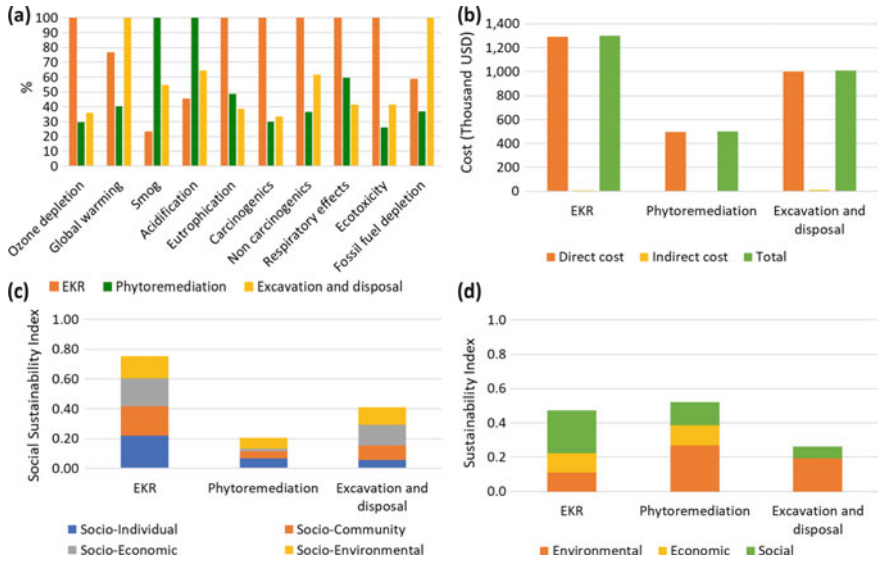


Fig. 3 Sustainability analysis of EKR, phytoremediation, and excavation and disposal options **a)** environmental, **b)** economic, **c)** social and **d)** overall sustainability

transportation and construction stages only. The impacts from the disposal of the construction waste generated were not included. The generalized subsurface soil profile at the site is shown in Kumar et al. [8]. The functional unit for the sustainability assessment of the two deep foundation systems was assumed to be five columns with each column carrying a load of 4448 kN (~1000 kips). Thus, the assessment compared the design and construction of five pile groups (i.e. $5 \times 14 = 70$ steel piles) and five caissons to support the five columns. The depth of both foundation systems required was 16.8 m (~55 ft.), which is the depth at which the base of the foundation was sufficiently within the hard clay.

The geotechnical engineering properties of soil layers including the shear strength (angle of internal friction (ϕ) for sands, and undrained shear strength (c) of clays) and the unit weight of the soil layers (γ) required for the technical design of the pile groups and caissons were determined based on the available site boring logs and laboratory/field testing [8]. Using these properties and the principles for design of pile foundations and caissons, the design of pile group and caisson was finalized. A detailed description of the technical design, the quantities and the unit cost of materials used and the fuel consumption of the equipment used for the construction of each of the two designs are provided by Kumar et al. [8].

A life cycle assessment (LCA) of the two design alternatives was performed using SimaPro software v8.5. The US life cycle inventory (LCI) database available in the software was used for the materials used in the construction of the two designs. The Tool for the Reduction and Assessment of Chemical and other

environmental Impacts (TRACI), a midpoint life cycle impact assessment (LCIA) method, developed by USEPA was used for the environmental impact assessment. The economic sustainability was assessed by evaluating the direct costs (e.g. cost of materials, equipment and machinery, labour and fuel) and indirect costs (e.g. social cost of carbon) associated with the design and implementation of the foundation system. The indirect costs were essentially based on an estimate of the monetized damages caused by an incremental increase in the carbon dioxide (CO₂) emissions in a given year [9, 10]. Based on SSEM approach, the functional and social impacts of each deep foundation system were assessed by conducting an online survey among professionals and academicians familiar with the two deep foundation systems. Questions for the survey were structured to evaluate the social impact of each of the deep foundation alternative on aspects at the functional, individual, community, economic and environmental levels. The indicators used for the social impact assessment are listed by Kumar et al. [8].

The sustainability index was calculated for each design alternative using the QUALICS framework as explained earlier. The results from the LCA showed that for the given functional unit and based on the site's geologic conditions, pile foundations had significantly higher environmental impacts under all the impact categories in the TRACI impact assessment method (Fig. 4a). Furthermore, it was found that the steel used in the manufacturing of the pipe piles was a major contributor to most of the environmental impacts in all the impact categories. Likewise, the direct costs associated with material, labour, equipment and fuel consumption along with the indirect cost from the predicted damages caused from CO₂ emissions (social cost of carbon) showed that pile foundation was an unsustainable choice due to its high cost (\$330,282) compared to the total cost of caissons (\$30,972) (Fig. 4b). The social impacts assessed based on a survey conducted among the experts also showed pile foundation to be a socially unsustainable choice (Fig. 4c). The overall sustainability index also showed caissons to be more sustainable than piles (Fig. 4d).

In conclusion, the authors suggested that the results from the analysis are site specific and may vary based on loading, geologic constraints as well as the weightages derived from the AHP for the analysis. However, such analysis involving the quantitative and holistic assessment of the net environmental, economic and social impacts from the project's activities will result in decisions made on a rational and sound basis.

4 Summary and Challenges

Civil, infrastructure and environmental engineering projects, including the geotechnical and geoenvironmental projects, are major contributors to the growing problem of global climate change due to the extensive use of energy and resources in the projects that lead to significant emissions and release of waste streams to the environment. Currently, there are well-established procedures in practice, at least in

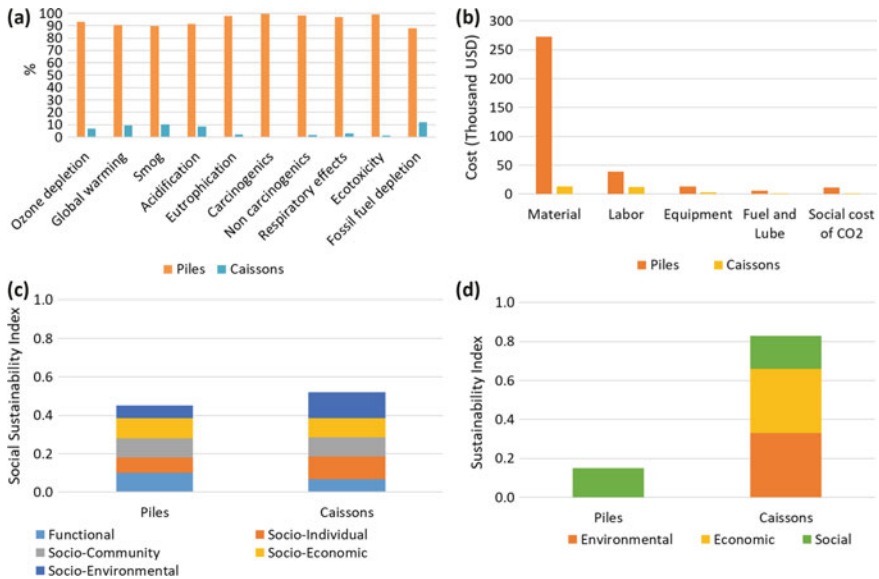


Fig. 4 Sustainability assessment of piles and caissons **a)** environmental, **b)** economic, **c)** social, and **d)** overall sustainability

the USA, to design and construct infrastructure in a technically sound basis. Similarly, significant advancements have been made to lay a strong technical framework to identify the hazard, characterize and remediate the contamination at the site, to a level that does not pose risk to human health and the environment using a suitable remediation technology. However, in the context of the global challenges faced by the world (e.g. exploding population and global climate change), the concept of sustainability and sustainable development is gaining wide prominence. Project activities in geotechnical and geoenvironmental projects utilize enormous amounts of energy and resources during the entire project life cycle. In this regard, quantifying the broader or secondary impacts from these project activities becomes important to identify the most effective and sustainable remedial option and consequently aid in contributing to the global sustainable development.

Recognizing the need and the importance of sustainable practices in infrastructure and environmental engineering projects, many federal agencies, international organizations and other academic researchers alike have proposed numerous qualitative and quantitative tools to identify a sustainable option among the different available potential design alternatives. However, these tools do not account for the broader economic and social impacts with a life cycle perspective. In addition, most tools focus on either of the three essential pillars of sustainability (environment, economy and society) with more inclination towards environmental impacts. Realizing this gap, a new quantitative assessment of life cycle sustainability (QUALICS) framework is proposed to aid in quantifying the secondary impacts and

identify the most sustainable design alternative in an engineering project. The QUALICS framework utilizes the MIVES and AHP, multi-criteria decision-making methods, to quantify the sustainability of different remedial options based on relative importance and relevance of the different criteria and indicators representative of the unique potential impacts envisioned to be arising for the project activities at the site. The method relies considerably on the knowledge and judgmental capacity of the experts and brings reality and complexity of the system in the sustainability assessment.

The applicability of the QUALICS framework is demonstrated using two case studies encompassing typical projects in geotechnical and geoenvironmental engineering. The QUALICS framework is used to identify the most sustainable design alternative/option to be implemented at the site. In addition, sensitivity analysis performed in the case studies discussed shows that the results on the sustainability index may vary based on the stakeholder's preferences (favoring one sustainability pillar over the other). The future research in this regard should focus on strengthening the economic aspects by involving the indirect costs and benefits that are otherwise unaccounted in most of the tools. Further, the tool used for social sustainability assessment in the QUALICS framework is still wanting. Therefore, a well-structured social sustainability assessment tool that can cater to assess the social sustainability in a rational manner (such as the life cycle assessment methodology) for any project has to be developed.

References

1. Damians, I.P., Bathurst, R.J., Adroguer, E.G., Josa, A., Lloret, A.: Sustainability assessment of earth-retaining wall structures. *Environ. Geotech.* **5**(4), 187–203 (2016)
2. Reddy, K. R., Kumar, G.: Addressing sustainable technologies in geotechnical and geoenvironmental engineering. In: *Geotechnics for Natural and Engineered Sustainable Technologies* (pp. 1–26). Springer, Singapore (2018)
3. Reddy, K. R., Kumar, G.: Green and sustainable remediation of polluted sites: new concept, assessment tools, and challenges. *ce/papers*, Special Issue: XVI DECGE 2018 Proceedings of the 16th Danube—European Conference on Geotechnical Engineering, 2(2–3), 83–92 (2018)
4. Reddy, K. R., Kumar, G., and Chetri, K. J.: Green and sustainable site remediation: incorporating broader economic impacts. In: *The 17th African Regional Conference on Soil Mechanics and Geotechnical Engineering* (2019)
5. Reddy, K. R., Sadasivam, B. Y., Adams, J. A.: Social sustainability evaluation matrix (SSEM) to quantify social aspects of sustainable remediation. In *ICSI 2014: Creating Infrastructure for a Sustainable World*, 831–841 (2014)
6. da S Trentin, A. W., Reddy, K. R., Kumar, G., Chetri, J. K., Thomé, A.: Quantitative Assessment of Life Cycle Sustainability (QUALICS): Framework and its application to assess electrokinetic remediation. *Chemosphere*, 230, 92–106 (2019)
7. Saaty, T.L.: Decision making with the analytic hierarchy process. *Int. J. Serv. Sci.* **1**(1), 83–98 (2008)
8. Kumar, G., Chetri, J. K., Reddy, K. R.: Sustainability assessment of deep foundations: case study. In: *44th Annual Conference on Deep Foundations*, Deep Foundations Institute

9. Raymond, A.J., Pinkse, M.A., Kendall, A., DeJong, J.T.: Life-cycle assessment of ground improvement alternatives for the Treasure Island, California, redevelopment. In: Geotechnical Frontiers, pp. 345–354. American Society of Civil Engineers, Reston, VA (2017)
10. USEPA (United States Environmental Protection Agency): The social cost of carbon: estimating the benefits of reducing greenhouse gas emissions. Available at: https://19january2017snapshot.epa.gov/climatechange/social-cost-carbon_.html. Accessed on 26 August 2019

Geological and Geotechnical Investigations and Interpretations Thereof for Statue of Unity Foundation



Sandeep Ghan

Abstract The statue of Unity, tallest statue of Late Sardar Vallabhaiji Patel, is constructed at around 3.50 km downstream of the Sardar Sarovar Dam. The statue is located on Sadhu Hill, one hill islanded in Narmada river waterway. The Sadhu Hill is around 250 m inside the Narmada waterway, and the top of the hill was at RL 72.0 m. Sardar Vallabhaiji Patel was a great Statesman and played a leading role in struggle for independence and guided into a united, independent nation. He forged a united India from British colonial premises and more than five hundred self-governing princely states. He was first deputy Prime Minister and first Home Minister of the country. To pay the respect to this great leader, Gujarat government decided to build a tallest statue of this leader in the world and the same is constructed at Sadhu Hill. The statue is 182 m tall and is of Bronze panels fixed on steel cladding which are fitted to concrete cores. This paper covers in detail the geological and geotechnical features of the statue site and surrounding area. It will be also detailing the difficulties faced during the design, the foundation and the basic structural design for such a tall structure. The statue is having two RCC cores and cladding around to support bronze sheets which are moulded to the statue shape. Considering the iconic importance of the structure, extensive geological and geotechnical investigations were carried out along with field tests.

Keywords Brecciated · Sandstone · Shale

S. Ghan (✉)

Chief Engineering Manager, Transportation Infrastructure IC, EDRC (RREC),
L & T Construction, Mumbai 400093, India
e-mail: Sandeep-Ghan@Intecc.com

1 Site Location and Topography

The proposed Statue of Unity is located on a rock promontory known locally as Sadhu Hill on the north side of the Narmada River bed. During periods of high river flow, this promontory is an island within the river channel. The top of the rocky promontory was at an elevation of R.L. 70.90 M above the mean sea level.

The Narmada River is the fifth largest river in India and drains a large area of central India to the west. River flow is very seasonal, reflecting the monsoon climate of the subcontinent. This has been reduced since the construction of the Sardar Sarovar Dam upstream of the proposed location for the Statue of Unity has taken place.

2 Regional Geology

The Narmada River flows along the ENE-WSW trending Narmada-Son Fault (NSF), a well-known seismotectonic feature. A major part of the course of the Narmada River falls within the rocky area comprising basaltic lava flow belonging to the Deccan Trap Formation. The river follows a constricted course in this reach characterized by waterfalls, rapids and gorges. The true alluvial reach of the Narmada is encountered in its lower part within the state of Gujarat. This reach is about 90 km in length and forms the southern margin of the N-S extending Gujarat alluvial plains.

The Narmada-Son Fault (NSF) divides the Indian plate into two halves and has a long tectonic history dating back to the Archaean times. This fault trends in ENE-WSW direction and is laterally traceable for more than 1000 km. It demarcates the Peninsular India into two geologically distinct provinces: the Vindhyan–Bundelkhand province (VBP) to the north and the Deccan province to the south regards the Narmada-Son Fault as a part of the composite tectonically controlled zone in the middle of the Indian plate and termed it as the SONATA zone (abbreviated form of Son-Narmada-Tapti Lineament zone). The Narmada and Tapti Rivers all throughout their course follow these tectonic trends. Geophysical studies in the central part of this zone reveal this to be a zone of intense deep-seated faulting.

The Narmada Basin has become reactivated in response to the collision of India with the Asian continent with uplift and subsidence taking place in a zone including the Son Narmada fault and along the pre-existing structures to the south of the Son-Narmada fault.

3 Geology of Sadhu Hill Area (Statue Location)

As mentioned above, the site chosen for the construction of the monument was an isolated hill mass in the Narmada river bed as shown in Fig. 1. The hillock is close to the right bank of the river. It comprises sedimentary rocks of Bagh Bed belonging to Cretaceous age. Main rock type is Quartzitic Sandstone. Minor shale beds are also present [1]. The area occupied by this hillock measures about 0.6 km² as could be assessed from the SOI contour map. The maximum height attained by the hillock is 70.90 m. The hillock is an inlier as it is surrounded by the younger Deccan trap basalt on all sides. The inlier may be formed due to tectonic activities during different geological periods. The hillock is in the form of a “horst structure” wherein the central block has come up relative to the adjacent block. The horst structure is formed due to “reverse faults” [2].

Due to tectonic activities at the end of Deccan Trap volcanism in the region, the sandstone beds have developed numerous joints as shown in Fig. 2.

The second abundant sedimentary rock type is medium- to dark-grey shale that apparently appears to be bituminous in nature (Fig. 3). Many of the shale contain considerable amount of fine-grained sand particles, and detrital muscovite mica. Argillaceous content has recrystallized into fine particles of sericite mica, leading to the development of an incipient phyllitic cleavage. The intrusive rocks are mainly dolerites and finer-grained basalts.

Fig. 1 Sadhu Hill in original condition [3]





Fig. 2 Mosaic texture in quartzitic sandstone



Fig. 3 Grey-coloured shale

The site falls in zone III of the seismic zoning map of India (BIS) where maximum expected magnitude of an earthquake is 6.0. Most of the area is covered by the Deccan traps and is along the Narmada-Son lineament, which is now inactive. Other faults nearby the study area are Piplod fault, Rajpardi fault, Borkhadi fault and Barwani-Sukta fault. The SSNNL is running a network of nine seismological stations comprising of short-period sensors since 1990 and recorded considerable amount of local seismicity.

Sadhu Hill abruptly rises with a vertical cliff. At the base of the hill lies the shale beds, and shale beds are encountered further in boreholes, but they are not exposed

on the surface of the Sadhu Hill. The youngest formations are exposed only in the north-western dwarf hillock, indicating that it forms the downthrown block.

The sandstone rock, with low dips of 15° – 22° westerly have very rough uneven surface, intersected by two prominent vertical joint sets. These joints formed large rectangular blocks of hard sandstone rock with crushed infillings within joints opening. Some of these blocks have been detached fully from their in situ positions on the bedding planes, whereas majority of them are still intact, but bit unstable with wider open gaps around them. It was necessary to assess correctly the engineering characteristics of rock mass through borehole identification.

Sadhu hillock is the isolated conical hill formed by erosional effect of Narmada River and can be defined as island in the river having flow of water on its all sides during flood season. Beautiful sections of this hillock have been exposed on its north eastern and south-western side by virtue of erosional effect by the Narmada River in the past. Thus, a complete subsurface rocks can be seen in these exposed sections which increase reliability of the borehole data drilled in the Sadhu Hill. Moreover, subsurface geology is clearer in these sections than in the borehole section.

In the case of drilling results of project area, a great variation in RQD values have been found.

A borehole, if drilled along the joint plane, will obviously intersect crushed infilling material, and poor RQD values are obtained. While another borehole, drilled just a meter away, will interact hard sandstone rock throughout its drilled depth with 100% RQD values.

Generally, the hard sandstone rock has been known for their excellent competency having uniaxial compressive strength generally more than 80 MPa along with high bearing capacity. Here also, these rocks appear to be very favourable to withstand the induced load of proposed statue with least variability in shear strength and bearing capacity through all zones of influence below the foundation.

4 Geotechnical Investigation at Sadhu Hill

The geotechnical investigation comprised 18 rotary cored boreholes to depths of 30 m to 90 m. The hydraulic rigs with triple tube core barrels were used to drill these deep boreholes. Three of the boreholes were inclined (45°) to investigate the rock mass immediately below the statue foundation. Five of the boreholes were surveyed using a down the hole televiewer to provide rock mass information and discontinuity orientations.

As already explained above, geophysical survey and surface geological rock outcrop mappings were performed to delineate major discontinuities, shear zones, geological setting for preliminary geological and geotechnical assessment of rock condition. The rock mass rating was calculated to know the response of rock mass and foresee the unexpected problematic zones as well as assessment of slope stabilization, foundation treatment if any, etc.

5 Geotechnical Assessment/Finding of Investigations

The main objective of geological and geotechnical survey was to summarize surface geological, subsurface geotechnical studies to work out with the following important attributes:

- i. Lithology,
- ii. Joints,
- iii. Discontinuities,
- iv. Permeability,
- v. Stratigraphy,
- vi. Geological setting.

The effect of the same was studied on the statue foundation and the global stability of Sadhu Hill. The additional objectives of the geotechnical investigation are to characterize the contact between overburden and in situ rock condition. To understand the porosity, permeability of rock and overburden materials which provide geotechnical inputs to the design mechanism of support system, rock excavation system for the foundation of 182 m high statue, slope stability analysis, blasting geometry, establishment of appropriate powder factor of blasts (PF) and road foundation, required for construction phase in appear Statue of Unity at Sadhu Hill site were carried out. The further objectives were assigned to provide comprehensive, graphic, geological, geotechnical, hydrological, geophysical and conceal surprises if any, weak zones, water in rushes information about the site conditions for technical purpose based on bore hole data to evolve an explicit, safe and economic design operation and selection of appropriate rock-friendly machinery.

6 Additional Testing at Sadhu Hill and Interpretation Thereof

Following testing was carried out at statue location to understand the various properties of the rocks.

- i. Borehole logging,
- ii. Packer permeability test,
- iii. High-pressure dilatometer,
- iv. Cross-hole shear test,
- v. Electrical resistivity test.

6.1 Interpretation of Borehole Logging

A feature of the strata noted from the borehole core is a degree of tectonic disturbance in places. This results in brecciation of the rock mass which in places has recemented, but in some horizons, a very weak reddish brown siltstone matrix is present between the breccia clasts. The degree of brecciation is variable with the more disturbed zones being described as fault breccia. The four main shale units are present in most boreholes. These thin (<2 cm) shale bands are intermittent and indurated.

6.2 Packer Permeability Test

It is measured with Lugeon testing. The reported Lugeon values are generally in the range of 1–5 which indicates tight discontinuities with a few higher values suggesting some of the discontinuities are open/partly open. The very low permeability recorded by the Lugeon data implies that the rock is better than as compared to the number of discontinuities and fractures observed are observed in the cores.

6.3 High-Pressure Dilatometer

Young's modulus is found to be in range of 4 GPa average.

6.4 Cross-Hole Shear Test

The general observation from the cross-hole seismic investigation indicates that the velocities of P and S waves vary from 2490–3132 to 1215–1628 m/sec, respectively. The value of Poisson's ratio varies from 0.28 to 0.34.

6.5 Electrical Resistivity Test

Measured values of resistance of the ground to passage of electrical current are 1450 to 7440 ohm which are less than typical values of the sandstone.

7 Engineering Parameters of the Rock

- i. Strength: The permeability of sandstone is recorded less than 1.50 Lugeon indicating high quality of sandstone.
- ii. Strength (in terms of UCS): The lower bound strength is taken at the 20th percentile of the combined UCS data giving a strength of 49 MPa.
- iii. Following parameters are worked out based on Hoek–Brown criterion (rock mass assessment)

UCS= 48 MPa; GSI= 40; D = 0.1; m = 17; E = 12 GPa

- iv. The joint roughness factor of approximately 8 is considered.
- v. From cross-hole seismic test, the S-wave velocity is approximately 1250–1500 m/s at 30 m. Similarly, P wave velocity varies from 2500 to 3000 m/s at 30 m which is consistent with fractured sandstone.
- vi. The E_i value of 42 GPa is indicated as a mean value which shows the stiffness of the rock.

8 Statue Foundation and the Challenges

The statue foundation is a raft foundation on quartzitic sandstone at RL 52.50 m on Sadhu Hill as shown in Fig. 4. The foundation for such a tall structure (tallest in the world) is designed with stringent design criterion and due weightage to geology, geotechnical assessments of the rock, structural aspects of the statue, seismic parameters, wind speed and other design considerations.

The foundation for statue is 3-m-thick raft with wide base of 44 x 34 m. The bearing capacity of 1500 KPa was computed for the founding strata of sandstone. The wide base combined with high safe bearing capacity has provided a good base to the statue which is stable against overturning and sliding effects. The entire raft has been cast in a single pour to avoid joints.

Fig. 4 Foundation construction



The design of statue foundation was a tough job considering following points:

- i. Stability of rock mass—Overall stability (considering the complex geology),
- ii. Local stability,
- iii. Sandwiched shale rock in between Quartzitic sandstone layers,
- iv. Seismic parameters pertaining to seismic zone V (although the area falls in zone IV),
- v. Basic wind speed of 50 m/s,
- vi. Scouring of the hill due to river water.

9 Solution to the Challenges

Looking at the complex geology and issues as elaborated above, the foundation design was going to be a challenge. Due to big variation in values of several parameters, the consideration of all these parameters into design was also a complicated job.

9.1 Stability of Rock Mass—Overall Stability (Considering the Complex Geology)

The available borehole information and 3D conceptual ground model shows the rock to be highly affected by tectonic action which has resulted in non-planar bedding and impersistent discontinuities due to the effects of local faulting. Locally, shale was observed in the boreholes above the highest shale band, but these are also impersistent. Furthermore, the brecciated zones within the rock mass have been found to be the results of local faulting and are found to be localized in the nature. There was no evidence of a plane of weakness within the rock mass that would give rise to global instability.

Numbers of checks have been given for confirming the global stability including worst-recorded bedding plane orientation in the area and the effects of a 15 m tension crack full of water the head of the wedge [4].

9.2 Local Stability

Where the erosion of shale by flood waters has results in overhanging sandstone, the shale shall be protected from further erosion by the use of shotcreting. The rock terracing is being done with slopes that may have unfavourable orientation in respect to the minor faults.

9.3 Sandwiched Shale Rock in Between Quartzitic Sandstone Layers

Although shale layers sandwiched between sandstone layers are very thin (<1000 mm), those are felt to be major plane of weakness. However, considering the depth of shale layers (>17 m) below the formation level, the major pressure will be getting dissipated before reaching to those layers.

The foundation of the statue was ensured to be resting on sandstone.

9.4 Seismic Parameters Pertaining to Seismic Zone IV

Although the site comes under zone III, the consideration for foundation design is taken as zone IV and the zone factor is taken as 0.24 g. The seismicity of the area is having a deep impact on the foundation design.

9.5 Basic Wind Speed of 50 m/s

The wind load for the statue structure has been estimated using a basic wind speed of 50 m/s and by carrying out a detailed wind tunnel studies. The wind effects are very high and due to which the foundation design has become very complicated. The very high anticipated sways in the structure have made the structural stability complicated. To reduce the effects of wind and excessive deflections of the structure, two numbers of tuned mass dampers have been provided to increase overall damping of structure.

9.6 Scouring of the Hill Due to River Water

Due to very high water currents during the flood discharges from the dam and even in the normal time, the banks and the other earth structures are subject to scouring action. The shale layers below the water are susceptible to water erosion more due to which the hill may get weakened in submerged portions. The proper treatment for this is still underway and will be firmed up once the inspection will be completed for submerged portions.

10 General Idea About Statue Structure

The statue is unique, not only in terms of its height and scale, but more significantly because it is a true (or near to as possible) representation of a man; Sardar Vallabhbhai Patel. As such, due to the primarily geometrical challenges that a human form creates, conventional solutions are generally inappropriate. Instead, bespoke solutions have been found, developed and implemented.

Devising an efficient structure for the statue raised several challenges, from both a design and construction perspective. The “spine” of the statue is formed by the reinforced concrete core, and this not only has to withstand and safely transfer significant wind and seismic forces to the foundations; it also has to provide support to the “skeletal frame” that creates the shape of the Statue figure. The skeletal frame not only has to respond to the complex geometrical shape of the figure, but at its extremities it has to provide fixture and support to the relatively heavy bronze “skin”, that ultimately creates the form of Sardar Vallabhbhai Patel. These complex design issues were similarly manifest as complex construction challenges. It was therefore essential that the design be developed with pro-active input from L&T and its key subcontractors and suppliers and the bronze cladding contractor.

The statue has been modelled using 3D finite element analysis as shown in Fig. 5. For schematic design, the core has been modelled using a grillage of 1D elements connected using “stiff arms”. This approach allowed for control of

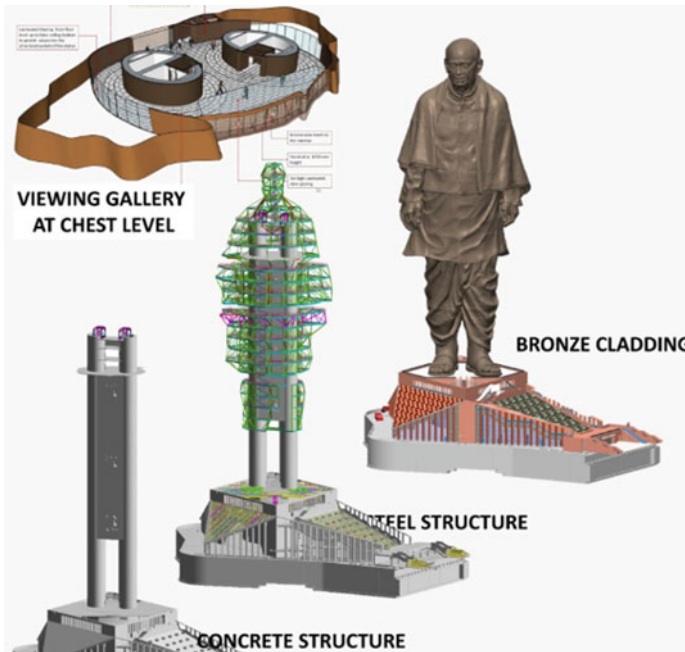


Fig. 5 Modelling of statue structure

in-plane and out-of-plane bending stiffness of walls and captured the effects of warping stiffness and shear stiffness. The output forces of the 1D analysis elements have been used to design the core wall sections. Only door and large service penetrations have been modelled.

The 182-m-tall statue is made up of a 25-m-high base and 157-m-tall statue. The base has high roofs with steel trusses and RCC slabs. The statue is divided into five parts—the lower and upper legs, lower and upper body and the shoulder and head.






The steel in the statue is in three layers: primary, secondary and tertiary. The primary frames are vertical trusses that interconnected with infill steel members and in turn connected to the RCC cores. These transfer all the load from the statue skin onto RCC cores. The secondary steel that is part of the primary layer are trusses that carry the load from the bronze cladding connected through the tertiary steel frames. These two layers form the basic skeleton of statue. The tertiary layer is set of steel trusses connected between secondary steel and bronze cladding that bridges the gap between the skin and the skeleton of the statue. Each tertiary steel frame is unique as each bronze panel is unique. Viewing galley at a height of 135 m from podium level has been provided as a unique experience for the visitors.

References

1. Choudhury, P., Rastogi, B. K, Kumar, S., Aggarwal, S: Seismic Hazard Analysis of the site selected for the construction of Sardar Patel Monument. ISR technical report No. 51 (2011)
2. Pancholi, D.: Report on Sadhu's hut site for locating statue of Sardar Patel. Vadodara, India (2010)
3. Ghan, S.: Geotechnical Investigation Report for the Statue of Unity. IGS (2015)
4. ARUP UK: Geotechnical Interpretive Report for Statue of Unity Project
5. Karanth, R.V., Patel, H., Gadhavi, M.: Report on geological mapping of Sadhu Hill Area. D. H. Geo Consulting, Ahmedabad (2015)

Early Warning of Water-Triggered Landslides



Vikas Thakur , Katherine Robinson, Emir Oguz, Ivan Depina, Ankush Pathania , Praveen Kumar , Prateek Chaturvedi, Kala Venkat Uday , and Varun Dutt 

Abstract Landslides are a major societal threat, causing adverse consequences to life, economy and environment. Mitigation of the potential negative effects of landslides commonly involves deployment of challenging and costly measures. This is often the case in the development and operation of linear infrastructures such as road, pipeline and railway networks in landslide-prone areas. One of the commonly employed measures for mitigating the adverse consequences involves monitoring of landslide triggering parameters and issuing timely warnings. Given that the landslide triggering parameters (e.g. large weather systems, local man-made triggers) and the linear infrastructures span varying spatial scales, there is a need for developing a landslide monitoring and early warning system for both regional and local scales. This paper presents a brief introduction of the Norwegian practice for early warning of landslides triggered by extreme weather on regional scale, which has proven to be effective. The criteria for issuing an early warning are based on the degree of saturation of soil and the supply of water to it through rainfall and snow melting. On other hand, monitoring of single slopes on local scales can be quite challenging and expensive. In order to provide landslide monitoring systems of single slopes in affordable price, Indian Institute of Technology Mandi developed a low-cost landslide monitoring and early warning system. These systems are deployed in Mandi district of Himachal Pradesh, India, and monitoring fifteen plus landslide locations. A recent case study is also discussed in this paper where these systems helped in alerting people and traffic from an impending landslide.

Keywords Landslides · Early warning system · Landslide monitoring

V. Thakur (✉) · K. Robinson · E. Oguz
Norwegian University of Science and Technology, 7491 Trondheim, Norway
e-mail: vikas.thakur@ntnu.no

I. Depina
SINTEF, S. P. Andersens veg 3, 7031 Trondheim, Norway
e-mail: ivan.depina@sintef.no

A. Pathania · P. Kumar · P. Chaturvedi · K. V. Uday · V. Dutt
Indian Institute of Technology, Mandi, Himachal Pradesh, India
e-mail: uday@iitmandi.ac.in

1 Introduction

Infrastructure development including building of roads, airports and railway networks on slopes is highly challenging and expensive due to the threat of landslides, i.e. down-slope movement of soil or rock along a failure plane. Landslides are triggered by combinations of natural and man-made causes such as severe rainfall, rapid snow melt, earthquake, or human activities. Moderate-to-steep slopes in weak soil or rock are most susceptible to landslides. Each year huge amount of property and human lives are lost due to landslides worldwide. UNISDR [1] quotes “*nearly 87% of disaster related spending goes on response, reconstruction and rehabilitation and only 13% goes towards managing the risks, which are driving these disasters including landslides in the first place*”.

It has become quite evident that changes in the climate cause a notable increase in the frequency of landslides. Triggering factors such as extreme rainfalls, rapid snow melts, permafrost melting and abrupt temperature change are the most common climate factors leading to naturally occurred landslides (referred as water-triggered landslides). Landslides cause major infrastructure damages and deaths in India. Paddhar landslide in 2017 in India exemplifies this, Ref. Fig. 1 for the details. More than INR 1000 crores/year economic losses and more than 1000 deaths/year is registered in India mostly confined to the Himalayan region. Due to landslides, average losses in Himachal Pradesh alone cost more than INR 300 crores per year and cause more than 200 deaths per year [2]. It is worth mentioning that majority of water-triggered landslides are along transport infrastructure such as roads, railroads and pipelines, which forms the lifeline of modern society. Their reliable and secure operation is paramount to national security and economic vitality.

Similarly, a significant part of European transport infrastructures is located on or in unsafe ground and are thus subjected to risks of landslides. At least 8,000–20,000 km of roads and railways are highly exposed to landslide [3, 4]. These risks result in high costs, with global annual losses of €18 billion caused by landslides. These losses comprise 17% of the €110 billion in global natural disaster losses each year. A majority of these costs are related to the repair and rehabilitation. In Italy, for example, total landslide-related damages in 2015 amounted to €3.9 billion [5]. Germany reported an annual total loss of about €68 million in 2015 from landslide damage to the highway system alone [5]. Another example involves the collapse of the ground beneath Norway’s Dovre Railway (Dovrebanen) in March 2012, for which direct repair costs exceeded €5 million. Indirect losses were significantly higher because Dovrebanen was closed for months for repair, and thus a major railroad connecting the Norwegian cities of Oslo and Trondheim was put out of commission.

The most frequent water-triggered landslides are seen in course-grained soils (sandy silty materials, tills, residual soils, debris). Sliding surface is often 1–2 metres deep in soil deposits as a direct result of infiltration of water in initially partially saturated soils. Shallow landslides, i.e., slides, debris slides and debris flows are the most common water-triggered landslides. Measures for mitigating of such landslide can be (a) structural solutions to reduce the frequency and severity of



Fig. 1 (Left) Water-triggered Paddhar landslide in 2017 in Himachal Pradesh due to intense and persistent rainfall. The failed slope was approximately 250 m high and 150 m in width. Approximately 300 000 m³ debris was displaced for approximately 950 metres resulting taking 46 lives (Courtesy Himachal Pradesh State Disaster Management Authority)

landslide events and (b) non-structural solutions to reduce the consequences through monitoring and prediction, improved land planning, rerouting, evacuation and early warning systems. Early warning (EW) systems have a great flexibility and costs much lower than structural solutions, which motivated the development of a wide range of solutions that are limited to varying degrees in terms of applicability, types of measurements, fabrication costs, maintenance and accuracy. In the last decade, studies on sensor-based solutions and real-time monitoring of slopes have enabled the development of landslide mitigation strategies based on EW systems. Due to the limitation in terms of the length of the paper, our focus is limited to describe a well-functioning EW method used in Norway and an ongoing effort in India by IIT Mandi to develop low-cost EW system for water-triggered landslides.

2 Prerequisites for Early Warning Systems

UNISDR [6] defines an EW system as “the set of capacities needed to generate and disseminate timely and meaningful warning information to enable individuals, communities and organizations threatened by a hazard to prepare and to act

appropriately and in sufficient time to reduce the possibility of harm or loss. An EW system shall consist of the following components: knowledge of and means of forecasting the water-triggered landslides; information from technical monitoring and field observation; preparedness plan to act or response; dissemination of warning to population exposed to landslide risk; and public awareness and preparedness. Selection of an EW system depends on several factors. However, landslide type and the scale of the landslide are the two major factors. Cruden and Varnes [7] classified landslides based the movements and the material types. They suggested five movement types: fall, topple, slide, spreads and flow and three material types, i.e., rock, coarse-grained soils and fine-grained soils.

The scale of EW can be either a slope scale or regional scale. A slope scale requires a set of monitoring technologies; operated either remotely or on site. Shallow landslides are not recurrent at a given location. However, they recur within a region. Therefore, EW of shallow landslides on a regional scale has been the approach that is more popular. The reliability of EW for water-triggered shallow landslides depends on accuracy of meteorological, hydrological, hydrogeological or geotechnical parameters. The EW of such landslide is often issued using intensity–duration curves for rainfall as thresholds with varying degree of accuracy.

Another crucial aspect related to early warning is time. A successful EW shall be able to identify and measure the initiation of a landslide, and issue warnings early enough to allow sufficient time to implement actions to protect life and properties. As the forecasting of temperature, rainfall is becoming accurate, a direct link between rainfall event and landslide occurrence is becoming increasingly efficient, in a statistical way, to provide early warning at small scale.

3 Norwegian Practice of Early Warning of Shallow Landslides on Regional Scale

Norwegian forecasting system for water-triggered landslide is developed and coordinated by Norwegian Water Resources and Energy Directorate (NVE). The EW is issued by NVE through www.varsom.no for the whole country with 1 km x 1 km resolution. The criteria for EW is based on relative water supply and the soil water saturation degree (see Fig. 2) using the real-time data, climate model and simulation of hydrological data using a distributed version of the hydrological HBV model [8]. The model divides Norway into 1 km² grid cells (total over 385 000 cells).

The relative water supply accounts for rainfall or the supply from melting of snow from the snowpack normalized with an annual average value for a 30-year period. Similarly, the relative degree of saturation (%) is the total water content normalized with annual average water content in the ground for a 30-year period. Figure 2 shows the national threshold used in Norway to issue early warning of water-triggered landslide. The EW has four danger levels; see Table 1 for the

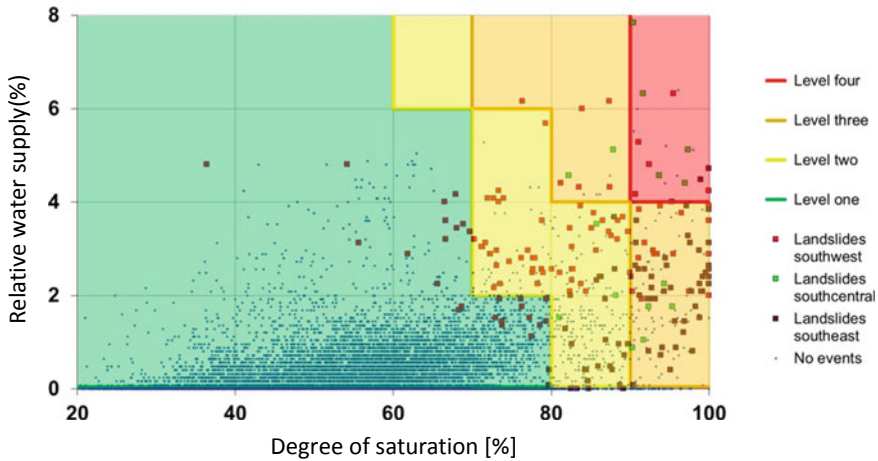


Fig. 2 National threshold for the early warning of water-triggered landslide in Norway (www.nve.no). Source www.nve.no and www.varsom.no

description. The accuracy of this EW is above 95%. The EW is being improved further by combining it with susceptibility maps and also by developing regional thresholds to issue warning. A detailed information about the EW can be found in Devoli et al. [9].

There are two major demanding issues related to the designing of an EW— firstly, the specification of appropriate threshold values for the alarms and secondly, number of false alarms and missed events. The consequences of false alarms and missed events are often so serious that every possible action must be taken to avoid them [10]. The criteria to assess the accuracy are based on how many false alarms are triggered for each danger level, ref. Table 2. The accuracy of the EW in Norway is close to 97% which can be considered quite effective [9].

4 IoT-Based Early Warning of Landslide on a Single Slope Scale

Recent developments in the domain of the environmental Internet of Things (IoT), however, have generated a spectrum of new opportunities for developing non-structural solutions for the prevention, detection, response and mitigation of geohazard risks with advanced monitoring and early warning (EW) systems. The IoT is a powerful concept of interacting with the physical world through a network of natural or man-made objects that are connected to the Internet and process the collected information automatically, with or without human intervention, to gain crucial insights that support more efficient management of limited resources. The flexibility and scalability of IoT-based EW systems support significant

Table 1 Awareness levels for landslide hazards used in Norway (www.nve.no)

Awareness levels	Description
Green awareness level (1)	Generally safe conditions
Yellow awareness level (2)	Situation that requires vigilance and may cause local damages Expected some landslide events, certain large events may occur Local flooding and/or erosional damage due to rapid increase of discharge in streams/small rivers, ice drift, ice in streams/rivers and frozen soil
Orange awareness level (3)	Severe situation that occurs rarely, requires contingency preparedness and may cause severe damages Flood: Return period of more than 5 years Expected many landslide events, some with considerable consequences Extensive flooding, erosional damage and flood damage to certain prone areas
Red awareness level (4)	Extreme situation that occurs very rarely, requires immediate attention and may cause severe damages Expected many landslide events, several with considerable consequences Extensive flooding, erosional damage and flood damage to buildings and infrastructure

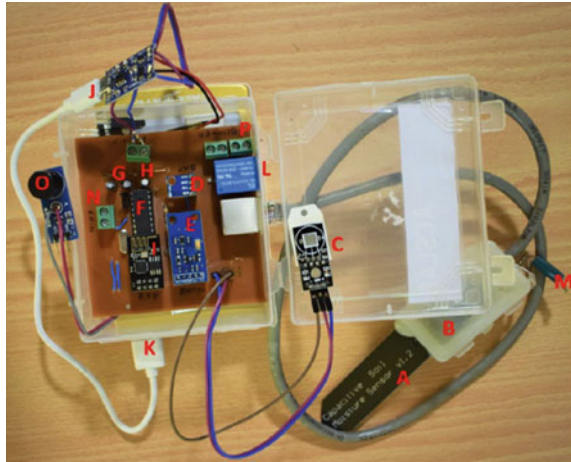
Table 2 Criteria used to evaluate the early warning system in Norway

Observed landslide events (debris slide/ debris avalanches, debris flows, small soil slides and slush flows)	>14	Miss	Wrong level	Wrong level	Ok
	6–10	Miss	Wrong level	Ok	Wrong level
	1–3	Miss	Ok	Wrong level	Wrong level
	0	Ok	False alarm	False alarm	False alarm
		Green	Yellow	Orange	Red
		Level sent			

automatization of landslide risk assessment through the implementation of advanced data analysis, statistical learning algorithms and efficient integration of data with advanced geohazards prediction models.

IoT technology can advance existing monitoring solutions with the deployment of cost- and power-efficient, scalable and flexible IoT devices. There are several ongoing projects investigating the advantages of IoT technologies in collecting and transferring data from sensors commonly employed in MEW systems for landslides [2, 11–14]. The Indian Institute of Technology (IIT) Mandi has developed a low-cost IoT solution for monitoring and EW of water-triggered landslides in India [2]. Figure 3 is a picture of the IoT system being developed by IIT Mandi. This IoT system is being used to monitor and issue early warning of landslides at 20 different locations in India. The IoT device has sensors that can be divided into several

Fig. 3 IoT device developed by IIT Mandi



categories: soil sensors, meteorological sensors, IoT device subcomponents and programmable local outputs. A brief description of the components included with the IoT device, and their functions is provided in the following section (Fig. 4).

The IoT device’s main unit contains the meteorological sensors. The meteorological factors that can be monitored include temperature, humidity, light intensity, barometric pressure and rainfall.

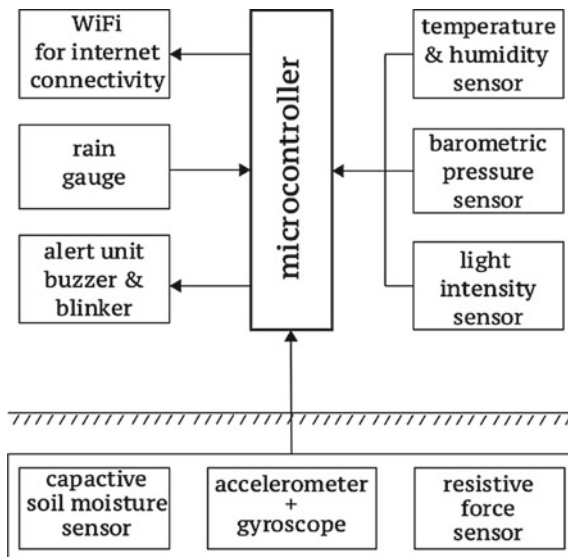
A: Capacitive Soil Moisture Sensor: Capacitive soil moisture sensor works on the principle of change in capacitance due to changes in the dielectric properties of the soil in contact with the sensor. The sensor measures the resonant frequency of an RC circuit, and this frequency value is linearly calibrated to volumetric water content of soil in percentage. The sensor’s range is between 0 and 100% moisture by volume, its accuracy is $\pm 5\%$, and its sensitivity is $\pm 1\%$.

B: Motion Processing Unit (MPU) Accelerometer: The accelerometer has both 3-axis accelerometer and 3-Axis gyroscope integrated on a single chip. The gyroscope measures rotational velocity or rate of change of the angular position over time, along the X-, Y- and Z-axis. It uses MEMS technology and the Coriolis effect for measuring. The outputs of the gyroscope are in degrees per second, so in order to get the angular position we just need to integrate the angular velocity.

C: Digital Relative Humidity and Temperature Sensor: The hygrometer is used to measure the humidity in the air, using the capacitance method. Since relative humidity is the relationship between amount of moisture in the air and the moisture capacity of the air, which is dependent on air temperature, and the hygrometer also measures air temperature. The air humidity can be used as a climatic indicator for precipitation and evapotranspiration potential, and can be used when computing energy balances.

D: Barometric pressure and Temperature Sensor: This sensor uses piezo-resistive technology to measure the air pressure at a certain elevation, meaning the sensor

Fig. 4 Architecture of the IoT device developed by IIT Mandi



monitoring elevation must be specified in the program. Since most barometric pressures are reported as coming from sea level, the pressure is also calibrated based on the elevation of the sensor and reported back as equivalent sea level pressure. The barometric pressure can give an indication of changing weather patterns and indicate if high- or low-pressure zones are approaching.

E: Digital Light Intensity Sensor: The light intensity sensor measures the amount of luminance in the surroundings using a photo-diode, which converts incoming light to a current directly proportional to the amount of incoming light. The luminance is the amount of light per second per unit target area on the sensor, measured in units of lux. The luminance can give an indication of the weather and short-wave radiation entering the atmosphere and could also be a useful measurement if solar panels are used to charge on-site batteries.

N: Rain Gauge: The device has pins for a rain gauge sensor. A rain gauge would provide a point measurement of precipitation at the slope location, instead of relying on weather stations which may not be near the site.

IoT device subcomponents: These subcomponents make up the hardware of the IoT device, connecting the microcontroller with the sensors, providing power and protecting the IoT device from high voltages.

F: Microcontroller: The microcontroller used in this IoT device is the same microchip used in the Arduino platform, through which the chip is programmed and connects with a computer. The microcontroller is an 8-bit, 28-pin plastic dual in-line package (PDIP), which runs the uploaded program and controls all the sensors in the IoT device. The program uploaded to the microcontroller controls the sensor reading frequency, data upload frequency and all information required to

read the sensors. Any program uploaded to the microcontroller is immediately activated.

G: Linear Voltage Regulator: This voltage regulator drops incoming voltage to the IoT device to a maximum of 5 V. The microcontroller and other components will not survive voltages higher than 5 V without burning out, so this regulator is very important should any voltage higher than 5 V be placed on the system. Since the input voltage coming from the battery and solar panel should never exceed 5 V, and there were issues with voltages being too low for the device to function properly; this regulator was eventually removed from the system.

H: Fixed LDO Voltage Regulator: This voltage regulator further drops the voltage to 3.3 V, which is the minimum required voltage for Wi-Fi module. Wi-Fi module is not capable of handling voltage more than 3.3 V. This regulator is a low voltage dropout (LDO) regulator, which can better handle small changes in voltage where other regulators require a larger voltage difference.

I: Wi-Fi module: The Wi-Fi module gives the microcontroller access to the Internet. The module can be programmed as an access point, which allows other devices to connect to it via Wi-Fi, or as a station, where it searches for a Wi-Fi network with specific credentials and connects to it when found.

J: Battery Charger with Protection Module: The battery charger provides power to the IoT device from either the battery or the power source with solar panel. This module allows the battery to be charged from the power source while still powering the IoT device and shuts off once the battery is charged.

K: Power Source: The power source is equipped with a solar panel to recharge the battery connected to the IoT device.

L: Relay module: Relay provides us the interface to switch on and off the alert unit for the local alerts.

M: Force Sensitive Resistor: A force-sensing resistor is a material whose resistance changes when a force, pressure or mechanical stress is applied. They are also known as “force-sensitive resistor” and are sometimes referred to by the initialism “FSR”.

The server then reports the data via a web-based interface, at the url: <http://landslidemonitoring.esy.es/index.php>. Some data recorded by the IoT device is shown in Fig. 5.

5 A Case Study of IoT-Based Early Warning of Paddhar Landslide on a Single Slope Scale

Kotropi, a village located 35-kilometres from Mandi bus stand along the NH 154 in Paddhar, witnessed a massive landslide in August 2017 (ref. Fig. 1) that killed more than 50 people. After the disaster, a temporary road was made through the debris for

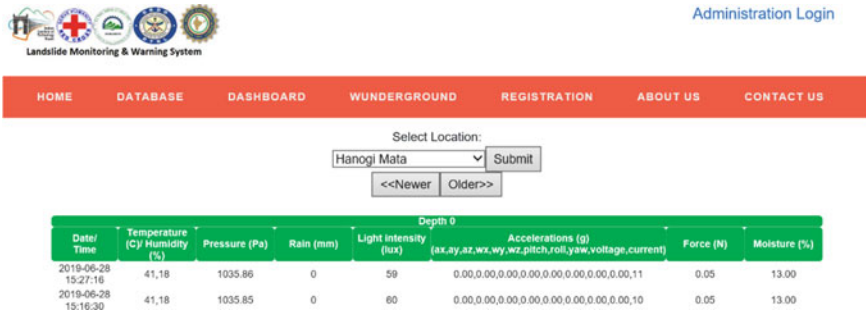


Fig. 5 Visualization of the portal for landslide monitoring and warning system by IIT Mandi

traffic flow. It is reported that Kotropi started experiencing a sewage overflow situation, which was originally a part of its old route due to substantial rainfall activity. For draining this sewage overflow, Public Works Department (PWD) had constructed a drainage facility. However, the internal water source was still active at some places underneath the temporary road, which was not easy to identify in the massive debris. When the monsoon started in July 2018, the sewage broke the integrity of soil and allowed water to go through as water finds its path through points of lowest energy. This breakage caused the movements in soil internally, and it started sliding. This internal slide of earth began to rupture the road from the corner with a way to release internal water. This complete scenario activated movements in the soil.

At 2:30 AM, on the night of 27 July 2018, it was raining heavily at Kotropi village, and a flash flood occurred. Underground water came rushing down towards the NH 154. However, between the water source and the road, there existed a low-cost landslide monitoring and warning system (LMWS), which the Mandi district administration had just deployed a few weeks back in collaboration with IIT



Fig. 6 Movement recorded by LMWS in X-, Y- and Z-direction between 29 June 2018 and 23 November 2018. The movement due to the flash flood at Paddhar on 27 July 2018 has been highlighted with a red oval

Mandi. The LMWS was triggered by rainwater, and the system sounded an alarm, which the police guards on the NH 154 heard in time. Figure 6 shows the movement recorded by LMWS at Kotropi between 29 June 2018 and 23 November 2018. In the figure, one can see rapid movements in all three directions on 27 July 2018. With the signals from the installed signal posts warning, the possibilities of rapid movements alerted the response team at site. Immediately, the disaster response team brought the traffic to halt which saved around 4–5 vehicles entering the sliding zone as per the report issued by district administration. This remains the one of the first positive alerts issued based on the monitoring of progressive movements observed at the site, subjected to rainfall induced landslide post a year of major incident happened in July, 2017.

6 Closing Remarks

This paper presented a brief introduction of the Norwegian practice for early warning of a landslide on regional scale. The criteria for issuing early warning are based on degree of saturation of soil and the supply of water to it through rainfall and snow melting. The paper also presented a promising development related to monitoring of single slopes. Indian Institute of Technology Mandi has developed a low-cost landslide monitoring and early warning system. These systems are deployed in Mandi district of Himachal Pradesh, India, and monitoring more than fifteen landslide locations in India. Through a case study, the usefulness of the systems was shown how it helped in alerting people and traffic from an impending landslide.

Acknowledgements The development of IoT devices at IIT Mandi was supported from grants (awards: IITM/NDMA/VD/184, IITM/DRDO-DTRL/VD/179 and IITM/DCoN/VD/204) to Varun Dutt and K.V. Uday. We are also grateful to Indian Institute of Technology Mandi for providing computational resources for this project. Support from the Research Council of Norway, the partners through the research project. KlimaDigital (www.klimadigital.no) and a strategic initiative by NTNU related to Resilient and Sustainable Water Infrastructure (www.sfiwin.com) are kindly acknowledged.

References

1. UNISDR <https://twitter.com/UNDRR/status/1065558323607601152> (2018)
2. Chaturvedi, P., Kishore Thakur, K., Mali, N., Uday, V., Kumar, S., Yadav, S., and Dutt, V: A Low-Cost IoT Framework for Landslide Prediction and Risk Communication, chapter 21, pp. 593–610. Wiley (2018)
3. Ko, C.K., Chowdhury, R., Flentje, R.: Hazard and risk assessment of rainfall-induced landsliding along a railway line. *Quarterly J. Eng. Geol. Hydrogeol.* **38**, 197–213 (2005)
4. Thakur, V., L'Hueruex, J. S., Locat, A.: Landslides in sensitive clays from research to implementation. Springer book series on Natural hazards. ISBN 978-3-319-56487-6 (2017)

5. Klose, M.: Landslide databases as tools for integrated assessment of landslide risk. Springer Theses—Recognizing Outstanding Ph.D. Research. Springer, Berlin, 156 pp. (2015)
6. UNISDR (United Nations International Strategy for Disaster Reduction). Terminology on disaster risk reduction. http://www.unisdr.org/files/7817_UNISDRTerminologyEnglish.pdf (2009).
7. Cruden, D. M., Varnes, D.J.: Landslide Types and Processes, Transportation Research Board, U.S. National Academy of Sciences, Special Report, **247**: 36–75 (1996)
8. Beldring, S., Engeland, K., Roald, L.A., Sælthun, N.R., Voksø, A.: Estimation of parameters in a distributed precipitationrunoff model for Norway. *Hydrol. Earth Syst. Sci.* **7**, 304–316 (2003). <https://doi.org/10.5194/hess-7-304-2003>
9. Devoli, G., Tiranti, D., Cremonini, R., Sund, M., Boje, S.: Comparison of landslide forecasting services in Piedmont (Italy) and Norway, illustrated by events in late spring 2013. *Nat. Hazards Earth Syst. Sci.* **18**(5), 1351–1372 (2018)
10. Calvello, M., Peduto, D., Arena, L.: Combined use of statistical and DInSAR data analyses to define the state of activity of slow-moving landslides. *Landslides* **14**(2), 473–489 (2017)
11. KLIMADIGITAL <https://www.sintef.no/en/latest-news/digitalization-of-geohazards-with-internet-of-things/> (2019)
12. Oguz, E., Robinson, K., Depina, I., Thakur, V.: IoT based strategies for risk management of rainfall induced landslides: A review. ISGSR, (2019)
13. Colleuille, H., Haugen, L. E., and Beldring, S.: A forecast analysis tool for extreme hydrological conditions in Norway, Poster presented at the Sixth World Friend conference, Marocco, 2010, Flow Regime and International Experiment and Network Data (2010)
14. Robinson, K.: Application of IoT Devices for Landslide Monitoring and Early Warning. Semester project report. NTNU (2018)